UNIVERSITY OF CALIFORNIA SAN DIEGO

# Chemoenzymatic Generation of Lipid Membranes

A Dissertation submitted in partial satisfaction of the requirements for the degree Doctorate of Philosophy

In

Chemistry

By

Satyam Khanal

Committee in charge:

Professor Neal K. Devaraj, Chair

Professor Michael D. Burkart, Co-chair

Professor Gourisankar Ghosh

Professor J. Andrew McCammon

Professor Roger K. Sunahara

Professor Haim Weizman

2022

The Dissertation of Satyam Khanal is approved and is acceptable in quality and form for publication on microfilm and electronically.

University of California San Diego

2022

## DEDICATION

Looking back at my PhD years, if someone were to ask me if I would do it all over again, I must be honest and say I would definitely pause and weigh both sides rather than give a quick yes or no. But in the end, it would be a yes; it has been a tough journey, but I have learned a lot about myself, the world (especially the molecular world) and I have made many amazing connections and had amazing experiences. And I have been able to go through with this journey because of the wonderful support system I have had.

The first person to thank for being my steady rock is my fiancée, Safalta Shrestha. She has been there for me throughout my 5 years, mostly on video call (she lived in Nepal for most of my PhD journey) and then in person. Her accepting my marriage proposal in the summer of 2021 was one of the highlights of my PhD years, even though it had nothing to do with chemistry. Despite not understanding much about chemistry at this depth (especially about lipid chemistry), she has patiently listened to me rant, whine, wallow and also rejoice over results during my research years. So, thank you so much, without your anchor I would have floated off somewhere in vacuum. I would also like to thank my parents, who have been nothing but wonderfully supportive to me over the years, my grandfather who always asks me for exciting news and updates, my brother and sister-in-law (and my niece more recently) for their love and support over the years and my entire family. Your love and care has let me stand up in this world.

I would also like to sincerely thank my primary advisor, Neal Devaraj. Neal is an absolute genius, so when I look back at the start of the program, I must have come off as such a newbie, having no background in lipid chemistry and molecular biology. He has been nothing but patient and helpful to me in the last 5 years and I have literally felt myself grow in skill (chemistry, oral presentation, and writing) as well as confidence under Neal's unwavering support and guidance. Neal is also a wonderful advisor for personal matters, and I have felt very comfortable talking with him about my mental health, my life in general and issues I have had over time, knowing that he would always give me the time and help me however he can. In the same vein, he is also very cognizant of the time-off that I needed from work, always respecting my wishes, and making sure I was in good health and mental space to work effectively. So, thank

you so much Neal. I would also like to thank my co-advisor, Mike Burkart. Mike has been such a great mentor in my journey. The greatest thing about Mike is his hands-off guidance method and his ideas. Troubleshooting chemistry with Mike and coming up with solutions has been integral to my growth as an independent scientist.

I would also like to thank both of the labs that I have had the absolute pleasure working with. They have been my mentors, my best friends in and out of lab, and great collaborators. Thanks to all the lab mates I have had over the years, I have made lifelong friends and connections. From Neal's lab: Eric Zhou, Xijun Piao, Andrés Seoane Fernandez, Roberto Brea, Henrike Neiderholtmeyer, Shuaijiang Jin, Mai Johnnson, Luping Liu, Jorge Jimenez, Youngjun Lee, Andrew Rudd, Ahanjit Bhattacharya, Alessandro Fracassi, Lalita Tanwar, Caroline Knittel, Chih-Chin Chi, Brandon Cisneros, Kayla Busby, Dongyang Zhang, Kira Podolsky, Hetika Vora, Judith Flores, Ember Tota, Christy Cho, Jiyue Chen, Jacob Vance, Alexander Harjung, Karen Guerrero, Stormi Chadwick, Zulfiqar Mohamedshah, Emily Tsai. Also a big thanks to Meli Tsai and Kailash Venkatraman for being honorary lab members and great friends. Special shoutout to Ahanjit for helping me kick start my project and letting me collaborate with him in his project, to Roberto and Alessandro for helping me immensely in my projects, to Andres for also helping me in my early years and finally my office mates (especially Judith, Ember, and Karen) as well as our lunch groups over the years. From Mike's lab: Jim La Clair, Tony Davis, Laetitia Misson-Mindrebo, Sho Konno, Brian Leon, Ashay Patel, Qing Zhe Ni, An Phung, Bhausaheb Rajput, Graham Heberlig, Jacque Faylo, Luca Bonanomi, Thomas Bartholow, Woojoo Eunice Kim, Jefferey Mindrebo, Katia Charov, Warren Chan, Troy Bemis, Terra Sztain-Pedone, Kelsey Trieger, Aochiu Chen, Joshua Corpuz, Rebecca Re, Brianna Kalaj, Jeffrey Chen, Desirae Mellor, Ziran Jiang, Javier Sanlley, Arthur Altunc, Yixing Suo, Lilit Vardanyan, Bashayer Althufairi, Yuta Moriuchi, Aaron Bruckbauer, Caitlin Hudecek, Matthew Miyada. Special thanks to Sho for helping me get started with my first project and to Leti and Josh for helping me with learning molecular biology techniques at the start. I would also like to thank lab alumni Dr. Bob Haushalter for helping me

figure out the nuances of the fatty acid synthase enzyme. Also, a special thanks to Rebecca, Josh, Brianna and Christy for being amazing cohort mates.

Thank you to my committee members, Gourisankar Ghosh, Haim Weizman, J. Andrew McCammon, Roger Sunahara for your helpful guidance, questions, and suggestions through my thesis work.

I would also like to thank my undergraduate advisor Seann P. Mulcahy, who took me under his wing in my very first year in college and let me work in his lab for the four-year duration of college. In his lab I kindled my love for chemistry lab work, and he has always been extremely encouraging and helpful to me over the years.

Finally, I would like to thank my friends who have been there for me through the tough years of graduate school. Special thanks to Sifeng Gu, Francois Louis Henri Vermersch, and Pyeongeun Kim for being my close friends, housemates, and surfing buddies over the last 5 years. We supported each other immensely in the last few years, especially during the lockdown of COVID. Being cohort mates brought us together, but we will be friends for life. I would also like to shoutout my lab sibling Judith Flores, without whom I cannot imagine being in lab. Finally, I would like to thank my other close friends, especially David Toro, Tara Moore, Mohammed Alshair, Ali Malik, Eduardo Lopez, Chris Baryiames, Shelby Scola, Max Molina, Chaz Davenport, and Mike DiGregorio whom I first befriended back in college but who have been amazing friends even though we haven't had a chance to hangout many times since then. Special shoutout to David for being my absolute homeboy, it was an honor to be your Best Man last summer.

## EPIGRAPH

An understanding of the natural world and what's in it is a source of not only a great curiosity but great fulfillment

Sir David Attenborough

**TABLE OF CONTENTS**

## LIST OF FIGURES

## ACKNOWLEDGEMENTS

Chapter Two, in full, is a reprint (with co-author permission) of the material as it appears in the publication: Khanal, S., Brea, R. J., Burkart, M., D., Devaraj, N., K. Chemoenzymatic Generation of Phospholipid Membranes Mediated by Type I Fatty Acid Synthase, *J. Am. Chem. Soc.* **2021**, 143, 23, 8533–8537. I would like to thank Roberto Brea for his contributions, especially the synthesis of the head groups and helping me with writing the manuscript. I would like to thank Neal Devaraj for his guidance and assistance in preparing the manuscript. I would like to thank Mike Burkart for his help and mentorship in the project as well.

Chapter Three consists of material that is being prepared into a manuscript that will be submitted for publication in the near future. I thank Alessandro Fracassi for his contributions to the work as well as Neal Devaraj for his oversight and assistance in this work. I would like to thank Mike Burkart for his support and mentorship in the project.

Chapter Four, in full, is a reprint of the material as it appears in the manuscript: Bhattacharya, A., Brea, R., J., Khanal, S., Salvador-Castell, M., Sinha, S., K., and Devaraj, N., K. Catalytic ion-directed synthesis of O-acylated sphingomyelin analogues in aqueous media and their self-assembly into vesicles. **2021**. *Submitted*. My contribution to this chapter was the optimization of the sphingolipid formation reactions under various conditions while using different metal ions. I would like to thank Ahanjit Bhattacharya for his contributions to this chapter, which includes the initial observations of different sphingolipid products made under different conditions, screening the reactions with various metal ions, optimization and characterization of the lipids made as well as, HPLC-MS, fluorescent microscopy as well as the biochemical assays. I would also like to thank Roberto Brea for the synthesis and characterization of the sphingolipid precursors as well as the lipids made and the microscopy experiments. Additionally, I would like to thank Marta Salvador-Castell for the x-ray diffraction experiments. I would like to thank Sunil Sinha for his insight and contributions to the manuscript. I would finally like to thank Neal Devaraj for his guidance for the project and assistance with the preparation of the manuscript.

# VITA

## Education

**2016** Bachelor of Science, Biochemistry, Providence College

**2019** Master of Science, Chemistry, University of California San Diego

**2022** Doctor of Philosophy, Chemistry, University of California San Diego

## Publications

**Khanal, S.**, Fracassi, A., Burkart, M., D., Devaraj, N., K. Utilizing Acetate as Carbon Feedstock in Membrane Generation. *In preparation*.

Bhattacharya, A., Brea, R., J., **Khanal, S.**, Salvador-Castell, M., Sinha, S., K., Devaraj, N., K. *Submitted*.

**Khanal, S.**, Brea, R., J., Burkart, M., D., Devaraj, N., K. Chemoenzymatic Generation of Phospholipid Membranes Mediated by Type I Fatty Acid Synthase. *J. Am. Chem. Soc.* **2021**, 143, 23, 8533–8537.

Saliba, B., S., **Khanal, S.**, O' Donnell, M., A., Queenan, K., E., Song, J., Gentile, M., E., Mulcahy, S., P. Parallel strategies for the synthesis of annulated pyrido[3,4-b]indoles via Rh(I)- and Pd(0)-catalyzed cyclotrimerization. *Tetrahedron Lett.* **2018**, 59(49), 4311-4314.

Varelas, J., G., **Khanal, S.**, O'Donnell, M., A., Mulcahy, S., P. Concise Synthesis of Annulated Pyrido[3,4-b]indoles via Rh(I)-Catalyzed Cyclization. *Org. Lett.* **2015**, 17 (21), 5512–5514.

## Fellowship and Awards

**2021** National Science Foundation Designer Cell Grant Recipient (NSF 21-531)

**2017** Roger Tsien Fellow for Interdisciplinary and Collaborative Work

**2015** Walsh Fellow for Undergraduate Summer Research

## ABSTRACT OF THE DISSERTATION

Chemoenzymatic Generation of Lipid Membranes

By

Satyam Khanal

Doctor of Philosophy in Chemistry

University of California San Diego, 2022

Professor Neal K. Devaraj, Chair

Professor Michael D. Burkart, Co-chair

The bottom-up generation of lipid membranes from minimal precursors is a key objective in synthetic biology research. In living cells, the synthesis of lipid assemblies is ubiquitously coordinated by several membrane-bound enzymes. However, these pathways are tough to replicate, owing to the difficulty of reconstituting the enzymes *in vitro*. Lipid membrane synthesis from simple metabolic building blocks remains challenging.

We demonstrate a chemoenzymatic schematic for lipid membrane generation, utilizing a bacterial fatty acid synthase (cgFAS I) to synthesize palmitoyl-CoA *in situ* from acetyl-CoA and malonyl-CoA as precursors. Palmitoyl-CoA spontaneously reacts with a cysteine-modified lysophospholipid via native chemical ligation (NCL), generating noncanonical amidophospholipids that self-assemble into micron-sized membranes. The results demonstrate that combining the specificity and efficiency of a type I fatty acid synthase with a selective bioconjugation reaction provides a biomimetic route for the *de novo* formation of membrane-bound vesicles. Utilizing this route, we further investigate the application of non-amphiphilic, minimal precursor pathway to generate lipid membranes. We explore the use of acetate as the carbon feedstock for the chemoenzymatic reaction strategy, generation palmitoyl-CoA *in situ* and coupling it with small molecule head group such as cysteine to form phospholipid analogs. Ubiquitous enzymes acetyl-CoA synthetase (ACS) from *E. coli* was used to generate acetyl-CoA from acetate and human acetyl-CoA carboxylase (ACC) was used to then synthesize malonyl-CoA from acetyl-CoA. Additionally, cgFAS catalyzed the *in situ* generation of palmitoyl-CoA from acetyl-CoA and malonyl-CoA. Finally, we explore the formation of a unique analog of sphingolipid membranes from water-soluble precursors that have markedly different biophysical properties to their natural counterparts. We show that numerous transition metal ions, particularly Cu(II), catalyze the selective O-acylation of the biologically occurring single-chain amphiphile sphingosylphosphorylcholine using fatty acyl phosphates or thioesters as acyl donors under mild aqueous conditions.

This work demonstrates the value of *de novo* membrane generation strategies starting from minimal, water-soluble precursors. Utilizing such approaches, we can control both the chemical structures of the lipid analogs as well as their biophysical properties in aqueous media. This effort contributes towards understanding the fundamental requirements for bottom-up generation of lipid membranes, providing alternative strategies to those previously shown.

# 1. Introduction

## 1.1 Motivation

An integral part of all living systems is the presence of compartments or boundaries that separate the living unit from the outside environment and perform critical functions vital to the proper functioning of living systems.[1] A form of compartment that we can easily visualize is the skin, which is the outer boundary for a lot of organisms, including us humans. The skin is our largest organ, protecting and insulating our body, especially our vital organs, from a diverse set of outer forces such as pathogens, UV radiation, excess heat and cold, among other things.[2] The skin controls what can and cannot enter our body while also maintaining homeostasis. Similar to the skin as our macro-boundary, all cells are compartmentalized (which we can think of as our micro-boundary). Existing cells utilize phospholipid membranes as the boundary to separate themselves from the external environment.[3] Membranes define the cell boundary, control exchange and transport of materials in and out of the cell, protect and segregate chemical reactions, and maintain ion gradients due to their impermeability to ions, among other functions.[4] Lipid membranes are extremely unique structures that can adopt numerous shapes and sizes depending on the particular requirements of the cells. Additionally, lipids can be generated rapidly, and can interact or be coupled with complex biological polymers (such as proteins and sugars) that confer transport and signaling functions.[5,6] All of these features are essential for highly compartmentalized cells to grow and divide.

In biologically relevant aqueous media, lipids have shown to spontaneously self-assemble into unique assemblies depending on the composition of the lipids. Phospholipids in particular assemble into membrane-bound structures called vesicles. Since phospholipids are amphiphilic, they self-assemble into vesicles in order to segregate the hydrophobic alkyl tails from the aqueous environment while exposing the hydrophilic heads to water. This process is driven by the segregation of the nonpolar fatty acyl chains of the phospholipid molecules from the aqueous solution to minimize their thermodynamically unfavorable

interaction with water molecules. Furthermore, phospholipids are complex amphiphiles and may not have evolved without a sophisticated biochemical machinery.[7] Previous work has suggested that the membranes of the earliest cells were made of single-chain amphiphiles such as fatty acids and fatty alcohols derived from geochemical processes and even extraterrestrial sources like meteorites.[8] These simple compartments are capable of encapsulating prebiotically important molecules and sustaining a few simple biochemical reactions.[9] Moreover, membrane-forming molecules evolved to be more complex to necessitate the early evolution of life. It has been theorized that the phospholipids gave a competitive edge to protocells bounded by them.[10] The presence of compartments in all forms of life indicates their significance in sustaining far-from-equilibrium biochemical systems and enabling Darwinian evolution.[11,12] Hence, it is vital to gain insight into the probable pathways that led to the early biosynthesis of phospholipids and other complex amphiphiles. To answer these critical questions about the role of compartmentalization in the evolution of life, the complementary methods of top-down and bottom-up synthetic biology explore the role of biochemistry in building a unit cell. While top-down synthetic biologists look to build a minimal unit by sequentially removing redundant genes in a biological cell,[13,14] bottom-up synthetic biologists work on using simple chemistries to synthesize components of life and combining them to form life-like matter.[13] Assembling artificial cells from the bottom up is a promising albeit ambitious approach to redefining life in chemical terms. The ultimate goal of artificial cell development is not just to explore how life started on Earth but also to construct systems that represent models to make sense of ubiquitous biological characteristics. In the absence of the limitations of prebiotic conditions, synthetic systems can be controlled and manipulated through an extended range of known functional groups and chemistries. Creating and assembling cell boundaries from the bottom up provides insight into which physicochemical characteristics lead to life-like attributes.

### 1.2 *In vitro* membrane generation strategies

In biological systems, membrane-forming lipids are ubiquitously synthesized in the endoplasmic reticulum via an enzyme-catalyzed, multi-step process involving several cofactors.[15] The diverse phospholipid membranes are enzymatically synthesized by membrane-bound acyl-transferases via the *de novo* Kennedy pathway.[16] These acyltransferases in part require membranes for correct integration, folding and function.[17] The fatty acids needed for these biochemical reactions are made by fatty acid synthases (FASs).[18] These enzymes catalyze these reactions in a highly efficient manner by the modularization of reactive domains as well as the use of carrier-mediated substrate shuttling.[19] The essential enzymes for phospholipid generation pathways are membrane-bound proteins that are difficult to reconstitute in functional form *in vitro*. The necessity of membrane proteins indicates that nascent membranes require pre-existing membranes for synthesis. Therefore, *de novo* membrane generation (i.e., the formation of membranes without previously existing membranes) is unlikely by reconstitution of native lipid synthesis pathways. Additionally, membrane-bound enzyme reconstitution in artificial membrane is an inefficient process, as shown by the low yield of synthesized membrane observed in past studies.[20,21] For example, Martin *et. al.* show that after incorporating beta-amyloid precursor protein cleaving enzyme (BACE) on artificial lipid bilayer surface, the activity of BACE was lower than 16% compared to the native counterpart. Typical issues arise from protein stability, proper folding during reconstitution, and correct orientation of the protein once integrated.[22] For the bottom-up design of an artificial cell, a completely different strategy is required. To remove the need for pre-existing membranes, the reactive precursors should not spontaneously assemble into membranes but rather react in a chemoselective fashion to form membrane-forming lipids. This method is known as *de novo* membrane generation. This approach was inspired by the Land's Cycle – a biochemical process used by organisms for phospholipid remodeling.[23,24] In this cycle, single-chain amphiphiles such as lysophospholipids and fatty acyl-CoA thioesters – react in the presence of lysophospholipid acyltransferase (LPLAT).[25,26] Membranes have been shown to be reconstituted from water-soluble precursors by utilizing the LPLAT activity of solubilized liver microsomal membranes, albeit inefficiently. It has been our goal to utilize simple, robust, and high-yielding reactions for this purpose.

Owing to the importance of understanding the parameters to set up biomimetic artificial cell systems, several groups have explored feasible approaches for the *de novo* formation of synthetic lipid membranes from reactive precursors. Synthetic lipid precursors can react non-enzymatically and assemble into biomimetic cell boundaries. By developing mutually compatible bioorthogonal chemistries, multifunctional synthetic membranes can be generated. One of the earliest examples based on a bioorthogonal approach used the copper(I) catalyzed azide–alkyne cycloaddition (CuAAC) reaction to drive membrane assembly.[24] This system employs a biomimetic coupling reaction to join an alkyne-functionalized lysophospholipid and an alkyl azide in the presence of a copper catalyst, which generates a triazole-linked phospholipid analog. Neither the alkyne nor azide precursors are capable of forming membranes in aqueous solution, but the lipid product, when hydrated, self-assembles to form stable membrane vesicles. Overall, the strategy is biomimetic, proceeding in aqueous medium with high specificity and a lack of background reactions.

Employing a similar strategy, Brea et al. used native chemical ligation (NCL) to chemoselectively couple a cysteine-functionalized lysophospholipid and a water-soluble fatty acyl thioester.[27] The reaction went to near completion under 30 minutes. The amidophospholipids showed physical properties similar to their natural counterparts. Brea et al. further showed that histidine ligation (HL) can similarly be utilized to generate amide-linked phospholipids.[28] The catalytic role of the imidazole ring of a histidine-functionalized lysolipid was utilized in particular to drive its coupling to a fatty acyl thioester, leading to unique amidophospholipids. The phospholipids thus formed can spontaneously self-assemble into micron-sized vesicles. Additionally, the chemoselectivity, and biorthogonality of this approach are key features that make it an effective tool for the efficient encapsulation of biomacromolecules like enzymes. Moreover, simple but robust chemoselective coupling reactions in mild aqueous media could be utilized to afford phospholipids *in situ*. In recent work, Bhattacharya *et. al.* also utilized a soluble enzyme FadD10 to activate fatty acid tails and generate lipids.[29] They used a high-yielding approach for *de novo* formation and growth of phospholipid membranes by forming fatty acyl adenylates that react with amine-functionalized lysolipids to afford phospholipids. Adding more precursors needed for lipid synthesis led to the growth of vesicles

encapsulating FadD10. Their findings showed that alternate chemistries can produce and maintain synthetic phospholipid membranes. These examples let us explore building a diverse toolbox for generating lipid membranes chemically.

### 1.3 Lipid formation from minimal precursors

In the given examples, the starting precursors are amphiphilic in nature. With these approaches, we can only get a partial picture of how lipids were generated. But in order to get a better idea, we need to start with even simpler, non-amphiphilic precursors. A key goal of lipid chemists is to reiterate the self-assembly of lipid analogs from simple, water-soluble precursors in an artificial cell system. If we think back to early protocells, complex biomolecules such as single-chain amphiphiles (fatty acids and monoacylglycerols), lipids and multi-domain enzymes were not present. To understand how these protocells evolved to the systems we see now, we need to deduct possible mechanisms of such evolution, starting from very minimal precursors and building up macromolecular assemblies. Recent examples from the Sutherland, Szostak and Powner groups have explored the formation of nucleotides, amino acids and lipids from activated, prebiotically plausible precursors.[30–32] These prebiotic building blocks, in turn, can be synthesized in complex reaction mixtures.[33–35] Moreover, utilizing cyanamide and imidazole as catalysts, a dried film of ammonium palmitate was reacted with glycerol at high temperatures to generate monopalmitoylglycerols, dipalmitoylglycerols and tripalmitoylglycerols.[36] Additionally, condensation reactions of lipids can similarly occur under hydrothermal conditions. For instance, monoacylglycerols, diacylglycerols and triacylglycerols have been made from various medium-chained fatty acids (ranging from $C_7$ to $C_{16}$) and an excess of glycerol under aqueous conditions. Purified monoacylglycerol products can form protocellular membrane structures after rehydration. The Deamer group suggested that phospholipids could be synthesized in evaporating tide pools containing glycerol, phosphate and cyanamide on hot sand under wet–dry cycling conditions, simulating a hydrothermal pool scenario of protocell formation. They were able to show that ether monoglycerols can be synthesized under wet-dry cycling only when dried completely. The resulting ether monoglycerol, was then mixed with various phospholipid precursors as well as clay,

generating low yields of phosphatidic acid, phosphatidylglycerol and phosphatidylglycerol phosphate.[37] Using alternative precursors, Oró and colleagues got yields of up to 45% of phosphatidic acid and other phospholipids under aqueous conditions evaporated to dryness.[38] Furthermore, phosphatidylcholine, one of the major phospholipids in eukaryotic cell membranes, was produced in a dry film of phosphatidic acid and choline in the presence of cyanamide.[39] Following up on this, two additional phospholipids, dioleoylphosphatidic acid (DOPA) and dioleoylphosphatidylethanolamine (DOPE), were abiotically generated from a racemic mixture of dioleolglycerol (phosphorylated in the presence of cyanamide or urea) and ammonium dihydrogen phosphate respectively, by evaporating the reaction mixtures to dryness.[40] The crude products, containing 30 to 60 mol% DOPA, formed stable giant vesicles that are able to encapsulate the water-soluble dye calcein. While these approaches are novel and based on minimal precursors, the reaction conditions are more indicative of the early earth with high temperatures. If we aim to understand alternative pathways using simple precursors in mid aqueous conditions comparable to more recent earth, we need to find approaches that depend on simple reactions that can be done under physiological conditions.

### 1.4 Fatty Acid Synthases (FASs)

Lipids consist of fatty acid units as their tails and fatty acids are primarily made by fatty acid synthases (FASs). FASs are ubiquitously found in all organisms and are theorized to be the steps of very ancient biochemical pathways.[41] The basic attributes of the FAS pathway, i.e., its fundamental chemical reactions and the identity of the respective component enzymes, were explicated more than three decades ago.[42–45] Evolutionarily speaking, numerous functionally differentiated FAS variations as well as a large family of FAS-related enzymes have been made which generate, by minor alteration of the FAS pathway, a broad spectrum of natural compounds. These FAS structural variants can be divided into three general classes. The first class consists of the dissociated type II FAS systems, which occur in most bacteria and in the organelles of procaryotic descent, such as mitochondria and chloroplasts. The constituent enzymes of type II fatty acid synthases are separate proteins which are encoded by a series of distinct genes. The individual FAS component enzymes are ac(et)yltransferase (AC), malonyl/acetyl- or malonyl/palmitoyl-

transacylase (AT, MPT), ketoacyl synthase (KS) ketoacyl reductase (KR), dehydratase (DH), enoyl reductase (ER), acyl carrier protein (ACP), and thioesterase (TE). The activities of AT and TE domains and those of the MPT domain are mutually exclusive and rely on the particular FAS system. The majority of cellular fatty acids generate via type II FAS typically contain 14–18 carbon atoms. In contrast to type II FASs, type I FASs are highly integrated multi-domain enzymes, which contain the numerous catalytic activities of the reaction sequence as discrete functional domains, either on a single polypeptide chain or, sometimes, on two different multifunctional proteins of similar size. Type I FASs are typically found in the eukaryotic cytoplasm[42,46] and, as a notable procaryotic exemption, also among the mycolic acid producing subgroup of the Actinomycetales.[47] The type I systems may be further subdivided corresponding to the domain organization of the multifunctional proteins and, concurrently, according to their subunit stoichiometry. Microbial type I FASs are hexamers with a domain sequence of AC-ER-DH-MPT/ACP-KR-KS forming either $\alpha_6\beta_6$ (fungi) or $\alpha_6$ (bacteria) oligomers (type Ia).[48] On the other hand, animal FASs are $\alpha_2$ dimers with the domain sequence KS-AT-DH-ER-KR-ACP-TE (type Ib).[18]

Despite there being substantial differences in the molecular structures of FASs from several sources, the reaction mechanism of *de novo* fatty acid synthesis is essentially the same in all living systems. Fatty acid biosynthesis is started by the AT, loading the acyl primer, typically acetate, from coenzyme A (CoA) to a specific binding site on FAS. By the end of the cycle, termination of chain elongation occurs by removing the product from FAS either by transesterification to the correct acceptor or by hydrolysis. The respective enzymes are generally MPT and TE. The reaction sequence between initiation and termination entails the elongation of enzyme-bound intermediates by numerous iterative cycles of a distinct set of reaction steps. Each cycle comprises of malonyl-transacylation from CoA to the enzyme by AT, condensation of acyl-enzyme with enzyme-bound malonate to 3-ketoacyl-enzyme by KS, reduction of the 3-keto- to the 3-hydroxyacyl intermediate by KR, dehydration of 3-hydroxyacyl enzyme to 2,3-trans-enoate by DH, and, finally, reduction of the enoate to the saturated acyl-enzyme by ER. A key role in substrate binding, processing of intermediates, and communicating of intermediates between the various catalytic

centers of FAS is performed by the prosthetic group, 4′-phosphopantetheine. This cofactor is covalently bound to a specific serine hydroxyl group of the ACP domain or, depending on the FAS system, to the ACP component of FAS. In some bacteria, the iterative sequence of elongation cycles may be interrupted, at a chain length of 10 carbons, by one cycle involving an intrinsic isomerase converting the 2-trans- into the 3-cis-decenoyl intermediate, which is subsequently not reduced but further elongated to long-chain monounsaturated fatty acids.[49,50]

An essential characteristic of every FAS is the specificity of its chain termination reaction, which defines both the chain length and the acceptor of the FAS product. In *Escherichia coli*, long-chain fatty acids are transacylated by specific glycerol phosphate transacylases from acyl-ACP directly to the membrane phospholipids. In contrast, certain shorter-chain intermediates may be diverted from the elongation process for other reactions such as lipopolysaccharide or coenzyme biosyntheses.[50] The type I FASs of yeast, mycobacteria, corynebacteria, and Euglena use an integral palmitoyl transferase activity for transacylation of palmitate from the enzyme to CoA.[42,47] Animal FAS, on the other hand, releases its products as free fatty acids after hydrolysis by an intrinsic thioesterase.[51,52] Additionally, the chain length of FAS products is undoubtedly an inherent property of every individual enzyme, even though the structural basis for this characteristic continues to be obscure. Depending on the particular organism and FAS system, the chain lengths of FAS products may vary over a wide range. For instance, Mangelsdorf group showed that the cell membrane fatty acid composition of *Chryseobacterium frigidisoli* PB4$^{T}$ changes in response to change in temperature as well as pH conditions.[53]

### 1.5 Type I FASs in Bacteria

The bacterial type I FAS enzyme has been isolated and purified from several mycobacterial strains[47,54,55] and from C. ammoniagenes.[56] In all of the cases, the purified enzymes were hexamers of identical subunits combining the entire set of catalytic FAS domains within a single polypeptide chain. Isolation and sequencing of the respective genes showed a domain organization of these multifunctional FAS proteins which was similar to a head-to-tail fusion of the yeast FAS subunits β and α.[55,57,58] Thus, the

microbial type I FASs, on the one hand, and animal FAS, on the other, represent different patterns of intramolecular and supramolecular organization. The size of the bacterial FAS subunits, containing about 3,000 amino acids, was in between those of animal FAS (about 2,500 amino acids) and the αβ dimer of yeast FAS (3,940 amino acids). Contrasting with the yeast FAS, the bacterial apoFAS activating phosphopantetheine transferase is encoded by a separate gene rather than being integrated into the FAS protein.[58,59] Even though this PPT gene is closely linked to the FAS-B reading frame in *C. ammoniagenes*, its product obviously functions as an independent enzyme activating both cellular FAS proteins, FAS-A and FAS-B.[60] Similarly, it appears that a single PPT coding sequence in the *M. tuberculosis* genome is sufficient for the activation of all pantetheinylated cellular proteins. *Corynebacterium glutamicum*, in particular, is used for the large-scale production of L-glutamate and L-lysine, currently produced in amounts of $1.2*10^6$ and $6*10^5$ tons per year, respectively.[61] It is established that the lipid content of *C. glutamicum* influences the amino acid excretion properties of this organism.[62] For example, an altered phospholipid composition of *C. glutamicum*, as done by overexpression of the cardiolipin synthetase gene cls, results in enhanced L-glutamate excretion.[63] Moreover, from studies with Mycobacterium species, we know that the outer lipid layer, comprising largely of mycolic acids bound to trehalose and the arabinogalactan polymer, contributes substantially to the flux properties of the cell envelope.[64]

### 1.6 Acetate as Carbon Feedstock for Membrane Formation

Following up on examples where simple chemical precursors were utilized to build a more complex phospholipid membrane system, we wanted to explore more avenues to build an artificial cell system starting from non-amphiphilic precursors. A novel and innovative approach would be to generate lipid membranes from simple, highly abundant and biologically relevant carbon feedstock such as acetate[65] and ubiquitous amino acids such as cysteine.[66] Using acetate as a carbon feedstock denotes a major departure from previous approaches. Moreover, from the point of view of bottom-up synthesis of *de novo* membranes, starting from acetate as feedstock and the sole source of carbon would be a stupendous achievement that is unexplored until now. Additionally, these simple precursors are membrane permeable and utilizing them

as a feedstock for lipid synthesis would avoid the detergent effect associated with single-chain amphiphilic precursors. However, efficiently generating long acyl chains from two-carbon precursors is extraordinarily challenging. Previously established systems either need high temperature and chemical reactants or they need a continuous addition of long-chain amphiphilic species to sustain the lipid formation. To date, there are no examples of such processes, and nearly all studies with synthetic membranes use preformed lipid species. In chapter two, we show a partial chemoenzymatic approach for generating synthetic phospholipid membranes from simple metabolic precursors. Instead of supplying the system with preformed fatty acid tails, we utilize a type I fatty acyl-coenzyme A (CoA) synthase from *Corynebacterium glutamicum* (cgFAS) to generate acyl-CoAs in situ from water-soluble precursor molecules, acetyl-CoA and malonyl-CoA.[1] Subsequently, the activated fatty acids chemically react with lysolipid precursors to form phospholipid membranes. By enzymatically generating acyl precursors and replacing the steps normally catalyzed by membrane-bound acyltransferases with chemical steps, we generate close analogs of biological phospholipids. However, this reaction scheme, while representing an important advance, still requires the use of lysolipid detergents. To realize our vision of an artificial membrane that can subsist on simple chemical feedstock, in chapter 3, we discuss the generation of phospholipid membranes entirely from non-amphiphilic, water-soluble precursors.

To generate the lipid tails, we utilize acetic acid as a carbon feedstock for lipid generation because of its simplicity, membrane permeability[67], abundance, and its industrial relevance.[68] Acetate can be enzymatically converted to acetyl-CoA, one of the central metabolic intermediates in living organisms participating in key processes such as the Kreb's cycle and serving as precursors for lipid synthesis, protein acetylation, metabolic acetylation, among others. Furthermore, various groups have shown that living organisms, especially heterotrophic bacteria, utilize acetate as carbon and energy source.[65,69,70] For our purposes, we use acetyl-CoA synthetase (ACS) from E. coli to generate acetyl-CoA from acetate. We then used human acetyl-CoA carboxylase (ACC) to produce malonyl-CoA from acetyl-CoA. Additionally, we utilize cgFAS I to generate palmitoyl-CoA from acetyl-CoA and malonyl-CoA. Once we optimize these

enzymatic steps, we reconstitute them into the chemoenzymatic one-pot reaction to generate fatty acyl-CoAs *in situ*. Finally, the fatty-acid tails generated *in situ* reacts with a cysteine to form a two-tailed phospholipid analogue.

### 1.7 Ion-directed O-acylated Sphingolipid Formation

In chapter 4, we explore the formation of sphingolipids in the presence of diverse metal ions. Sphingolipids are an essential class of lipids occurring universally in eukaryotes. They are structural components of membranes and are also important in biochemical signaling processes. Sphingolipids are made up of a sphingoid base with two hydroxyl (-OH) groups at positions $C_1$ and $C_3$ and an amine ($-NH_2$) group at position $C_2$. The amine is normally acylated by a fatty acid chain via an amide linkage. Sphingomyelins may be an attractive choice for building blocks for stable synthetic cells thanks to their hydrolytic stability. One of the simplest forms of acylated sphingolipids is ceramide, where the $OH(C_1)$ group remains unmodified. The $OH(C_1)$ group of ceramides may be enzymatically altered by addition of polar head groups like phosphocholine and phosphoethanolamine to generate sphingomyelins, and with sugar moieties to generate glycosphingolipids. Additionally, in sphingolipids, the $OH(C_3)$ group on the sphingoid base chain typically remains free. However, sphingolipid species where the $OH(C_3)$ is acylated, but $NH_2(C_2)$ is free have not been previously reported. Native sphingomyelins having phosphocholine headgroups are known to self-assemble into vesicles in aqueous media. Vesicle formation has also been reported from N-acylated sphingomyelins containing small structural modifications. Here we show that numerous transition metal ions, particularly Cu(II), catalyze the selective O-acylation of the biologically occurring single-chain amphiphile sphingosylphosphorylcholine (also known as lysosphingomyelin) using fatty acyl phosphates or thioesters as acyl donors under mild aqueous conditions. We further show that the O-acylated sphingomyelin analogues self-assemble into vesicles having markedly different physical properties as compared to the vesicles formed from N-acylated sphingomyelins.

## 2. Chemoenzymatic Generation of Phospholipid Membranes Mediated by Type I Fatty Acid Synthase

### 2.1 Introduction

All living organisms use phospholipid membranes to control the exchange of materials with the extracellular matrix, isolate and protect sensitive chemical reactions, and maintain homeostasis inside cells.[4] Furthermore, cells require phospholipid membranes for energy production, membrane protein synthesis, and cell signaling.[5,6] Phospholipids are enzymatically generated by membrane-bound acyl-transferases as part of the Kennedy lipid synthesis pathway.[15,17] The fatty acids needed for these biochemical reactions are in turn made by fatty acid synthases (FASs). FASs are ubiquitous proteins that catalyze the synthesis of fatty acids in a highly efficient manner through modularization of enzymatic functions and the use of carrier-mediated substrate shuttling.[18,46,71] Drawing inspiration from the biochemical pathways for phospholipid synthesis, various research groups have devised strategies for the bottom-up construction of phospholipid membranes.[27,72] Although recent studies have shown that phospholipids can be generated abiotically using chemical coupling reactions,[22,24] the alkyl chains are typically synthesized in advance and provided externally. Currently, there are no known biomimetic strategies that synthesize phospholipids *de novo* by coupling in situ formed fatty acid tails with single-chain amphiphiles. Instead of externally adding alkyl species, we sought to harness a FAS for the formation of fatty acyl-CoAs from simple metabolic building blocks such as acetyl-CoA and malonyl-CoA. FASs can be rationally engineered to modulate the type of fatty acid species made in live organisms.[48] However, we wanted to reconstitute FAS function outside of cells to produce fatty acyl-CoAs *in situ*. Subsequently, the fatty acyl-CoAs could chemically react with lipid precursors to form phospholipid membranes. Such a chemoenzymatic scheme would better mimic biological phospholipid synthesis compared to previous synthetic strategies and would enable the use of medium-chain acyl-CoAs to drive membrane formation. Here, we employ a bacterial type I FAS (cgFAS I), in combination with native chemical ligation (NCL), to spontaneously generate membrane-forming synthetic phospholipids from simple water-soluble fatty acid precursors. Our chemoenzymatic

approach enables *de novo* membrane formation, that is, membrane formation in the absence of preexisting membranes. Chemoenzymatic phospholipid formation may provide simpler strategies to generate membrane compartments in synthetic cells,[3,24,27,28] support the advancement of methods for reconstituting membrane proteins,[73,74] and facilitate the synthesis of natural and noncanonical lipids.[75]

### 2.2 Expression and Functional Verification of Bacterial Type I FAS

We first identified an appropriate FAS for the *in situ* formation of activated fatty acids. While type II FASs are comprised of multiple enzymes working in a coordinated fashion, type I FASs consist of a single multi-enzyme complex with catalytic domains that interact with each other in a cooperative manner to form fatty acids.[18] Through iterative cycles, a type I FAS utilizes acetyl-CoA and malonyl-CoA to produce medium-chain fatty acids in a stoichiometric fashion (Figure 2.1.A). We considered that a type I FAS would be an ideal enzyme for our system as it would require reconstituting a single multi-domain protein. Additionally, some type I FASs, such as yeast and bacterial FASs, produce fatty acyl-CoA as their final product.[46] As coenzyme A is a good leaving group, we reasoned that the bacterial type I FAS would be an appropriate enzyme for generating fatty acyl-CoAs that could be efficiently coupled with appropriate thioester-reactive lysophospholipids to form noncanonical phospholipids *in situ*. We chose to work with type I FAS B from Corynebacterium glutamicum (cgFAS I) as it has been shown to primarily produce palmitoyl-CoA[76] (Figure 2.1.A) and has been efficiently expressed in *E. coli*.[77]

N-terminal $His_6$-tagged type I cgFAS was expressed in *E. coli* and purified by adapting a previously published procedure.[71] The integrity of the protein, as well as its oligomeric state, were verified using size exclusion chromatography (SEC) on a fast protein liquid chromatography (FPLC) column (Figure 2.1.B). The fractions were then subjected to a nicotinamide adenine dinucleotide phosphate (NADPH) consumption assay to verify cgFAS activity (Figure 2.1.C).[71] First, we treated cgFAS I (100 nM) with acetyl-CoA (100 μM), malonyl-CoA (700 μM), and NADPH (1 mM) in 1 mM phosphate ($Na_2HPO_4$/ $NaH_2PO_4$) buffer, pH 7.4 containing 1 mM tris(2-carboxyethyl)phosphine hydrochloride (TCEP) at 37 °C. Subsequently, we monitored NADPH oxidation to NADP+ over time by the decrease in fluorescence at

470 nm. The amount of NADPH consumed was verified by making a calibration curve using commercially available NADPH (Figure 2.6.B). In agreement with previous reports, we observed that palmitoyl-CoA **1** was the major product of the cgFAS I-catalyzed reaction.[76,77] Using gas chromatography−mass spectrometry (GC-MS)[48,71] after fatty acid methyl ester (FAME) formation (Figure 2.1.D, Figure 2.4), we observed that **1** comprised 93% of the total fatty acid species formed. Moreover, using the NADPH consumption assay together with high performance liquid chromatography−mass spectrometry (HPLC-MS), we observed that 41 µM of **1** was produced by the cgFAS I-mediated reaction, corresponding to a 40.6% yield.

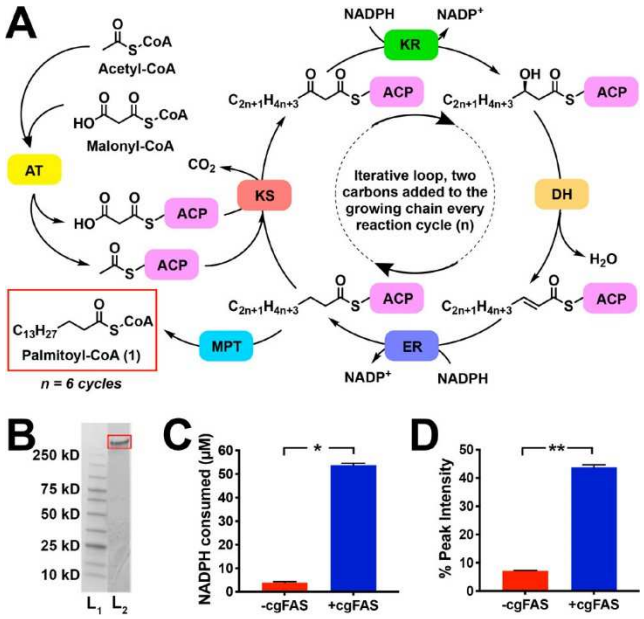


**Figure 1. In situ synthesis of palmitoyl-CoA 1 mediated by bacterial type I FAS (cgFAS).**

**A.** Schematic representation of the iterative fatty acid elongation cycle. Malonyl-palmitoyltransferase (MPT) transfers the final palmitoyl moiety to a CoA molecule to form 1 [AT: acyl transferase; ACP: acyl carrier protein; KS: ketosynthase; KR: ketoreductase; DH: dehydratase; ER: enoyl reductase]. **B.** SDS-PAGE analysis of the His-tagged cgFAS after FPLC purification. Lane 1 (L1): ladder; Lane 2 (L2): purified His-tagged cgFAS (325 kDa). **C.** NADPH consumption assay analysis, verifying cgFAS activity. Significance was determined using an unpaired t test. *P < 0.0005. **D.** GC-MS FAME analysis of the cgFAS-catalyzed formation of 1 over 1 h. Significance was determined using an unpaired t test. **P < 0.001. Error bars represent standard deviations (SD) (n = 3).

## 2.3 Characterization of Phospholipid Vesicle Formation

We next proceeded to select an appropriate thioester reactive lysophospholipid for chemical coupling with cgFAS I-synthesized palmitoyl-CoA. We had previously prepared a novel class of cysteine-modified lysophospholipids that can undergo spontaneous acylation by NCL reaction with long-chain thioesters.[3,27,78] We therefore hypothesized that cysteine-modified lysolipids would react by NCL with palmitoyl-CoA **1** generated in situ by cgFAS I. As a test, we synthesized cysteine-modified lysophospholipid **2** and demonstrated NCL coupling with commercially available palmitoyl-CoA, forming phospholipid **3**. Briefly, we treated lysophospholipid **2** (1 mM) with palmitoylCoA (1 mM) in 10 mM phosphate ($Na_2HPO_4/NaH_2PO_4$) buffer, pH 7.4 containing 10 mM TCEP at 37 °C. Phospholipid formation was followed using HPLC-MS combined with evaporative light-scattering detection (ELSD) and corroborated by chemically characterized standards. Using calibration curves, we determined that 820 μM of phospholipid **3** was formed after 3 h, corresponding to a yield of 82%.

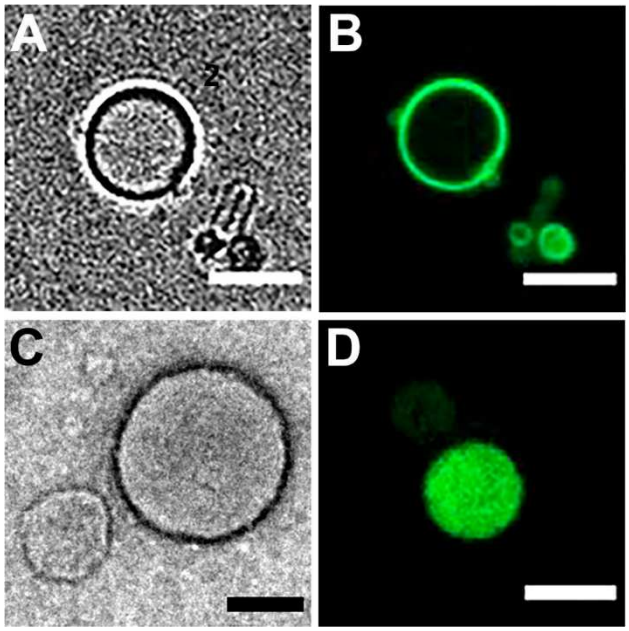


**Figure 2. Characterization of phospholipid 3 vesicular structures.**

**A.** Phase-contrast microscopy image of membrane-bound vesicles resulting from the self-assembly of **3**. Scale bar denotes 5 μm. **B.** Fluorescence microscopy image of vesicles formed by hydration of a thin film of **3**. Membranes were stained with 0.1 mol % BODIPY-FL DHPE. Scale bar denotes 5 μm. **C.** TEM image of negatively stained vesicles of **3**. Scale bar denotes 100 nm. **D.** Fluorescence microscope image demonstrating the encapsulation of HPTS in vesicles of **3**. Scale bar denotes 5 μm.

In previous work, we have observed that amphiphilic species are preferentially acylated by amphiphilic reactants, likely promoted by co-assembly in micelles or membranes.[24,28,78] To better understand the role self-assembly plays in the formation of the phospholipid product, we investigated the reactivity of lysophospholipid **2** with non-amphiphilic small-chain thioesters. Malonyl- and acetyl-CoA were selected as reactive thioester partners with **2**. Although both substrates contain a reactive thioester moiety that can react by NCL with cysteine-modified lysophospholipid **2**, the absence of a long-chain hydrophobic tail precludes assembly into structures such as micelles. Therefore, we anticipated a difference in their reactivity with **2** in comparison to the previously tested palmitoyl-CoA **1**. As expected, when we attempted to react **2** with malonyl- or acetyl-CoA under our standard NCL reaction conditions, we were unable to detect product formation. To determine the ability of noncanonical phospholipid **3** to form membrane-bound vesicles, microscopy studies were performed. Neither palmitoyl-CoA **1** nor lysophospholipid **2** formed membranes in aqueous solution. Phospholipid **3** readily formed membrane-bound assemblies when hydrated. Lipid vesicles were initially identified by phase-contrast and fluorescence microscopy using the membrane-staining dye BODIPY-FL DHPE. Under these conditions, vesicles of 1−10 μm diameter were observed after hydration and tumbling of **3** in phosphate buffer, pH 7.4 at 37 °C for 1 h. Transmission electron microscopy (TEM) also corroborated the formation of vesicular structures. The encapsulation ability of the phospholipid vesicles was demonstrated by hydrating a thin lipid film of **3** in the presence of 8-hydroxypyrene-1,3,6- trisulfonic acid (HPTS), a highly polar fluorescent dye, followed by removal of excess dye by spin-filtration and vesicle characterization using fluorescence microscopy.

Having characterized the individual enzymatic and chemical reactions, we next explored combining enzymatic palmitoylCoA **1** synthesis with chemical phospholipid **3** synthesis in a one-pot reaction. Briefly, we added lysophospholipid **2** (400 μM) to 10 mM phosphate (Na2HPO4/NaH2PO4) buffer, pH 7.4 containing cgFAS I (1 μM), acetyl-CoA (1 mM), malonyl-CoA (1 mM), and NADPH (10 mM) along with TCEP (10 mM) at 37 °C. Phospholipid formation was followed using HPLC-MS-ELSD measurements. Optimization of the reaction conditions enabled rapid coupling between cgFAS I generated **1** and **2**. The one-pot reaction afforded the corresponding phospholipid **3** as the prominent product within

30 min. All of lysophospholipid **2** was consumed in less than 4 h (Figure 4 B) to afford 367 μM of phospholipid **3**. After 30 min of reaction, small vesicular structures were detected by fluorescence microscopy using BODIPY-FL DHPE. After leaving the reaction tumbling overnight at 37 °C, we observed larger vesicles in the range of 1−2 μm in diameter.

### 2.4 *In situ* Chemoenzymatic Phospholipid Membrane Formation

We next investigated the one-pot chemoenzymatic formation of membranes in the presence of biologically relevant cell membrane components, including cholesterol,[79] ionic small molecules such as guanidine hydrochloride (GuHCl),[80–82] and short-chain alkanols such as decanol.[83] Natural cell membranes are heterogeneous bilayers composed of multiple phospholipids, as well as other lipid species such as cholesterol.[84,85] Since the lipid profile of our vesicles is homogeneous, we wanted to explore the effect of incorporating biologically relevant additives into our system. Therefore, we added cholesterol (400 μM), GuHCl (400 μM) and 1-decanol (400 μM) to the one-pot *in situ* chemoenzymatic reaction forming phospholipid **3**. It has been suggested that stoichiometric addition of cholesterol, GuHCl, and decanol leads to the curvature stabilization and fusion of fatty acid vesicles.[82] We expected similar interactions of such additives with our phospholipid vesicles. We observed that the additives did not perturb the formation of phospholipid **3** membranes and led to the formation of larger, more stable vesicles. Vesicles were stable over 48 h at 37 °C, as observed by fluorescence microscopy using BODIPY-FL DHPE.

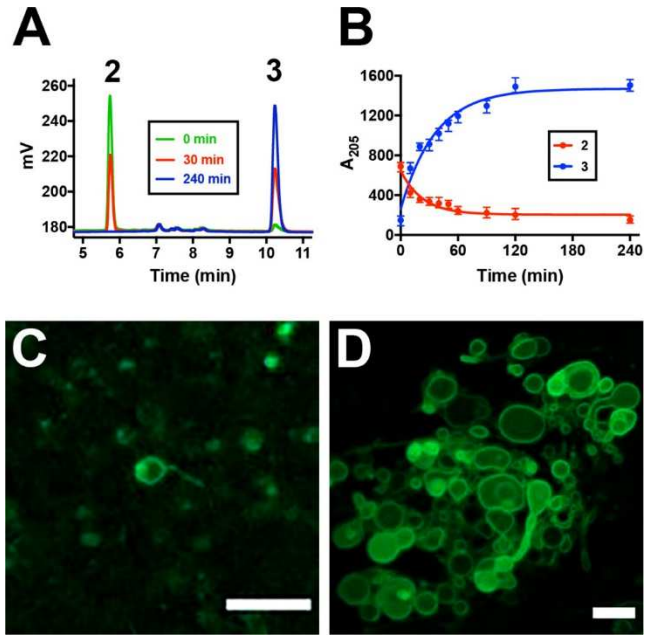


**Figure 3. One-pot chemoenzymatic formation and self-assembly of phospholipid 3.**

**A.** HPLC/ELSD traces corresponding to the NCL-based synthesis of phospholipid **3** from enzymatically generated **1** and lysophospholipid **2. B.** Kinetic plots of lysophospholipid **2** consumption and phospholipid **3** formation during one-pot synthesis. Absorption at 205 nm was monitored and the area under the peak for compounds **2** and **3** were plotted over time. Data was collected in triplicates. **C.** Fluorescence microscopy image of phospholipid **3** vesicles after 4 h of chemoenzymatic reaction. **D.** Fluorescence microscopy image of chemoenzymatically formed vesicles of **3** in the presence of GuHCl, decanol and cholesterol. Membranes were stained with 0.1 mol % BODIPY-FL DHPE. Scale bar denotes 5 μm.

## 2.5 Conclusion

In summary, we have developed a chemoenzymatic route to synthesize noncanonical phospholipids from water-soluble precursors. Given our approach, there should be flexibility to diversify the lipid species generated in the reaction. Even though we utilized cgFAS I to selectively produce palmitoyl-CoA, the use of fatty acid synthases from other organisms could enable the formation of a diverse array of fatty acyl-CoA species, which could be subsequently coupled to reactive lysophospholipids to give several noncanonical lipid species. For instance, many bacterial FASs are known to synthesize terminally branched iso-, anteiso-, or omega-alicyclic fatty acids from branched, short-chain carboxylic acid precursors such as methylmalonyl-CoA.[46,86,87] We plan on utilizing the *in situ* synthesis of diverse phospholipid species to facilitate investigations of how lipid membrane composition affects vesicle assembly, growth, and division.

## 2.6 Experimental Methods

### *2.6.1 General Information*

Commercially available 1-oleoyl-2-hydroxy-sn-glycero-3-phosphocholine (Lyso $C_{18:1}$ PC-OH) was used as obtained from Avanti® Polar Lipids. N-Boc-L-Cys(Trt)-OH, N-Fmoc-L-Cys(Trt)-OH, 2,4,6-trichlorobenzoyl chloride (TCBC), 4-dimethylaminopyridine (DMAP), N,N'-diisopropylcarbodiimide (DIC), O-(7-azabenzotriazol-1-yl)-1,1,3,3-tetramethyl-uronium hexafluorophosphate (HATU), dichloromethane ($CH_2Cl_2$), N,N-dimethylformamide (DMF), N,N-diisopropylethylamine (DIEA), trifluoroacetic acid (TFA), triethylsilane (TES), 4-methylpiperidine, palmitic acid and tris(2-carboxyethyl)phosphine hydrochloride (TCEP) were obtained from Sigma-Aldrich. Texas Red® 1,2-dihexadecanoyl-sn-glycero-3-phosphoethanolamine, triethylammonium salt (Texas Red® DHPE) was obtained from Life Technologies. BODIPY FL DHPE was obtained from ThermoFisher Scientific. Deuterated chloroform ($CDCl_3$) and methanol ($CD_3OD$) were obtained from Cambridge Isotope Laboratories. All reagents obtained from commercial suppliers were used without further purification unless otherwise noted. Solvent mixtures for chromatography are reported as v/v ratios. HPLC analysis was carried out on an Eclipse Plus C8 analytical column with Phase A/Phase B gradients [Phase A: $H_2O$ with 0.1% formic acid; Phase B: MeOH with 0.1% formic acid]. HPLC purification was carried out on Zorbax SB-C18 semipreparative column with Phase A/Phase B gradients [Phase A: $H_2O$ with 0.1% formic acid; Phase B: MeOH with 0.1% formic acid]. GC-MS analysis was carried out on an Agilent 7890A GC system connected to a 5975C VL MSD quadrupole MS (EI). Samples were separated on a 60m DB23 Agilent GCMS column using helium as carrier gas and a gradient of 110 °C to 200 °C at 15 °C/min, followed by 20 min at 200 °C. Proton nuclear magnetic resonance (1 H NMR) spectra were recorded on a Varian VX500 MHz spectrometer, and were referenced relative to residual proton resonances in $CDCl_3$ (at δ 7.24 ppm) or $CD_3OD$ (at δ 4.87 or 3.31 ppm). Chemical shifts were reported in parts per million (ppm, δ) relative to tetramethylsilane (δ 0.00). 1 H NMR splitting patterns are assigned as singlet (s), doublet (d), triplet (t), quartet (q) or pentuplet (p). All first-order splitting patterns were designated on the basis of the appearance

of the multiplet. Splitting patterns that could not be readily interpreted are designated as multiplet (m) or broad (br). Carbon nuclear magnetic resonance ($^{13}$C NMR) spectra were recorded on a Varian VX-500 MHz spectrometer, and were referenced relative to residual proton resonances in $CDCl_3$ (at δ 77.23 ppm) or $CD_3OD$ (at δ 49.15 ppm). Electrospray Ionization-Time of Flight (ESI-TOF) spectra were obtained on an Agilent 6230 Accurate-Mass TOF-MS mass spectrometer. Spinning-disk confocal microscopy images were acquired on a Yokagawa spinning-disk system (Yokagawa, Japan) built around an Axio Observer Z1motorized inverted microscope (Carl Zeiss Microscopy GmbH, Germany) with a 63x, 1.40 NA oil immersion objective to an Evolve 512x512 EMCCD camera (Photometrics, Canada) using ZEN imaging software (Carl Zeiss Microscopy GmbH, Germany). A condenser/objective with a phase stop of Ph2 was used to obtain the phase-contrast images. The fluorophores were excited with a 20 mW DPSS laser (Texas Red®). NanoDrop 2000C spectrophotometer was used for UV/Vis measurements. Fluorescence measurements were carried out on a Tecan infinite F200 plate reader instrument. Transmission electron microscopy (TEM) images were recorded on a FEI TecnaiTM Sphera 200 kV microscope equipped with a LaB6 electron gun, using the standard cryotransfer holders developed by Gatan, Inc.

### *2.6.2 Expression and purification of cgFAS*

pBbE5c (a pET22b[+] derivative) was kindly provided by Dr. Robert Haushalter from Professor Dr. Jay Keasling's lab in University of Berkeley.[77] This plasmid contained the *Corynebacterium* type I FAS gene [codon optimized]. It has been shown that Corynebacteria have two type I FASs, type IA and type I B.[88] Type I A is the essential FAS since it makes the bulk of the fatty acid whereas type I B variant supplements palmitoyl-CoA. For this project, we required *in situ* palmitoyl-CoA formation, so we utilized type I B of *Corynebacterium*. We then added a C□terminal histidine $His_6$□tag onto the plasmid using forward and reverse primers for $His_6$-tag. The ACP domain of type I bacterial FASs requires activation by an external phosphopantetheine transferase (sfp) that adds a phosphopantetheine arm onto a conserved serine residue on the ACP. Dr. Haushalter also provided us with *Escherichia coli* having the phosphopantetheine transferase (Sfp) embedded into its genome and we made competent cells out of the

provided sample in order to express the cgFAS gene with an activated ACP domain. For making competent *E. coli* cells, we used an established protocol provided by New England Biolabs (NEB).[89] The pBbE5c plasmid was then transformed into the competent *E. coli* cells and grown overnight at 37 °C in Luria-Bertani (LB) broth containing 0.1 mg/mL of kanamycin. Afterwards, 1 mL of the overnight culture was used to inoculate 1 L of freshly autoclaved LB medium containing 0.1 mg/mL of kanamycin. The rest of the overnight culture was stored as 25% glycerol stocks at -80 °C. The culture was grown at 37 °C in a shaker-incubator till the $OD_{600}$ reached 0.6. Overexpression of cgFAS was induced by addition of 1 mM isopropyl 1-thio-D-galactopyranoside (IPTG). The cells were then grown for 16 h at 18 °C, after which they were harvested by centrifuging at 6,000 rcf for 20 min at 4 °C. The pellet was resuspended by vortexing in 10 mL of lysis buffer containing 25 mM Tris buffer, pH 8.0, 0.5 M NaCl, 2 mM β-mercaptoethanol, 1 mg/mL lysozyme and a cocktail of protease inhibitors (SigmaFast®). Following cell lysis by an ultrasonicator probe, debris were removed by centrifuging (13,000 rcf, 20 min, 4 °C). The supernatant was incubated in a gravity column with $Ni^{2+}$-nitrilotriacetate (Ni-NTA) agarose resin pre-equilibrated with 10 mM imidazole on a shaker table for 3 h at 4 °C. Next, the flow-through was discarded and the resin was washed with 10 mL each of 20 mM imidazole and 50 mM imidazole solutions. Finally, $His_6$-tagged cgFAS was eluted with 250 mM imidazole and collected in 1 mL fractions. The fractions were analyzed by SDS-PAGE to check for considerable impurities, and subsequently concentrated in a centrifugal filter with a 100,000 nominal molecular weight limit (Amicon Ultra-4, Merck Millipore). The sample was further purified by size-exclusion chromatography (Fig. 2B) (column: Superose 6 10/300GL, GE Healthcare, buffer G: 100 mM $Na_2HPO_4/NaH_2PO_4$ pH 7.4, 100 mM NaCl) and examined for its oligomeric state. Fractions were pooled, concentrated and aliquoted to a final concentration of 1 μM of protein containing 10% glycerol each and stored at -80 °C. Protein $A_{280}$ and concentration measurements carried out using a NanoDrop (ThermoFisher Scientific).

### *2.6.3 cgFAS I activity assay*

To test the activity of cgFAS I, NADPH consumption assay was carried out on a 50 µL scale, including 35 µL of 100 mM $NaH_2PO_4/Na_2HPO_4$ buffer, pH 7.4 (containing 10 mM TCEP), 5 µL of 1 mM acetyl-CoA (in sterile $H_2O$), 5 µL of 10 mM NADPH (in sterile $H_2O$) and 5 µL of cgFAS I (1 µM in elution buffer) at 37 °C. After 1 min of recording the emission at 470 nm using a Spark multimode plate reader (Tecan), the reaction was started by the addition of 5 µL of 7 mM malonyl-CoA and the emission was continuously measured for 1 h. NADPH consumption was closely followed, and a calibration curve was made to observe the amount of NADPH consumed in the reaction. After subtracting non-specific decay of signal, we observed that 602 µM of NADPH was being consumed in the reaction, which correlates to 43 µM fatty acid species being made in the reaction. After conducting NADPH consumption assay experiments in triplicate, we plotted the corresponding results. For our control experiment, we set up the experiment as shown above but without addition of cgFAS I. Statistical analysis was done on the results. P value equals 0.0002, showing the difference in data to be statistically significant. T = 13.68 and standard error of difference = 3.651. Mean value for –cgFAS I = 3.81, for +cgFAS I = 53.76. Error bars were set from standard deviations for both (-cgFAS, SD = 0.30; +cgFAS, SD = 6.31).

### *2.6.4 GC-MS FAME analysis of FAS product*

The product from the cgFAS I activity assay was subjected to GC-MS fatty acid methyl ester (FAME) analysis to investigate the fatty acid product. After 1 h of NADPH consumption assay, the reaction was centrifuged to remove protein debris and the sample was then resuspended in 300 µL of 1 M methanolic acid and incubated at 65 °C for 30 min. The FAMEs were extracted using 300 µL of hexanes and then separated by GC-MS. As expected, the major peak was the methyl palmitate. Using area under the curve, we observed that 93% of the fatty acid species was palmitoyl-CoA (1), with a small peak (4%) of stearoyl-CoA. The peak was corroborated using commercially available palmitoyl-CoA after conversion into FAME. For our control experiment, we set up the experiment as shown above but without addition of cgFAS I before preparing the FAMEs. We plotted the corresponding results of the GC output. Statistical analysis was done on the results. P value equals 0.0005, showing the difference in data to be statistically

significant. T = 10.07 and standard error of difference = 3.635. Mean value for –cgFAS I = 7.19, for +cgFAS I = 43.81. Error bars were set from standard deviations for both (- cgFAS, SD = 0.56; +cgFAS, SD = 6.27).

**A)**

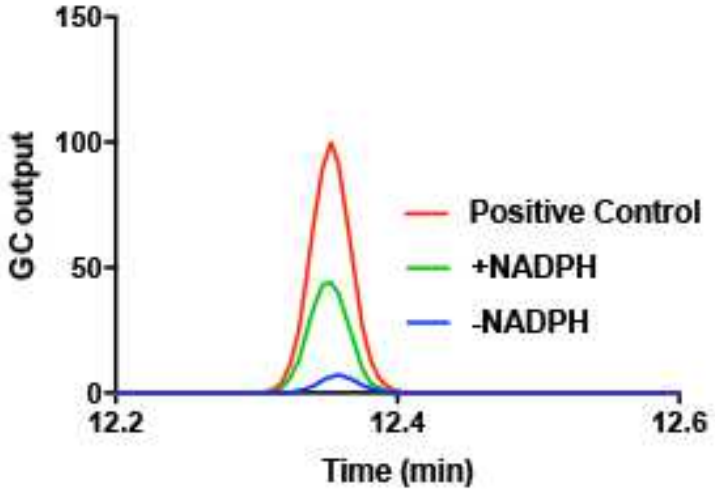


**B)**

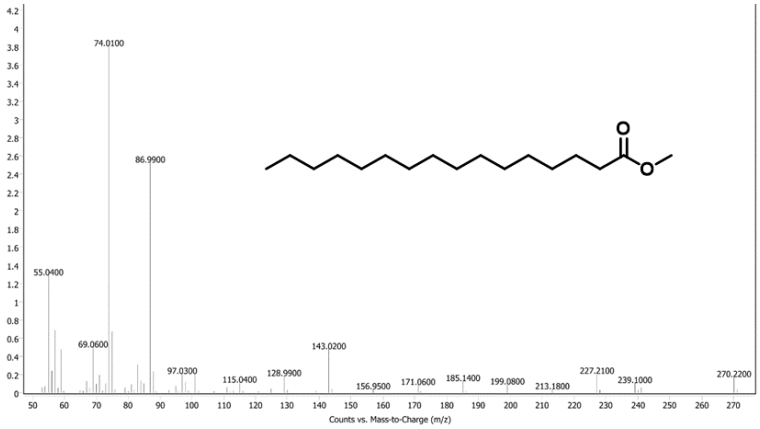


**Figure 4. FAME analysis of cgFAS-mediated palmitoyl-CoA (1) formation.**

**A.** Representative FAME spectral analysis. The product is compared to the methyl ester of commercially available palmitoyl-CoA. **B.** EI-MS of the peak at 12.38 min, as palmitic acid.

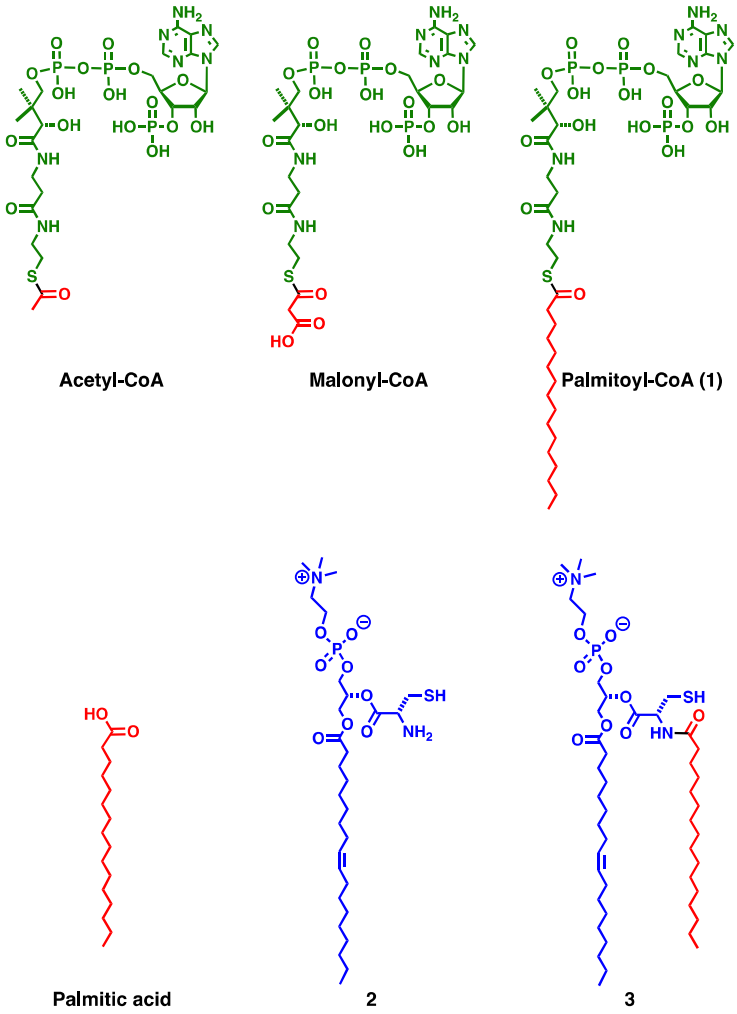


**Figure 5. Chemical structures of all the lipids used in this study.**

*2.6.5 HPLC-MS quantification of palmitoyl-CoA (**1**) product*

Chromatographic separation was performed with a mobile-phase system with gradients based on Phase C (water, 10 mM triethylamine/acidic acid buffer, adjusted to pH 9.0) and Phase D (acetonitrile). A multistep gradient at a flow rate of 0.25 ml/min was used with the starting condition of Phase D at 7%, a linear increase to 60% until 6 min, then to 70% until 9.5 min and finally to 90% until 10 min runtime. cgFAS I-mediated palmitoyl-CoA (**1**) formation was set up as described in the activity assay and monitored over 1 h using HPLC-MS. For each HPLC-MS run, a small aliquot (10 µL) of the reaction was taken and centrifuged to remove protein debris before loading onto the column. For the quantification, the UV trace

at 205 nm was used. The amount of palmitoyl-CoA made was 41 µM, which closely agreed with the amount previously calculated from NADPH consumption (43 µM).

**A)**

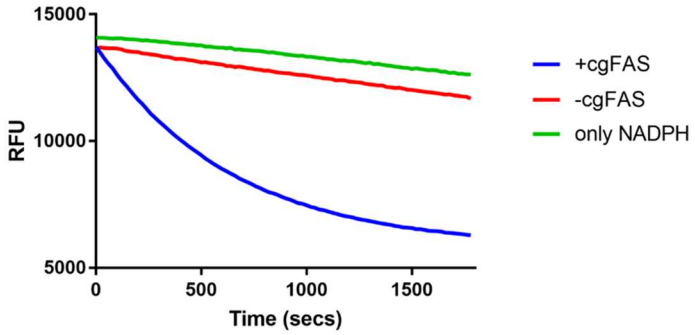


**B)**

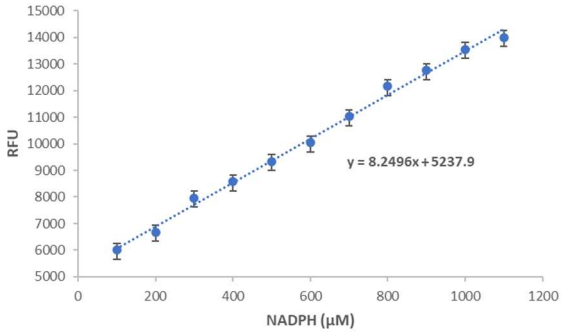


**C)**

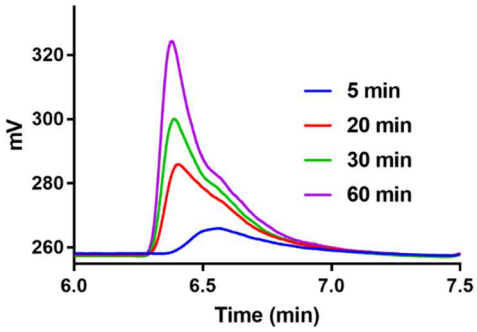


**Figure 6. cgFAS-mediated palmitoyl-CoA (1).**

**A.** Representative NADPH consumption assay. Fluorescence emission of NADPH is measured as the cgFAS-mediated palmitoyl-CoA formation consumes NADPH to convert it to $NADP^+$. **B.** Calibration curve for NADPH. **C.** HPLC-MS traces of palmitoyl-CoA formation over 1 h.

*2.6.6 Synthesis of Lysophospholipids*

Lysophospholipid **2** was synthesized.

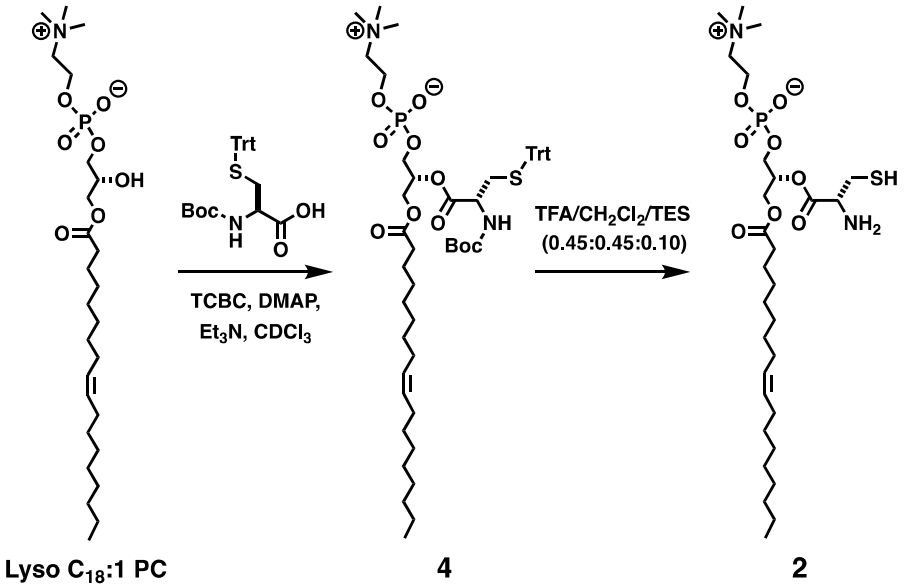


**Figure 7. Synthesis of lysophospholipid 2 (A) and phospholipid 3 (B).**

**1-oleoyl-2-[N-Boc-L-Cys(Trt)]-sn-glycero-3-phosphocholine** (**4**).[74] A solution of 1-oleoyl-2-hydroxy-sn-glycero-3-phosphocholine (Lyso $C_{18:1}$ PC-OH, 25.0 mg, 47.9 µmol), N-Boc-L-Cys(Trt)-OH (55.5 mg, 119.8 µmol), DMAP (35.1 mg, 287.5 µmol) and $Et_3N$ (23.4 µL, 167.7 µmol) in $CDCl_3$ (1.875 mL) was stirred at r.t. for 10 min. Then, TCBC (48.7 µL, 311.5 µmol) was added. After 12 h stirring at r.t., $H_2O$ (125 µL) was added to quench the acid chloride, and the solvent was removed under reduced pressure to give a pale yellow solid. The corresponding residue was dissolved in MeOH (1 mL), filtered using a 0.2 µm syringe-driven filter, and the crude solution was purified by HPLC, affording 39.6 mg of lysophospholipid 4 as a white solid [86%, tR = 7.8 min (Zorbax SB-C18 semipreparative column, 100% Phase B, 15.5 min)]. 1 H NMR ($CDCl_3$, 500.13 MHz, δ): 7.38 (d, J = 7.5 Hz, 6H, 6 × $CH_{Ar}$), 7.33-7.26 (m, 6H, 6 × $CH_{Ar}$), 7.25-7.19 (m, 3H, 3 × $CH_{Ar}$), 5.40-5.29 (m, 2H, 2 × CH), 5.27-5.13 (m, 1H, 1 × CH), 5.07 (d, J = 9.0 Hz, 1H, 1 × NH), 4.41-3.88 (m, 7H, 3 × $CH_2$ + 1 × CH), 3.77-3.57 (m, 2H, 1 × $CH_2$), 3.25 (s,

9H, 3 × $CH_3$), 2.74-2.48 (m, 2H, 1 × $CH_2$), 2.31-2.09 (m, 2H, 1 × $CH_2$), 2.07-1.93 (m, 4H, 2 × $CH_2$), 1.61-1.43 (m, 2H, 1 × $CH_2$), 1.42 (s, 9H, 3 × $CH_3$), 1.31-1.17 (m, 20H, 10 × $CH_2$), 0.88 (t, J = 7.0 Hz, 3H, 1 × $CH_3$). 13C NMR ($CDCl_3$, 125.77 MHz, δ): 173.5, 170.4, 163.9, 155.3, 144.4, 130.1, 129.9, 129.7, 129.6, 128.2, 128.2, 127.1, 80.1, 72.3, 67.2, 66.5, 63.8, 62.7, 59.4, 54.6, 52.7, 34.1, 34.1, 34.0, 32.0, 29.9, 29.9, 29.7, 29.5, 29.5, 29.4, 29.4, 29.3, 29.2, 29.2, 28.5, 28.5, 27.4, 27.3, 24.9, 24.8, 22.8, 14.3. MS (ESI-TOF) [m/z (%)]: 989 ([M +Na]$^+$ , 20), 967 ([MH]$^+$ , 100). HRMS (ESI-TOF) calculated for $C_{53}H_{80}N_2O_{10}PS$ ([MH]$^+$ ) 967.5266, found 967.5269.

*Alternative method*:[90] A solution of N-Boc-L-Cys(Trt)-OH (88.9 mg, 191.7 μmol) in $CH_2Cl_2$ (7.5 mL) was stirred at rt for 10 min, and then DIC (45.0 μL, 287.5 μmol) and DMAP (11.7 mg, 95.8 μmol) were successively added. After 10 min stirring at rt, 1-oleoyl-2-hydroxy-sn-glycero-3-phosphocholine (25.0 mg, 47.9 μmol) was added. After 12 h stirring at rt, the solvent was removed under reduced pressure, and the crude was purified by HPLC, affording 34.6 mg of **3** as a colorless foam [75%].

**1-oleoyl-2-(L-Cys)-sn-glycero-3-phosphocholine** (**2**). A solution of 1-oleoyl-2-[N-Boc-L-Cys(Trt)]- sn-glycero-3-phosphocholine (**3**, 5.0 mg, 5.2 μmol) in 200 μL of TFA/$CH_2Cl_2$/TES (90:90:20) was stirred at rt for 30 min. After removal of the solvent, the residue was dried under high vacuum for 3 h. Then, the corresponding residue was dissolved in MeOH (500 μL), filtered using a 0.2 μm syringe-driven filter, and the crude solution was purified by HPLC, affording 3.1 mg of the lysophospholipid 2 as a colorless foam [82%, tR = 8.6 min (Zorbax SB-C18 semipreparative column, 50% Phase A in Phase B, 5 min, and then 5% Phase A in Phase B, 10 min)]. 1 H NMR ($CD_3OD$, 500.13 MHz, δ): 5.46-5.26 (m, 3H, 3 × CH), 4.49-4.35 (m, 1H, 1 × CH), 4.34-4.19 (m, 3H, 1.5 × $CH_2$), 4.16-3.99 (m, 3H, 1.5× $CH_2$), 3.72-3.59 (m, 2H, 1 × $CH_2$), 3.29-3.26 (m, 1H, 0.5× $CH_2$), 3.23 (s, 9H, 3 × $CH_3$), 3.19-3.00 (m, 1H, 0.5× $CH_2$), 2.35 (t, J = 6.7 Hz, 2H, 1 × $CH_2$), 2.09-1.90 (m, 4H, 2 × $CH_2$), 1.69-1.53 (m, 2H, 1 × $CH_2$), 1.41-1.22 (m, 20H, 10 × $CH_2$), 0.90 (t, J = 6.7 Hz, 3H, 1 × $CH_3$). $^{13}$C NMR ($CD_3OD$, 125.77 MHz, δ): 174.9, 172.3, 131.6, 130.8, 73.7, 67.4, 64.9, 63.4, 63.2, 60.6, 54.6, 34.9, 33.7, 33.1, 30.8, 30.8, 30.7, 30.6, 30.5, 30.4, 30.3, 30.3,

30.2, 28.1, 26.0, 23.8, 14.5. MS (ESI-TOF) [m/z (%)]: 625 ([MH]$^+$ , 100). HRMS (ESI-TOF) calculated for $C_{29}H_{58}N_2O_8PS$ ([MH]$^+$ ) 625.3651, found 625.3647.

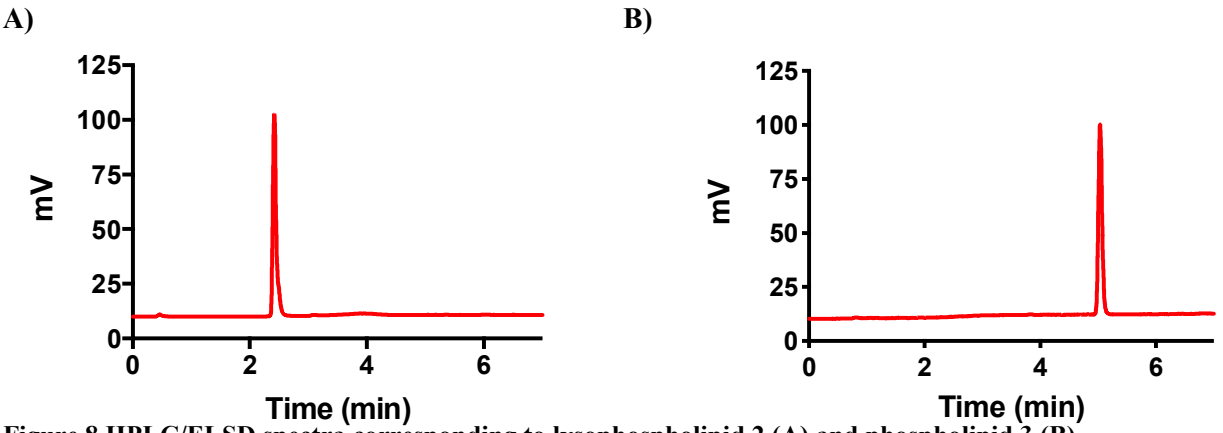


**Figure 8 HPLC/ELSD spectra corresponding to lysophospholipid 2 (A) and phospholipid 3 (B).**

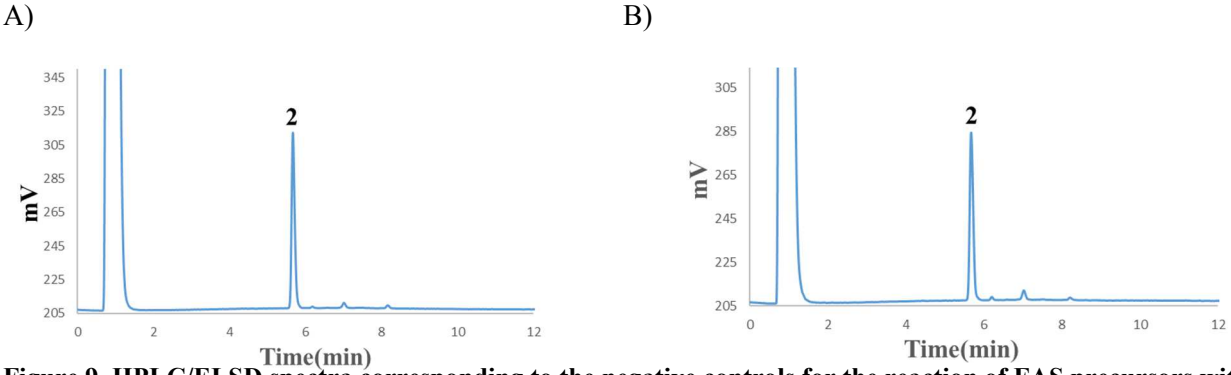


**Figure 9. HPLC/ELSD spectra corresponding to the negative controls for the reaction of FAS precursors with lysophospholipid 2 under NCL reaction conditions.**

**A.** Acetyl-CoA reaction with 2. **B.** Malonyl-CoA reaction with 2. Retention times ($t_R$) were verified by mass spectrometry.

### *2.6.7 Synthesis of Phospholipids*

Phospholipid 3 was synthesized. The pure compound was used to corroborate by HPLC/ELSD/MS the formation of 3 using our NCL-FAS I approach.

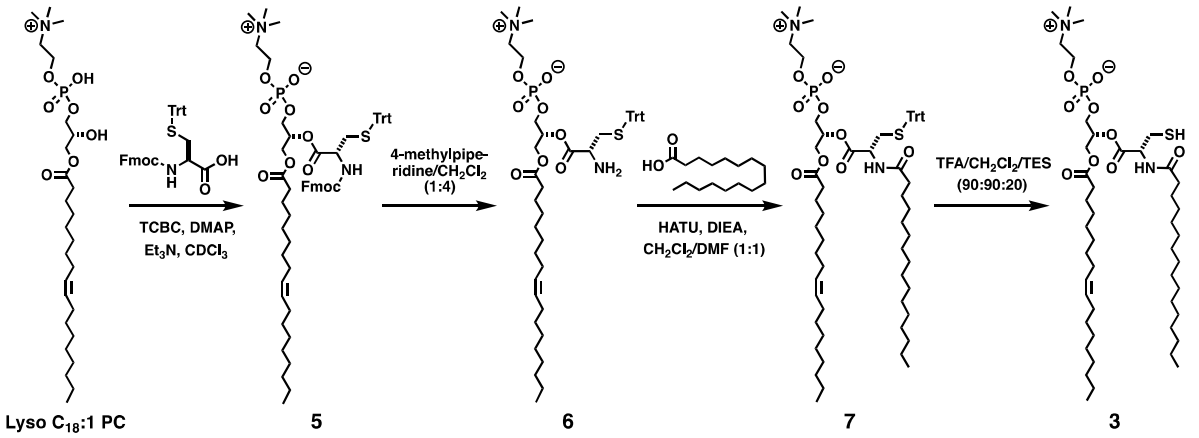


**Figure 10. Synthesis of lysophospholipid 2 (A) and phospholipid 3 (B).**

**1-oleoyl-2-[N-Fmoc-L-Cys(Trt)]-sn-glycero-3-phosphocholine** (**5**). A solution of 1-oleoyl-2-hydroxy-sn-glycero-3-phosphocholine (Lyso $C_{18:1}$ PC-OH, 25.0 mg, 47.9 µmol), N-Fmoc-L-Cys(Trt)-OH (70.2 mg, 119.8 µmol), DMAP (35.1 mg, 287.5 µmol) and $Et_3N$ (23.4 µL, 167.7 µmol) in $CDCl_3$ (1.9 mL) was stirred at r.t. for 10 min. Then, TCBC (48.7 µL, 311.5 µmol) was added. After 12 h stirring at r.t., $H_2O$ (125 µL) was added to quench the acid chloride, and the solvent was removed under reduced pressure to give a pale yellow solid. The corresponding residue was dissolved in MeOH (500 µL), filtered using a 0.2 µm syringe-driven filter, and the crude solution was purified by HPLC, affording 42.7 mg of lysophospholipid 5 as a white solid [82%, tR = 7.8 min (Zorbax SB-C18 semipreparative column, 100% Phase B, 25 min)]. MS (ESI-TOF) [m/z (%)]: 1111 ($[M+Na]^+$ , 100), 1089 ($[MH]^+$ , 72). 1-oleoyl-2-[L-Cys(Trt)]-sn-glycero-3-phosphocholine (6). A solution of 1-oleoyl-2-[N-Fmoc-LCys(Trt)]-sn-glycero-3-phosphocholine (**5**, 7.5 mg, 6.9 µmol) in 125 µL of 4-methylpiperidine/$CH_2Cl_2$ (25:100) was stirred at rt for 30 min. After removal of the solvent, the residue was dried under high vacuum for 3 h. Then, the corresponding residue was dissolved in MeOH (250 µL), filtered using a 0.2 µm syringe-driven filter, and the crude solution was purified by HPLC, affording 5.2 mg of the lysophospholipid 6 as a colorless film

[87%, tR = 8.3 min (Zorbax SB-C18 semipreparative column, 50-0% Phase A in Phase B, 2.5 min, and then 100% Phase B, 15 min)]. MS (ESI-TOF) [m/z (%)]: 889 ([M +Na]$^+$ , 60), 867 ([MH]$^+$ , 100).

**1-oleoyl-2-[L-Cys(Trt)-(palmitoyl)]-sn-glycero-3-phosphocholine** (**7**). A solution of palmitic acid (0.6 mg, 2.3 μmol) in $CH_2Cl_2$/DMF (1:1) (200 μL) was stirred at 0 ºC for 10 min, and then HATU (1.0 mg, 2.5 μmol) and DIEA (1.6 μL, 9.2 μmol) were successively added. After 10 min stirring at 0 ºC, 1-oleoyl-2-[L-Cys(Trt)]-sn-glycero-3-phosphocholine (**6**, 2.0 mg, 2.3 μmol) was added. After 1 h stirring at rt, the mixture was concentrated under reduced pressure. The corresponding residue was dissolved in MeOH (250 μL), filtered using a 0.2 μm syringe-driven filter, and the crude solution was purified by HPLC, affording 2.0 mg of **7** as a colorless film [79%, tR = 25.0 min (Zorbax SB-C18 semipreparative column, 50-0% Phase A in Phase B, 2.5 min, and then 100% Phase B, 20 min)]. MS (ESI-TOF) [m/z (%)]: 1127 ([M +Na]$^+$ , 37), 1105 ([MH]$^+$ , 100).

**1-oleoyl-2-[L-Cys-(palmitoyl)]-sn-glycero-3-phosphocholine** (**3**). A solution of 1-oleoyl-2-[LCys(Trt)-(palmitoyl)]-sn-glycero-3-phosphocholine (**7**, 1.0 mg, 0.9 μmol) in 200 μL of TFA/$CH_2Cl_2$/TES (90:90:20) was stirred at rt for 30 min. After removal of the solvent, the residue was dried under high vacuum for 3 h. Then, the corresponding residue was dissolved in MeOH (250 μL), filtered using a 0.2 μm syringe-driven filter, and the crude solution was purified by HPLC, affording 0.7 mg of the amidophospholipid 3 as a colorless film [83%, tR = 16.4 min (Zorbax SB-C18 semipreparative column, 50- 0% Phase A in Phase B, 2.5 min, and then 100% Phase B, 15 min)]. 1 H NMR ($CD_3OD$, 500.13 MHz, δ): 8.54 (s, 1H, 1 × NH), 5.41-5.33 (m, 2H, 2 × CH), 5.32-5.22 (m, 1H, 1 × CH), 4.67-4.62 (m, 1H, 1 × CH), 4.46-4.36 (m, 1H, 0.5 × $CH_2$), 4.33-4.19 (m, 3H, 1.5 × $CH_2$), 4.12-3.96 (m, 2H, 1 × $CH_2$), 3.74-3.58 (m, 2H, 1 × $CH_2$), 3.23 (s, 9H, 3 × $CH_3$), 3.04-2.85 (m, 2H, 1 × $CH_2$), 2.34 (t, J = 7.5 Hz, 2H, 1 × $CH_2$), 2.30-2.23 (m, 2H, 1 × $CH_2$), 2.10-1.95 (m, 4H, 2 × $CH_2$), 1.71-1.53 (m, 4H, 2 × $CH_2$), 1.39-1.26 (m, 44H, 22 × $CH_2$), 0.90 (t, J = 6.8 Hz, 6H, 2 × $CH_3$). $^{13}$C NMR ($CD_3OD$, 125.77 MHz, δ): 176.4, 174.9, 171.0, 130.9, 130.8, 73.3, 67.4, 64.9, 63.5, 60.6, 56.2, 54.7, 36.7, 34.9, 33.1, 30.9, 30.9, 30.9, 30.8, 30.8, 30.8, 30.7, 30.7, 30.7, 30.6, 30.5, 30.5, 30.5, 30.4, 30.4, 30.4, 30.3, 30.3, 30.2, 28.2, 27.0, 26.7, 26.0, 23.8, 14.5.

MS (ESI-TOF) [m/z (%)]: 863 ([MH]$^+$ , 100). HRMS (ESI-TOF) calculated for $C_{45}H_{88}N_2O_9PS$ ([MH]$^+$ ) 863.5948, found 863.5947.

*2.6.8 Rehydration of phospholipid **3***

5 μL of a 10 mM solution of purified phospholipid 3 in CHCl**3** was added to a 1 mL vial, placed under N**2** and dried for 15 min to prepare a lipid film. Then, 95 μL of $H_2O$ was added and the solution was tumbled at 25 ºC for 1 h. Afterwards, to 10 μL of this 500 μM aqueous solution of phospholipid **3** was added 0.1 μL of a 100 μM BODIPY-FL DHPE solution in EtOH, and the mixture was briefly agitated. The corresponding mixture was finally monitored by phase-contrast and fluorescence microscopy in order to determine the vesicle structure. We observed that the phospholipid product **3** spontaneously self-assemble into vesicles. Initially, the vesicles were observed to be in close proximity to each other (91±13 vesicles counted) and with varying diameter (ranging from 1 to 7 μm), but upon overnight tumbling at 25 ºC, they dispersed homogenously in solution. Encapsulation of HPTS 10 μL of a 10 mM solution of pure phospholipid **3** in MeOH/$CHCl_3$ (1:1) was added to a glass vial, placed under a steady flow of $N_2$, and dried for 10 min to prepare a lipid film. Then, 100 μL of 0.1 mM HPTS aqueous solution was added to the lipid film and briefly vortexed. The solution was tumbled at room temperature for 30 min. Afterward, the resulting cloudy solution was diluted with an additional 200 μL of $H_2O$ and transferred to a 100 kDa molecular weight cut-off (MWCO) centrifugal membrane filter and centrifuged for 3 min at 10,000 rcf (Eppendorf 5415C). The solution was similarly washed for additional 5× to remove any non-encapsulated dye. Then, 1 μL of the vesicle solution were placed on a clean glass slide, secured by a greased cover slip, and imaged on a spinning disc confocal microscope (488 nm laser) to observe encapsulation of HPTS. Consistent with the previously described membrane-staining rehydration experiments, the phospholipid **3** in the presence of HPTS spontaneously self-assembled into vesicular structures with 0.5-8 μm diameter (163±24 vesicles counted). These HPTS-encapsulating vesicles were observed to be in close proximity to each other, but upon overnight tumbling at 25 ºC, they dispersed homogenously in solution.

### *2.6.9 Transmission Electron Microscopy (TEM) Studies*

General. A deposition System Balzers Med010 was used to evaporate a homogeneous layer of carbon. The samples were collected over 400 mesh Cu grids. The grids were then negatively stained with a solution of 1% (w/w) uranyl acetate. Micrographs were recorded on a FEI TecnaiTM Sphera microscope operating at 200 kV and equipped with a LaB6 electron gun, using the standard cryotransfer holders developed by Gatan, Inc. For image processing, micrographs were digitized in a Zess SCAI scanner with different sampling windows.

TEM measurements. Copper grids (formvar/carbon-coated, 400 mesh copper) were prepared by glow discharging the surface at 20 mA for 1.5 min. Once the surface for vesicle adhesion is ready, 3.5 µL of a 5 mM solution of phospholipid **3** in $H_2O$ (previously hydrated at 37 ºC for 1 h) was deposited on the grid surface. This solution was allowed to sit for 10 seconds before being washed away with 10 drops of glass distilled $H_2O$ and subsequent staining with 3 drops of 1% w/w uranyl acetate. The stain was allowed to sit for 10 seconds before wicking away with filter paper. All grid treatments and simple depositions were on the dark/shiny/glossy formvar-coated face of the grid (this side face up during glow discharge). Samples were then imaged via TEM, revealing the presence of several populations of spherical compartments (50-950 nm in diameter), consistent with the vesicle architecture.

### *2.6.10 Phospholipid **3** formation from lysophospholipid 1 and commercially available palmitoyl-CoA*

In a typical *de novo* phospholipid synthesis reaction, to a 5 µL of standard palmitoyl-CoA (10 mM stock in sterile $H_2O$), 5 µL of lysophospholipid **2** solution (10 mM stock in sterile $H_2O$) was successively added along with 40 µL of 100 mM $NaH_2PO_4/Na_2HPO_4$ buffer, pH 7.4 containing 10 mM TCEP, and the solution was mixed by gentle tapping. The reaction mixture was tumbled at 37 °C. HPLC-MS analysis was done after 4 h to analyze the formation of the corresponding product. Using UV traces at 205 nm, we observed that 820 µM phospholipid **3** was being made in the reaction. The product peak was comparable to the chemically synthesized phospholipid **3**.

### *2.6.11 Chemoenzymatic one-pot phospholipid formation mediated by cgFAS I*

*In situ vesicle formation (without additives).* For this reaction, lysophospholipid **2** was added to a scaled-up version of the cgFAS I-mediated palmitoyl-CoA (**1**) formation. In a typical *de novo* chemoenzymatic phospholipid synthesis reaction, to a 2 μL of lysophospholipid **2** solution (10 mM stock in sterile $H_2O$) was successively added 33 μL of 100 mM $NaH_2PO_4/Na_2HPO_4$ buffer, pH 7.4 containing 10 mM TCEP, along with 5 μL of 10 mM acetyl-CoA (in sterile H2O), 5 μL of 100 mM NADPH (in sterile $H_2O$), and 5 μL of cgFAS (1 μM in elution buffer). Then, 5 μL of 70 mM malonyl-CoA (in sterile $H_2O$) was added, and the solution was mixed by gentle tapping. The reaction mixture was tumbled at 37 °C. Small aliquots (~2 μL) were taken out at various time points and placed on a glass slide for microscopic observations. Initially the vesicles were hard to visualize because of their small size, having sub-micrometer diameters. However, after tumbling overnight at 37 °C, some bigger vesicles were more evident, at 0.5-2 μm in diameter (133±12 vesicles counted). *In situ* vesicle formation (with additives). For the *de novo* phospholipid reaction with additives, the reaction was set up exactly as above, with the addition of 2.5 μL of guanidine hydrochloride (GuHCl) (10 mM in sterile $H_2O$), 2.5 μL of decanol (10 mM in sterile $H_2O$) and 2.5 μL of cholesterol (10 mM in EtOH) to the one-pot reaction. Cholesterol was added initially to the vial and $N_2$ gas was passed until all of the EtOH evaporated. Then, 2.5 μL of lysolipid **2** solution (10 mM in sterile $H_2O$) was added along with 25 μL of 100 mM $NaH_2PO_4/Na_2HPO_4$ buffer, pH 7.4 containing 10 mM TCEP, along with 5 μL of 10 mM acetyl-CoA (in sterile $H_2O$), 5 μL of 100 mM NADPH (in sterile $H_2O$), and 5 μL of cgFAS (1 μM in elution buffer). Then, 5 μL of 70 mM malonyl-CoA (in sterile $H_2O$) were added, and the solution was mixed by gentle tapping. The reaction mixture was tumbled at 37 °C. Small aliquots (~2 μL) were taken out at various time points and placed on a glass slide for microscopic observations. After 30 min, vesicles with 2.5-3 μm in diameter were evident in the reaction (Fig. 4D). HPLC quantification of chemoenzymatic phospholipid **3** formation Chromatographic separation was performed with a Phase A/Phase B gradients. A multistep gradient at a flow rate of 0.25 ml/min was used with the starting condition of Phase B at 5%, a linear increase to 50% until 7 min, then to 70% until 10 min and

finally to 95% until 14 min runtime. For each HPLC-MS run, a small aliquot (10 μL) of the reaction was taken and then centrifuged to remove protein debris before loading onto the column. For the quantification, the UV traces at 205 nm were used, determining that the amount of phospholipid **3** made was 367 μM. The product peak was comparable to the chemically synthesized phospholipid **3**.

A) B)

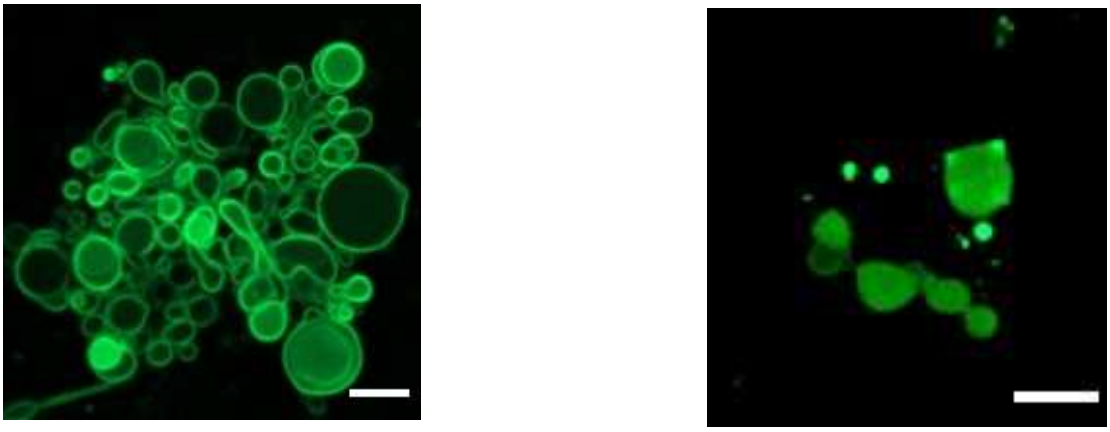

**Figure 11. Spinning-disk confocal fluorescence microscope images demonstrating the spontaneous self-assembly of phospholipid 3 into membranous vesicles.**

**A.** Fluorescence microscopy image of **3**. Membranes were stained with 0.1 mol % BODIPY FL DHPE. **B.** Encapsulation of HPTS in membrane vesicles of **3**. Scale bars denote 5 μm.

## 2.7 NMR Spectra

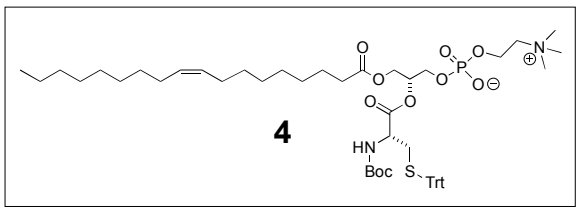


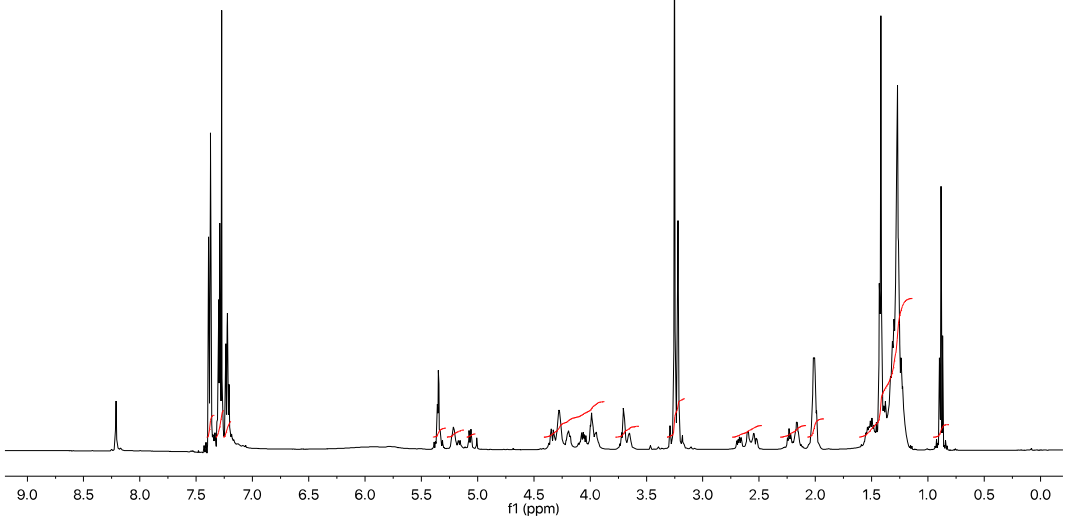


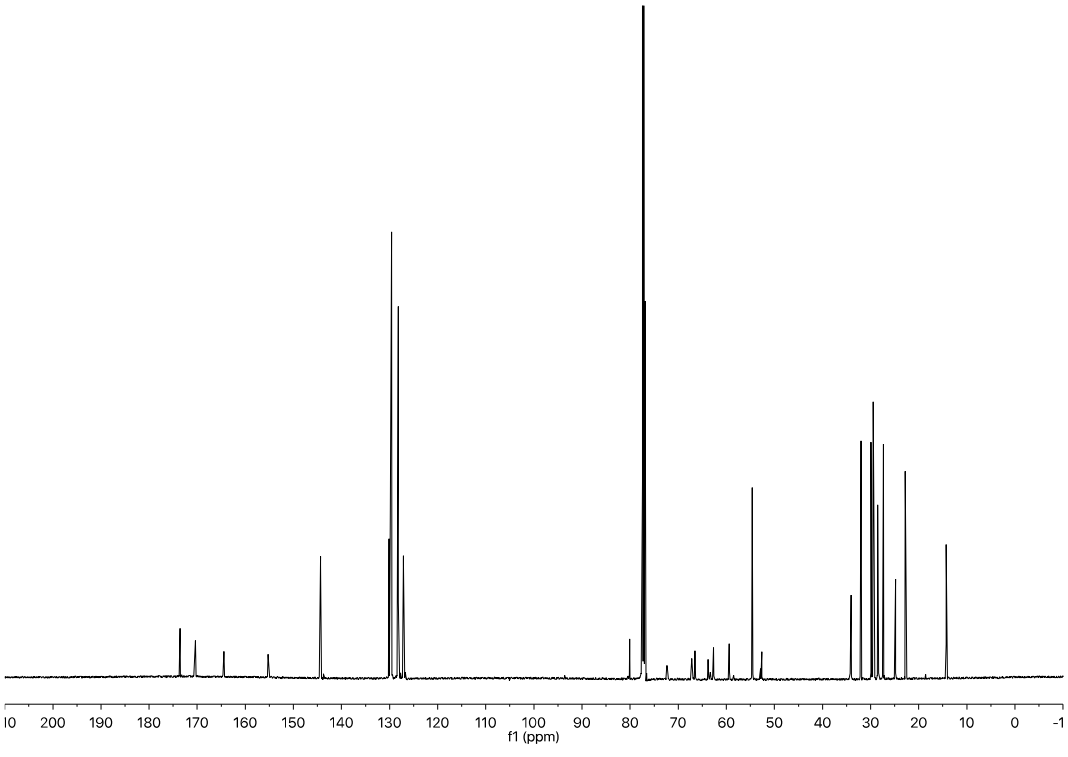

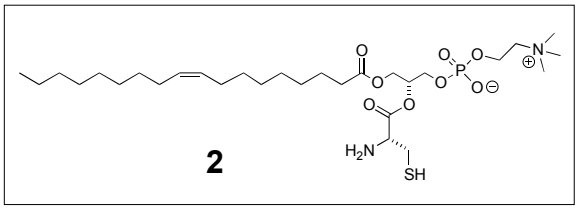
2

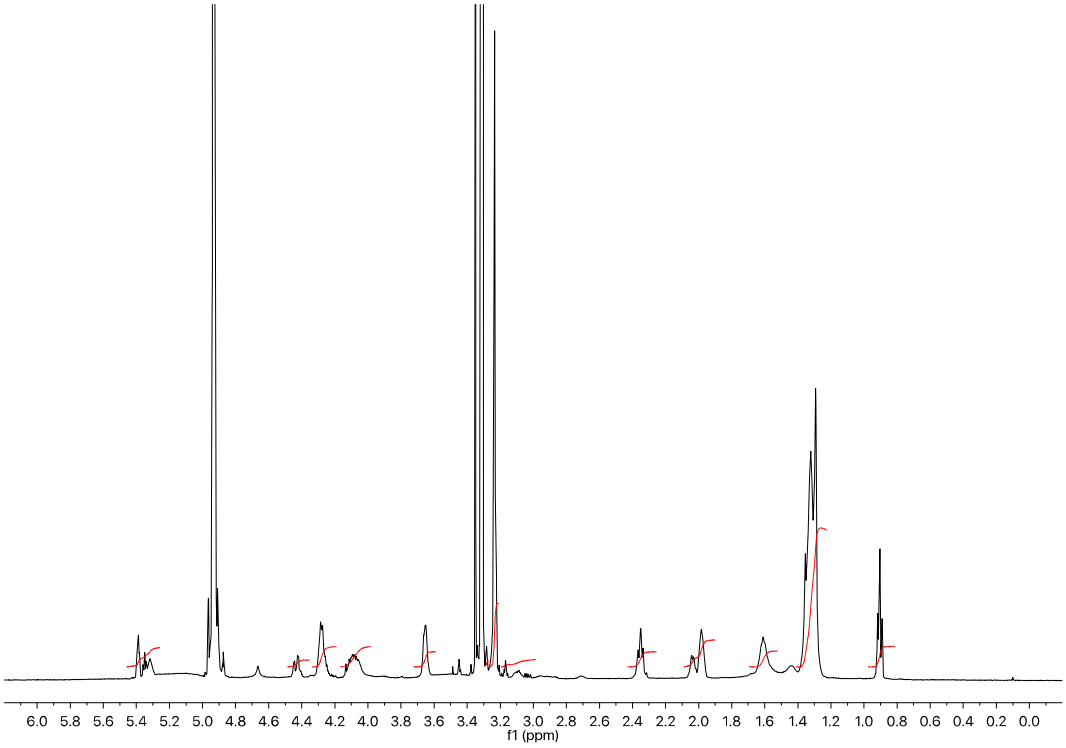
6.0 5.8 5.6 5.4 5.2 5.0 4.8 4.6 4.4 4.2 4.0 3.8 3.6 3.4 3.2 3.0 2.8 2.6 2.4 2.2 2.0 1.8 1.6 1.4 1.2 1.0 0.8 0.6 0.4 0.2 0.0
f1 (ppm)

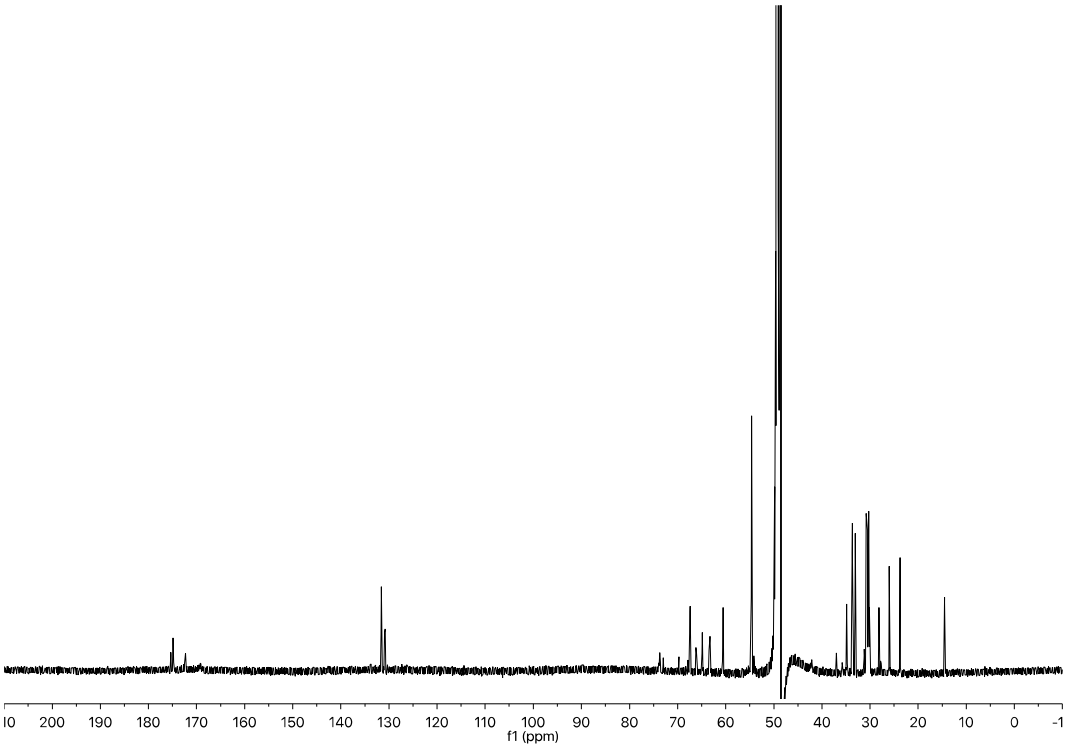
10 200 190 180 170 160 150 140 130 120 110 100 90 80 70 60 50 40 30 20 10 0 -1
f1 (ppm)

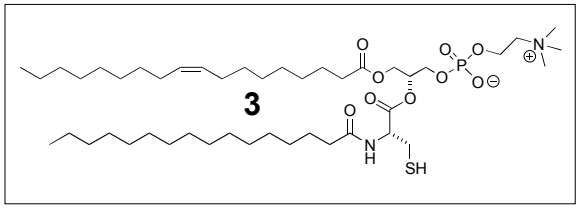
3
O
O
O
O
O
O
O
O
O
N
H
SH
N


9.0
8.5
8.0
7.5
7.0
6.5
6.0
5.5
5.0
4.5
4.0
3.5
3.0
2.5
2.0
1.5
1.0
0.5
0.0
f1 (ppm)

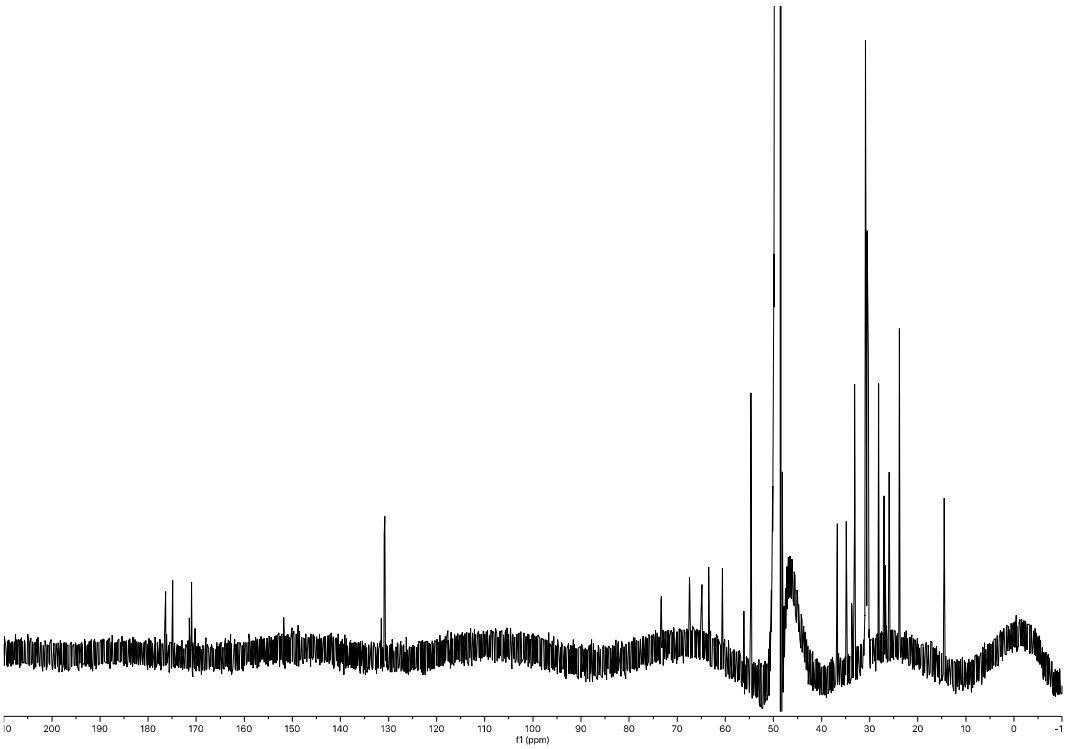
200
190
180
170
160
150
140
130
120
110
100
90
80
70
60
50
40
30
20
10
0
f1 (ppm)

## 2.8 Acknowledgements

Chapter Two, in full, is a reprint (with co-author permission) of the material as it appears in the publication: Khanal, S., Brea, R. J., Burkart, M., D., Devaraj, N., K. Chemoenzymatic Generation of Phospholipid Membranes Mediated by Type I Fatty Acid Synthase, *J. Am. Chem. Soc.* **2021**, 143, 23, 8533–8537. I would like to thank Roberto Brea for his contributions, especially the synthesis of the head groups and helping me with writing the manuscript. I would like to thank Neal Devaraj for his guidance and assistance in preparing the manuscript. I would like to thank Mike Burkart for his help and mentorship in the project as well.

# 3. Utilization of Acetate as Feedstock for Membrane Generation

## 3.1 Introduction

As we discussed earlier, the biosynthesis of phospholipid membranes involves a sophisticated mechanism involving transmembrane proteins embedded in the endoplasmic reticulum (ER).[15,16] This is very challenging to recreate in an artificial cell setting, because of the difficulty in reconstituting membrane proteins in a functional form. In fact, if we want to shed some light on the primitive generation of the first examples of lipids in nature, we want to start with the simplest forms of carbon-containing small molecules as possible. Previous works have developed nonenzymatic chemical approaches to generate phospholipids from reactive single chain precursors such as fatty thioesters.[91] Various chemical reactions have been shown to form both natural and noncanonical phospholipid membranes.[3,24,27,28] Our work on the *de novo* chemical synthesis of lipid-based vesicles demonstrated a significant progress in the development of biomimetic membranes.[1] However, previously made systems need a continuous addition of long-chain amphiphilic species, which are complex molecules in their own right. Additionally, the use of amphiphilic reactants can hinder a *de novo* membrane generation system as long-chain amphiphiles such as lysophospholipids or fatty acids act as detergents in solution.[92] Therefore, addition of large concentrations of these precursors may disrupt any membranes formed via detergent solubilization.[6,93] A novel and innovative approach would be to generate lipid membranes from simple, highly abundant and biologically relevant carbon feedstock such as acetate[65] and ubiquitous amino acids such as cysteine.[66] Using acetate as a carbon feedstock denotes a major departure from previous approaches. Moreover, from the point of view of bottom-up synthesis of *de novo* membranes, using acetate as feedstock and the sole source of carbon would be a stupendous achievement that is unexplored until now. Additionally, these simple precursors are membrane permeable and utilizing them as a feedstock for lipid synthesis would avoid the detergent effect associated with single-chain amphiphilic precursors. However, efficiently generating long acyl chains from two-carbon precursors without the use of enzymes is extraordinarily challenging.

In the last chapter, we showed a partial chemoenzymatic approach for generating synthetic phospholipid membranes from simple metabolic precursors. Instead of supplying the system with preformed fatty acid tails, we utilized a type I fatty acyl-coenzyme A (CoA) synthase from *Corynebacterium glutamicum* (cgFAS) to generate acyl-CoAs *in situ* from water-soluble precursor molecules, acetyl-CoA and malonyl-CoA. Subsequently, the activated fatty acids chemically reacted with lysolipid precursors to form phospholipid membranes. By enzymatically generating acyl precursors and replacing the steps normally catalyzed by membrane-bound acyltransferases with chemical steps, we generated close analogs of biological phospholipids. However, this reaction scheme, while representing an important advance, still requires the use of lysolipid detergents. To realize our vision of an artificial membrane that can subsist on simple chemical feedstock, the idea is to generate phospholipid membranes *entirely* from non-amphiphilic, water-soluble precursors.

To form the fatty acid tails, we utilize acetate as carbon feedstock for lipid generation because of its simplicity, membrane permeability,[67] abundance, and its industrial relevance.[68] Acetate can be enzymatically converted to acetyl-CoA, one of the central metabolic intermediates in living organisms participating in key processes such as the Kreb's cycle[94] and serving as precursors for lipid synthesis[95], protein acetylation[96], metabolic acetylation, among others. Furthermore, various groups have shown that living organisms, especially heterotrophic bacteria, utilize acetate as carbon and energy source.[65,69,70] For our purposes, we used acetyl-CoA synthetase (ACS) from *E. coli* to generate acetyl-CoA from acetate. We then used human acetyl-CoA carboxylase (ACC) to produce malonyl-CoA from acetyl-CoA. Additionally, we utilized cgFAS I to generate palmitoyl-CoA from acetyl-CoA and malonyl-CoA. Our preliminary results show that we can indeed generate palmitoyl-CoA from acetate and coenzyme A as the starting precursors in the presence of ACS, ACC and FAS.

Additionally, we were also able to couple commercially available palmitoyl-CoA with cysteine to give a diacylated cysteine lipid analog. When we observed the product under the microscope in the presence of

cholesterol, we were able to observe micron-sized membrane-bound vesicles. The final idea is to then combine the enzymatic reactions with the diacylation of cysteine and monitor for the lipid analog.

### 3.2 Functional Validation of the Enzymatic Steps of the Chemoenzymatic Reaction

We first identified an appropriate way to make acetyl-CoA *in situ*. We utilized *E. coli* ACS as it has been shown to generate acetyl-CoA in a high titer.[97] Cells generate acetyl-CoA from glucose, fatty acid, and amino acids.[98] During glycolysis, glucose is catabolized into two three-carbon molecules of pyruvate. The mitochondrial pyruvate dehydrogenase complex then catalyzes the oxidative decarboxylation of pyruvate to produce acetyl-CoA, a two-carbon acetyl unit that is ligated to the acyl-group carrier, CoA.[99] In *E. coli* specifically, acetyl-CoA generation is dependent on one acetate activation pathway, while under accelerated growth conditions, utilization requires an alternate pathway. This pathway, uses acetate as the starting precursor along with coenzyme A and is catalyzed by the enzyme acetyl-CoA synthetase (Acs; acetate:CoA ligase [AMP forming]), proceeding through an enzyme-bound acetyladenylate (acetyl-AMP) intermediate.[100] Cells use this high-affinity pathway to scavenge for small concentrations of acetate.[97,101]

N-terminal $His_6$-tagged ACS was expressed in *E. coli* and purified by adapting a previously published procedure.[102] The pETM11 vector containing the ACS gene was purchased from Addgene that was deposited by the Schultz lab.[102] To test the activity of ACS, we utilized two different assays. First, we set up an indirect method by following adenosine triphosphate (ATP) consumption. Acetyl-CoA is generated from acetate and coenzyme A and this reaction uses ATP as fuel. Adenosine monophosphate (AMP) is formed in the reaction as acetyl-CoA is being made. For quantifying this reaction, we used an AMP-Glo (detection) kit purchased from Promega. ATP consumption assay was carried out on a 50 µL scale, including 35 µL of 100 mM $NaH_2PO_4/Na_2HPO_4$ buffer, pH 7.4 (containing 10 mM tris(2-carboxyethyl)phosphine (TCEP)), 5 µL of 1 mM acetate (in sterile $H_2O$), 5 µL of 1 mM coenzyme A (in sterile $H_2O$), 5 µL of 10 mM ATP (in sterile $H_2O$) and 5 µL of ACS (1 µM in elution buffer) at 37 °C. After completing the enzymatic reaction, adding AMP-Glo Reagent I terminates the reaction, removes any remaining ATP, and converts AMP to ADP. Adding AMP Detection Solution drives the conversion of ADP

to ATP and the detection of ATP through the luciferase reaction. The amount of AMP produced by the reaction is proportional to the light measured and can be extrapolated using a standard curve. From this reaction, we demonstrated that 64% of ATP was being consumed. To have a more direct assay, we utilized an acetyl-CoA detection kit from Sigma Aldrich. The reaction conditions were identical to the one mentioned above. Acetyl-CoA concentration is then determined by a coupled enzyme assay, which results in a fluorometric output proportional to the acetyl-CoA present. After calibrating it with standard acetyl-CoA, we ascertained that the yield for the reaction was 69%.

We then moved on to generate malonyl-CoA from acetyl-CoA and bicarbonate *in situ*. For this, we purchased purified human acetyl-CoA carboxylase (ACC 1) from Sigma Aldrich. ATP consumption was done exactly as for *E. coli* ACS, since the carboxylation also requires ATP as fuel. ATP consumption assay was carried out on a 50 µL scale, including 35 µL of 100 mM $NaH_2PO_4/Na_2HPO_4$ buffer, pH 7.4 (containing 10 mM TCEP), 5 µL of 1 mM acetyl-CoA (in sterile $H_2O$), 5 µL of 1 mM sodium bicarbonate (in sterile $H_2O$), 5 µL of 10 mM ATP (in sterile $H_2O$) and 5 µL of ACC (1 µM in elution buffer) at 37 °C. After the luminescence output reading, 71% of ATP was consumed. We also utilized a human malonyl-CoA detection ELISA assay from MyBioSource for direct detection of malonyl-CoA. This assay uses the quantitative sandwich enzyme immunoassay technique. Antibody specific for malonyl CoA has been pre-coated onto a microplate. Standards and samples are pipetted into the wells and any malonyl CoA present is bound by the immobilized antibody. After removing any unbound substances, a biotin-conjugated antibody specific for malonyl CoA is added to the wells. After washing, avidin conjugated Horseradish Peroxidase (HRP) is added to the wells. Following a wash to remove any unbound avidin-enzyme reagent, a substrate solution is added to the wells and color develops in proportion to the amount of malonyl CoA bound in the initial step. The color development is stopped and the intensity of the color is measured. We were able to see 73% yield of malonyl-CoA after reaction using standard acetyl-CoA.

We then proceeded to do a one-pot reaction starting from acetate and utilizing both ACS and ACC and followed by both ATP consumption as well as malonyl-CoA detection. The reaction scale was 50 µL scale,

including 35 μL of 100 mM $NaH_2PO_4/Na_2HPO_4$ buffer, pH 7.4 (containing 10 mM TCEP), excess amount of acetate (in sterile $H_2O$), excess amount of ATP (in sterile $H_2O$), 5 μL of 1 mM coenzyme A, 5 μL of ACS, 5 μL of 1 mM bicarbonate and 5 μL of ACC (1 μM in elution buffer) at 37 °C. We were able to demonstrate an overall yield of 41% for malonyl-CoA production.

Finally, we set up FAS reaction similar to our previously shown protocol.[1] We again utilized type I FAS B from *Corynebacterium glutamicum* (cgFAS I) as it has been shown to primarily produce palmitoyl-CoA[76] (Figure 2.1.A) and has been efficiently expressed in *E. coli*.[77] N-terminal $His_6$-tagged type I cgFAS was expressed in *E. coli* and purified by adapting a previously published procedure.[71] The integrity of the protein, as well as its oligomeric state, were verified using size exclusion chromatography (SEC) on a fast protein liquid chromatography (FPLC) column. The fractions were then subjected to a nicotinamide adenine dinucleotide phosphate (NADPH) consumption assay to verify cgFAS activity.[71] First, we treated cgFAS I (100 nM) with acetyl-CoA (100 μM), malonyl-CoA (700 μM), and NADPH (1 mM) in 1 mM phosphate ($Na_2HPO_4$/ $NaH_2PO_4$) buffer, pH 7.4 containing 1 mM TCEP at 37 °C. Subsequently, we monitored NADPH oxidation to NADP+ over time by the decrease in fluorescence at 470 nm. The amount of NADPH consumed was verified by making a calibration curve using commercially available NADPH. In agreement with previous reports, we observed that palmitoyl-CoA **1** was the major product of the cgFAS I-catalyzed reaction.[76,77] Using GC-MS[48,71] after fatty acid methyl ester (FAME) formation, we observed that **1** comprised 91.8% of the total fatty acid species formed. Moreover, using the NADPH consumption assay together with HPLC-MS, we observed that 38.3 μM of **1** was produced by the cgFAS I-mediated reaction, corresponding to a 39.6% yield.

### 3.3 Diacylation of Cysteine from Palmitoyl-CoA

We next proceeded to select an appropriate thioester reactive small molecule precursor for chemical coupling with cgFAS I-synthesized palmitoyl-CoA. We had previously prepared a novel class of cysteine-modified lysophospholipids that can undergo spontaneous acylation by NCL reaction with long-chain thioesters.[3,27,78] We also demonstrated palmitoyl-CoA coupling with a cysteine-modified lysolipid with a

choline head group in the previous chapter. Similar to the previous reactive lysolipid, we decided to choose cysteine as our reactive head group. After we verified the enzymatic part, we wanted to validate the chemical part by testing the reaction between a small molecule polar head group and the product of the enzymatic reaction, palmitoyl-CoA. Hence, we explored the NCL coupling of cysteine with commercially available palmitoyl-CoA. Briefly, we treated cysteine (1 mM) with palmitoyl-CoA (1 mM) in 10 mM bicine buffer, pH 7.4 containing 100 mM TCEP at 37 °C. However, at this pH, we did not notice an effective conversion of the precursors into the respective lipid analog. We theorized that the pH needed to be raised in order to be closer to the pKa of the thiol (-SH) group in order for the reaction to proceed efficiently and rapidly. With this in mind, we set the reaction up at pH 8.5 as well as pH 9 and monitored for product formation. The yield of the product was 49% in 4 hours at pH 8.5 and it went to completion overnight whereas it was completed under 4 hours at pH 9. We rationalized this as the pKa of cysteine is 8.6, hence the thiol is much more reactive at pH 9 compared to pH 7.4. Formation of diacylated product was followed using HPLC-MS combined with evaporative light-scattering detection (ELSD). Preliminary microscopy experiments were conducted on the lipid product formed. None of the precursors, including palmitoyl-CoA, formed membranes in aqueous solution. The diacylated cysteine product, on the other hand, formed low micron range vesicles in the presence of the same additives as described in chapter 2, especially cholesterol.

### 3.4 Conclusion and Future Directions

In summary, in this chapter we explored a chemoenzymatic lipid generation strategy starting from acetate as the simple carbon feedstock. As mentioned earlier, our approach should have flexibility to diversify the lipid species generated in the reaction. Even though we utilized cgFAS I to selectively produce palmitoyl-CoA, the use of fatty acid synthases from other organisms could enable the formation of a diverse array of fatty acyl-CoA species, which could be subsequently coupled to reactive lysophospholipids to give several noncanonical lipid species. Similarly, we aim to utilize other cysteine-derived reactive head groups to couple with palmitoyl-CoA to form the lipid species. The aim is to set up the one-pot reaction similar to chapter 2 and monitor lipid formation starting from acetate as the primary carbon source and characterize

the processes involved. We envision obtaining membrane vesicles as our product and be able to show that this is a viable method to generated lipid analogs starting from non-amphiphilic, water-soluble precursors.

### 3.5 Acknowledgements

Chapter Three consists of material that is being prepared into a manuscript that will be submitted for publication in the near future. I thank Alessandro Fracassi for his contributions to the work as well as Neal Devaraj for his oversight and assistance in this work. I would like to thank Mike Burkart for his support and mentorship in the project.

# 4. Ion-directed Sphingolipid Membranes from Minimal Precursors

## 4.1 Introduction

Sphingolipids are an important class of lipids occurring universally in eukaryotes.[103] They are structural components of biological membranes and are also involved in biochemical signalling processes.[104,105] Sphingolipids consist of a sphingoid base which has two hydroxyl (-OH) groups at positions $C_1$ and $C_3$ and an amine ($-NH_2$) group at position $C_2$. The amine is typically acylated by a fatty acid chain via amide linkage (Fig. 4.1.A). One of the simplest acylated sphingolipids is ceramide, where the $OH(C_1)$ group remains unmodified. The $OH(C_1)$ group of ceramides may be transformed enzymatically by addition of polar head groups like phosphocholine and phosphoethanolamine to generate sphingomyelins, and with sugar moieties to generate glycosphingolipids (Fig. 4.1.A).[106] Regardless of the head group modification, in sphingolipids, the $OH(C_3)$ group on the sphingoid base chain typically remains free. There is a report mentioning the occurrence of a three-tailed sphingomyelin in new-born pig plasma where the $OH(C_3)$ is also acylated with a fatty acid.[107] However, to our knowledge sphingolipid species where the $OH(C_3)$ is acylated, but $NH_2(C_2)$ is free have not been previously reported. In this work we show that several transition metal ions, particularly Cu(II), catalyze the selective O-acylation of the biologically occurring single-chain amphiphile sphingosylphosphorylcholine[108,109] (also known as lysosphingomyelin) using fatty acyl phosphates or thioesters as acyl donors under mild aqueous conditions (Fig. 4.1.B). We further show that the O-acylated sphingomyelin analogues self-assemble into vesicles having markedly different physical properties as compared to the vesicles formed from N-acylated sphingomyelins. Native sphingomyelins having

phosphocholine headgroups are known to self-assemble into vesicles in aqueous media.[110,111] Vesicle formation has also been reported from N-acylated sphingomyelins containing small structural modifications.[112] Sphingomyelins may be an attractive choice for building blocks for stable synthetic cells thanks to their hydrolytic stability.

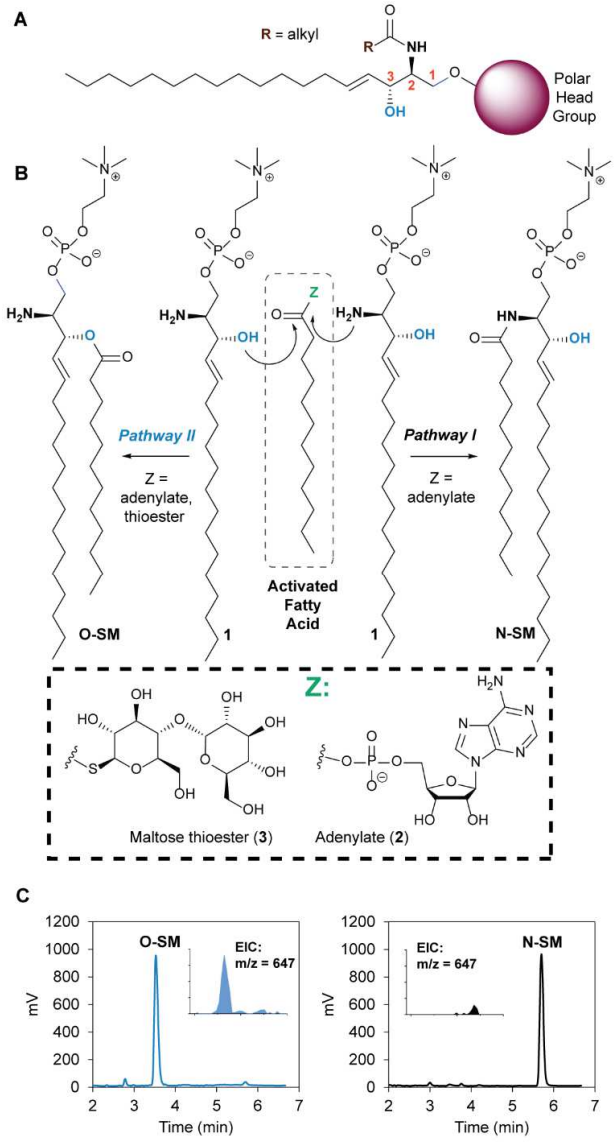


**Figure 12. Synthesis of isomers of sphingomyelin.**

**A.** General structure of a sphingolipid molecule. **B.** Reaction schemes showing the acylation of sphingosylphosphorylcholine (1) with activated fatty acid derivatives – adenylate (2) and maltose thioester (3). **C.** The HPLC-ELSD chromatograms of O-SM and N-SM are shown with extracted ion chromatograms. (EIC) corresponding to m/z = 647 in inset.

## 4.2 Metal Ion-mediated Acylation

Recent work described a chemoenzymatic strategy for synthesis of phospholipids analogues by the reaction between amine-functionalized lysophospholipids and fatty acyl adenylates.[113] The resulting amidophospholipids self-assembled into cell-mimetic vesicular compartments. Following the same method, we attempted to synthesize sphingomyelins via acylation of the $NH_2(C_2)$ group on sphingosylphosphorylcholine (**1**) with dodecanoyl-AMP (**2**). Indeed, we found using HPLC-ELSD-MS that when **1** and **2** are mixed, the expected product N-SM (m/z = 647) is produced (Fig. 4.1.B, *Pathway I*). However, the reaction was sluggish due to the location of the $2NH_2$ group on a secondary carbon. When we carried out the reaction in the presence of $Mg^{2+}$ ions, the rate of reaction significantly increased. This is likely due to the greater electrophilicity of the carbonyl carbon of **2** resulting from coordination of the $Mg^{2+}$ ion to the acyl phosphate moiety. Inspired by this result, we

screened a series of common metal salts to assess their catalytic effect on the acylation reaction. Using HPLC-ELSD-MS to characterize the reaction products, we observed an additional peak at a lower retention time (compared to the N-SM) when the reaction was carried out in the presence of certain metal ions (Fig. 4.1.B, *Pathway II*). This peak had an m/z value of 647 as well. As acylation at $NH_2(C_2)$ or at $OH(C_3)$ are both possible outcomes, we assigned the peak at the lower retention time (~3.5 min) to the O-acylated product (O-SM) as it would be expected to be more polar due to protonation of the free -$NH_2$ group under the eluent solvent conditions (Fig. 4.1.C). Further, the corresponding mass spectra showed strong molecular ion $[M+H]^+$ (m/z = 647) signal, which could be due to ionization of the amine group (Fig. 4.1.C). In comparison, the peak at higher retention time (~5.7 min) which was previously confirmed to be N-SM gave significantly suppressed $[M+H]^+$ (m/z = 647) signal (Fig. 4.1.C). To validate that the newly formed product is indeed the O-acylated analogue of sphingomyelin, we carried out further characterization experiments. We carried out the organic synthesis of compound O-SM to verify the retention times in HPLC-ELSD-MS and characterized the structure using nuclear magnetic resonance (NMR) spectroscopy. Notably, $^{13}C$ NMR spectrum of O-SM gave carbonyl peak at 172.4 ppm (ester) while that of N-SM gave a carbonyl peak at ppm 174.5 (amide) (Fig. 4.6). Infrared (IR) spectroscopy of the sphingomyelin isomers gave carbonyl stretching bands at 1718 $cm^{-1}$ (ester) and 1646 $cm^{-1}$ (amide) for O-SM and N-SM respectively. Finally, O-SM gave a significantly smaller peak in the 205 nm chromatogram as compared to that from the same amount of N-SM (Fig. 4.6).

### 4.3 Screening different Metal Ions

Among the metal ions we screened, the hard cations promote N-acylation exclusively while relatively soft or borderline cations promote O-acylation to various degrees. A summary of the outcomes of the reactions between **1** and **2** in presence of miscellaneous water-soluble metal salts at pH 7.5 is provided in Table 4.1. The ratios between O-SM and N-SM products were estimated based on standard calibration curves generated from HPLC peak areas. Among all the cations screened, Cu(II) was found to promote O-acylation with the highest selectivity (~95%). We tested several water soluble salts (50 mol% with respect

to 1 and 2) like $CuSO_4$, $CuCl_2$, and $Cu(OAc)_2$ and observed similar product ratios. We obtained 76% and 72% O-acylation when 10 mol% and 2.5 mol% Cu(II) were used respectively. We reason that upon coordination to Cu(II), the $OH(C_3)$ group is deprotonated, which makes it more nucleophilic compared to $NH_2(C_2)$ and therefore, attack of $OH(C_3)$ on the carbonyl group of 2 is favored.[114]

| Species | Metal salt | **O-SM:N-SM** |
|---|---|---|
| Li(I) | LiCl | 0:100 |
| Mg(II) | $MgCl_2,6H_2O$ | 0:100 |
| Ca(II) | $CaCl_2,2H_2O$ | 0:100 |
| Mn(II) | $MnCl_2$ | 0:100 |
| Fe(II) | $FeSO_4,7H_2O$ | 40:60 |
| Co(II) | $Co(NO_3)_2,6H_2O$ | 66:34 |
| Ni(II) | $NiSO_4,6H_2O$ | 80:20 |
| Cu(II) | $CuSO_4,5H_2O$ | 95:5 |
| | $Cu(OAc)_2,2H_2O$ | 96:4 |
| Zn(II) | $ZnCl_2$ | 66:34 |
| | $Zn(OAc)_2,2H_2O$ | 73:27 |

**Figure 13. Table summarizing metal ion-dependent acylation of sphingosylphosphorylcholine (1).**

In each of these reactions, **1** (1 mM) was incubated with **2** (1 mM) in HEPES-Na (100 mM, pH 7.5) in presence of 10 mM of various metal salts.

We studied the effect of pH on the outcome of Cu(II)-catalyzed acylation of **1** with **2**, and we found that over a pH range of 5-8, O-acylation nearly exclusively took place (Fig. 4.2.A). At pH 9, the product ratio was completely reversed, and N-SM was the majority product. Next, we studied the effect of stereochemistry on the outcome of the reactions. The 1,2- aminoalcohol moiety on **1** has D-erythro (2S, 3R) configuration and $NH_2(C_2)$ and $OH(C_3)$ are placed *anti* to one another. However, when we carried out the reaction between the corresponding L-threo (2S, 3S) isomer and **2** at pH 7.5, an approximately 3:1 ratio between O- and N-acylated products was obtained (Fig. 4.7). A likely explanation is that $NH_2(C_2)$ and $OH(C_3)$ are placed *syn* to one another in the L-threo isomer, and thus intramolecular O→N acyl transfer may be taking place, which is prevented in the erythro isomer.[115] In addition to acyl phosphates, thioesters are ubiquitously found in biochemistry as activating groups for carboxylic acids to enable acylation chemistries.[116] We were curious if Cu(II) species can drive O-acylation of 1 with fatty acyl thioesters. We

tested the reaction between 1 (1 mM) and an amphiphilic maltose thioester 3[74] (1 mM) at pH 7.5 and 37 °C, but no acylation of 1 could be detected. However, when the reaction was carried out in presence of 50 mol% of Cu(II), we found that acylation went to completion in ~30 min yielding O-SM as the major product with traces of N-SM. In addition, we observed similar outcome when biologically occurring thioesters, namely when fatty acyl-CoAs such as palmitoyl-CoA were used as acyl donors (Fig. 4.8). Compared to the adenylates, we observed a similar trend of product ratio when the reaction was carried out at different pH values over the range of 5-9 (Figure 4.2.B). At pH 5, exclusively O-SM was synthesized and remained the overwhelming major product till pH 8. At pH 9, about 93% of the product is N-SM.

## 4.4 Characterizing the Sphingolipids

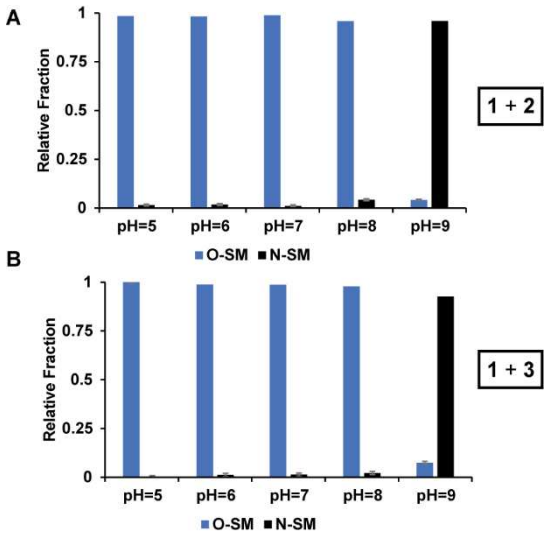


**Figure 14. HPLC-MS analysis of the relative fractions of O-SM and N-SM generated at pH 5-9 via the reaction between A. 1 and 2, B. 1 and 3. Error bars represent standard deviation ($n$ = 3).**

Having developed a facile synthetic route to O-acylated sphingomyelin, we next sought to characterize the structural properties of the membranes formed from pure lipid and compare with the natural counterpart. X-ray diffraction methods have been widely applied to lamellar lipid multilayers and are well-established to quantitatively study lipid bilayer structures.[117,118] We prepared multi-layered oriented films from O-SM

and N-SM on silicon wafers and carried out X-ray diffraction experiments. We obtained five Bragg peaks at equal q-spacing corresponding to a lamellar phase (Fig. 4.3.A). We calculated the electron density profiles (EDPs) of O-SM and N-SM bilayers (Fig. 4.3.B) from which we obtained the distance between lipid headgroups ($d_{hh}$) and the thickness of the water layer between lipid bilayers ($d_w$). We obtained a lamellar repeat distance (d-spacing) of 51.6 Å and a membrane thickness of 39.8 Å for O-SM multilayers. For N-SM multilayers, we obtained a slightly lower d-spacing value of 51.0 Å and a membrane thickness of 39.2 Å (Fig. 4.3.B). For both samples, the water thickness between lipid bilayers was established as 11.8 Å, suggesting similar headgroup hydration (Fig. 4.3.B).

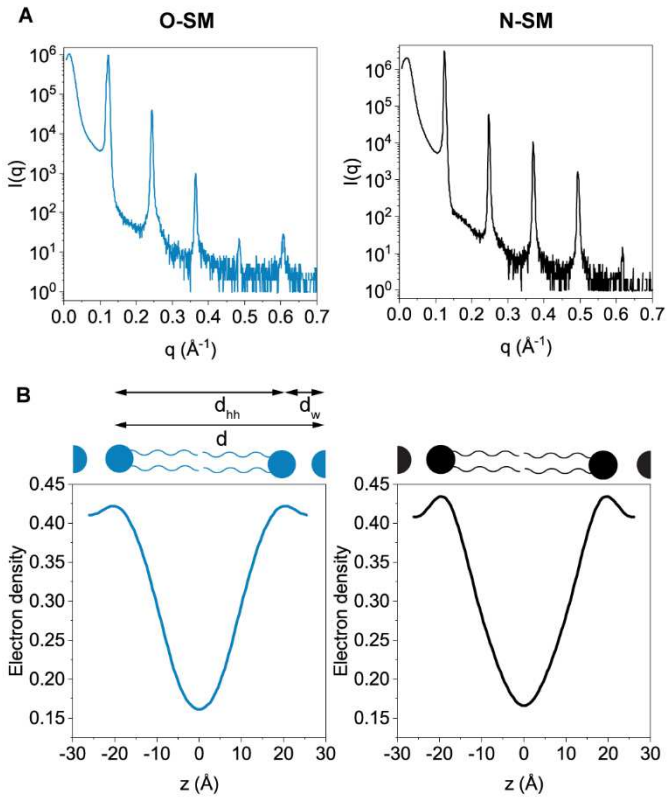


**Figure 15. X-ray diffraction studies on oriented multilayer films of sphingomyelin isomers.**

**A**. Intensity profiles showing Bragg peaks. **B**. Electron density profiles calculated from the intensity profiles. 0 on the *x*-axes represents the bilayer midplane.

The X-ray studies suggest that the two isomers of sphingomyelin present similar structural properties when organized as a stack of lipid multilayers. However, the vesicles formed from the lipids showed marked differences. In water or in buffered solutions, both lipids formed membrane bound vesicles upon gentle

hydration of a thin film. Vesicles also were able to encapsulate water-soluble dyes like Alexa Fluor 488 (Fig. 4.4.B, Fig. 4.9). Interestingly, unlike membranes formed from N-SM or glycerophospholipids, the O-SM membranes could not be visualized by fluorescence microscopy by staining with lipophilic dyes such as Nile Red and Texas Red DHPE (Fig. 4.8). A likely explanation is that the presence of a free -$NH_2(C_2)$ group at the hydrophobic-hydrophilic interface of O-SM quenched the fluorescence of the lipophilic dyes. On the other hand, the presence of free interfacial -$NH_2(C_2)$ group allowed O-SM membranes to bind negatively charged macromolecules such as green fluorescent protein (sfGFP) (Fig. 4.4.C) and a fluorescently labelled DNA oligonucleotide (5′-FAM $dN_{20}$) (Fig. 4.4.D). In contrast, such binding behavior was not observed with N-SM vesicles (Fig. 4.9).

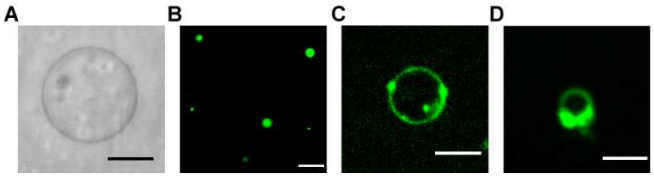


**Figure 16. Self-assembly of O-acylated sphingomyelin O-SM into vesicles.**

**A.** Phase contrast microscopy of a vesicle in water. **B.** Encapsulation of Alexa Fluor 488. **C.** Binding of sfGFP to membranes. **D.** Binding of 5′-FAM-labeled DNA oligonucleotide to membranes. Scale bars in A and B represent 10 μm and in C and D represent 5 μm.

## 4.5 Conclusion

In summary, we report the catalytic aqueous synthesis of an unusual analogue of sphingomyelin and described its self-assembly properties. Given that our method of generating O-acylated sphingomyelin relies on biologically relevant amphiphiles and metal ions, it may be worth exploring if similar reactions take place in cellular membranes and whether these lipids have any bioactive roles. Our method of synthesis of sphingomyelin analogues involved selective O-acylation of a hydroxyl group when in the presence of an adjacent free amine. Such transformations are generally regarded as challenging, particularly in aqueous media.[119,120] Therefore, our method may facilitate development of mild strategies for selective functionalization of organic molecules and biomolecules. Another area where we foresee applications of

our methodology is the development of artificial metalloenzymes capable of catalyzing acylations.[121] Finally, exploring selective high-yielding acylation reactions in aqueous media is important in the context of prebiotic chemistry.[91] Our findings may provide hints at how non-enzymatic acylation reactions took place, particularly in the context of the synthesis of phospholipids and other complex membrane lipids.[122]

## 4.6 Experimental Methods

### *4.6.1 General Information*

Commercially available D-*erythro*-Lysosphingomyelin (d18:1) and L-*threo* Lysosphingomyelin (d18:1) was used as obtained from Cayman Chemicals. Dodecanoic acid, Di-*tert*-butyl dicarbonate, Adenosine 5′-monophosphate monohydrate (5'-AMP.$H_2O$), 2,4,6-trichlorobenzoyl chloride (TCBC), 4-dimethylaminopyridine (DMAP), O-(7-azabenzotriazol-1-yl)-1,1,3,3-tetramethyl-uronium hexafluorophosphate (HATU), dichloromethane ($CH_2Cl_2$), N,N-dimethylformamide (DMF), N,N-diisopropylethylamine (DIEA), trifluoroacetic acid (TFA), triethylsilane (TES), 4-methylpiperidine, palmitic acid and tris(2-carboxyethyl)phosphine hydrochloride (TCEP) were obtained from Sigma-Aldrich. Texas Red® 1,2-dihexadecanoyl-sn-glycero-3-phosphoethanolamine, triethylammonium salt (Texas Red® DHPE) was obtained from Life Technologies. BODIPY FL DHPE was obtained from ThermoFisher Scientific. Deuterated chloroform ($CDCl_3$) and methanol ($CD_3OD$) were obtained from Cambridge Isotope Laboratories. All reagents obtained from commercial suppliers were used without further purification unless otherwise noted. Solvent mixtures for chromatography are reported as v/v ratios. HPLC analysis was carried out on an Eclipse Plus C8 analytical column with Phase A/Phase B gradients [Phase A: $H_2O$ with 0.1% formic acid; Phase B: MeOH with 0.1% formic acid]. HPLC purification was carried out on Zorbax SB-C18 semipreparative column with Phase A/Phase B gradients [Phase A: $H_2O$ with 0.1% formic acid; Phase B: MeOH with 0.1% formic acid]. GC-MS analysis was carried out on an Agilent 7890A GC system connected to a 5975C VL MSD quadrupole MS (EI). Samples were separated on a 60m DB23 Agilent GCMS column using helium as carrier gas and a gradient of 110 °C to 200 °C at 15 °C/min, followed by

20 min at 200 °C. Proton nuclear magnetic resonance (1 H NMR) spectra were recorded on a Varian VX500 MHz spectrometer, and were referenced relative to residual proton resonances in $CDCl_3$ (at δ 7.24 ppm) or $CD_3OD$ (at δ 4.87 or 3.31 ppm). Chemical shifts were reported in parts per million (ppm, δ) relative to tetramethylsilane (δ 0.00). 1 H NMR splitting patterns are assigned as singlet (s), doublet (d), triplet (t), quartet (q) or pentuplet (p). All first-order splitting patterns were designated on the basis of the appearance of the multiplet. Splitting patterns that could not be readily interpreted are designated as multiplet (m) or broad (br). Carbon nuclear magnetic resonance ($^{13}C$ NMR) spectra were recorded on a Varian VX-500 MHz spectrometer, and were referenced relative to residual proton resonances in $CDCl_3$ (at δ 77.23 ppm) or $CD_3OD$ (at δ 49.15 ppm). Electrospray Ionization-Time of Flight (ESI-TOF) spectra were obtained on an Agilent 6230 Accurate-Mass TOF-MS mass spectrometer. Spinning-disk confocal microscopy images were acquired on a Yokagawa spinning-disk system (Yokagawa, Japan) built around an Axio Observer Z1motorized inverted microscope (Carl Zeiss Microscopy GmbH, Germany) with a 63x, 1.40 NA oil immersion objective to an Evolve 512x512 EMCCD camera (Photometrics, Canada) using ZEN imaging software (Carl Zeiss Microscopy GmbH, Germany). A condenser/objective with a phase stop of Ph2 was used to obtain the phase-contrast images. The fluorophores were excited with a 20 mW DPSS laser (Texas Red®). NanoDrop 2000C spectrophotometer was used for UV/Vis measurements. Fluorescence measurements were carried out on a Tecan infinite F200 plate reader instrument. Transmission electron microscopy (TEM) images were recorded on a FEI TecnaiTM Sphera 200 kV microscope equipped with a LaB6 electron gun, using the standard cryotransfer holders developed by Gatan, Inc.

### *4.6.2 X-ray diffraction studies on lipid multilayers*

*Preparation of lipid multilayers and data acquisition*. X-ray diffraction experiments were performed on multi-stacks of oriented lipid bilayers deposited on freshly cleaned hydrophilic silicon [100] wafers. Silicon substrates, cut to 18×20 mm, were sonicated three times for 15 min in methanol followed by another 15 min in deionized water (18 MΩ $cm^{-1}$, Milli-Q; Millipore, Billerica, MA). Substrates were then nitrogen-dried and exposed to short-wavelength UV radiation for 30 min to make the surface hydrophilic. For lipid

deposition, the wafers were placed on an accurate leveled platform and 2 μmol of the corresponding lipid was deposited drop by drop on it. The wafers were left about 2 hours covered at the fume hood for slow evaporation, and then placed under high vacuum for 24 hours to completely evaporate the solvents. The lipid dried films were equilibrated under 96% relative humidity (RH) at 50 °C for 48 hours and finally, they were equilibrated 24 h at room temperature under different RH, i.e. 98%, 93.5%, 83% and 75%, achieved by a reservoir of different saturated salt solutions: $K_2SO_4$, $KNO_3$, KCl and NaCl, respectively.[123] X-ray diffraction measurements were carried out using an in-house Cu $K_\alpha$ tube spectrometer with wavelength 1.54 Å operating in the horizontal plane. During the in-house X-ray diffraction measurements, we used a specially constructed humidity cell designed for high accuracy and sensitivity in RH.[124] The scattered intensity was plotted as a function of $q$ (intensity of scattering vector), which is directly related to the scattering angle by $q = 4\pi \sin(\theta)/\lambda$, where $\lambda$ is the X-ray wavelength. Therefore, we obtained one-dimensional I($q$) profiles for each RH with Braggs peaks indicating the presence of a lamellar phase for both lipids. The diffraction peaks were fitted by a Gaussian after background subtraction. The repeat distance (or *d*-spacing) of the lamellar phase was calculated by $D = 2\pi/\Delta q$, where $\Delta q$ corresponds to the slope of a linear fit of peak position ($q$) vs. diffraction order ($n$).

*Calculation of electron density profiles (EDP)*. The integrated intensity $I_n$ of $n^{th}$ order peaks were then used to calculate the electron density profiles as follows:[125]

$$\rho_{bilayer}(z) = \frac{2}{D}\sum_{n=1}^{M} f_n \, v_n \cos(\frac{2n\pi}{D} z)$$

Where $D$ is the lamellar spacing, coefficient $f_n$ is found by the relationship $I_n=|fn|^2/q_z$, where $q_z$ is the Lorentz correction factor equal to $q$ for oriented bilayers and $I_n$ is the integrated intensity of the $n^{th}$ Bragg peak and $v_n$ is the phase factor for the $n$-th order reflection.[126] Because of the mirror symmetry of the bilayers in the z direction, the phase factors can only be +/- 1.[127] For each phase, intensities of all diffraction orders are normalized by the sum of all peak intensities in that phase to account for the full beam intensity normalization correction. We established the phase factors by following the swelling method,[128]

corresponding to -,-,+,-,+ for both lipids at 98% RH. For each phase, intensities of all diffraction orders were normalized by the sum of all peak intensities in that phase to account for the full beam intensity normalization correction. Finally, the distance between the two characteristic maxima of the density profile was attributed to the lipid headgroup to headgroup distance ($D_{hh}$) and the water layer thickness between lipid bilayers was defined as $D_w = D - D_{hh}$.[129]

### *4.6.3 Synthesis of Lipid Species*

**Dodecanoyl-AMP (1)**.[29] At first, anhydrous $Et_2O$ (7 mL) was used to dissolve solid dodecanoic acid (241.2 mg, 1.20 mmol) and stirred for 10 min at RT. Then, a 1 M solution of DCC in $CH_2Cl_2$ (1.2 mL) previously diluted with anhydrous $Et_2O$ (4 mL) was added dropwise for 10 min. The white suspension that was produced was continuously stirred at RT for 12 h. Afterward, the mixture was filtered, and the filtrate was evaporated in vacuo to afford a white solid. The corresponding dodecanoic anhydride was dried under high vacuum for 3 h and used without further purification. 5′-AMP.$H_2O$ (147.8 mg, 0.40 mmol) was dissolved in a solution of 8 mL of 1:1 $H_2O$: pyridine (v/v) containing NaOH (20 mg, 0.50 mmol) taken in a long vessel. Following this, a solution of dodecanoic anhydride dissolved in 8 mL of THF was added to the mixture in three portions. Upon addition, a white suspension formed readily, and the mixture was stirred at RT continuously. In about 15 min, the suspension turned into nearly clear solution. Next, $Et_2O$ (20 mL) was added and the two-phase mixture was stirred vigorously for about 2 min. Then, the two-phase system was allowed to rest briefly and the upper phase was removed carefully. This process was repeated three times. After this, a small volume of distilled water (~3 mL) was added, and the pH was lowered to ~3 by dropwise addition of aqueous HCl (5%). The gel was transformed into a white suspension and $Et_2O$ (3 × 15 mL) was used to extract the latter by vigorous stirring. The top organic layer is separated continuously after each round. The white solid was transferred to a Büchner funnel and the residual suspension was filtered. Finally, the solid is washed with acetone (3 × 5 mL) and $Et_2O$ (2 × 5 mL). The residue is dried in vacuo, and dodecanoyl-AMP **1** is obtained as a white powder [125.2 mg, 60%]. $^1$H NMR ($d_6$-DMSO, 500.13 MHz, δ): 8.55 (s, 1 H, 1 × $CH_{Ar}$), 8.30 (s, 1 H, 1 × $CH_{Ar}$), 5.94 (d, $J$ = 5.6 Hz, 1 H, 1 × CH), 4.57 (t, $J$ = 5.3 Hz, 1 H,

1 × CH), 4.24–3.98 (m, 4 H, 2 × CH + 1 × $CH_2$), 2.33 (t, $J$ = 7.3 Hz, 2 H, 1 × $CH_2$), 1.55–1.35 (m, 2 H, 1 × $CH_2$), 1.31–1.09 (m, 16 H, 8 × $CH_2$), 0.88 (t, $J$ = 6.8 Hz, 3 H, 1 × $CH_3$). $^{13}$C NMR ($d_6$-DMSO, 125.77 MHz, δ): 163.3, 152.8, 148.8, 148.5, 140.8, 118.7, 87.3, 83.6, 73.8, 70.4, 66.0, 34.6, 31.3, 29.0, 29.0, 28.9, 28.7, 28.7, 28.3, 24.1, 22.1, 14.0. MS (ESI-TOF) [m/z (%)]: 530 ([MH]$^+$, 100). HRMS (ESI-TOF) calculated for $C_{22}H_{37}N_5O_8P$ ([MH]$^+$) 530.2374, found 530.2374.

**Dodecanoyl maltose thioester (2)**.[74] A solution of dodecanoic acid (263.3 mg, 131.5 µmol) in DMF (500 µL) was stirred at 0 ºC for 10 min, and then HATU (55.0 mg, 144.6 µmol) and DIEA (25.2 µL, 144.6 µmol) were successively added. After 10 min stirring at 0 ºC, 1-thio-b-maltose sodium salt (50.0 mg, 131.5 µmol) was added. After 1 h stirring at rt, the mixture was concentrated under reduced pressure. The corresponding residue was diluted in MeOH (500 µL), filtered using a 0.2 µm syringe-driven filter, and the crude solution was purified by HPLC, affording 45.3 mg of 1 as a white solid [64%, tR = 4.7 min (Zorbax SB-C18 semipreparative column, 5% Phase A in Phase B, 15.5 min)]. 1 H NMR (CD3OD, 500.13 MHz, d): 5.18 (d, J = 3.9 Hz, 1H, 1 × CH), 5.06 (d, J = 10.3 Hz, 1H, 1 × CH), 3.87-3.77 (m, 3H, 3 × CH), 3.72-3.56 (m, 5H, 1 × CH + 2 × CH2), 3.49-3.42 (m, 2H, 2 × CH), 3.38-3.33 (m, 1H, 1 × CH), 3.29-3.23 (m, 1H, 1 × CH), 2.69-2.54 (m, 2H, 1 × CH2), 1.75-1.56 (m, 2H, 1 × CH2), 1.43-1.19 (m, 16H, 8 × CH2), 0.90 (t, J = 7.0 Hz, 3H, 1 × CH3). 13C NMR (CD3OD, 125.77 MHz, d): 198.6, 102.9, 83.9, 81.1, 80.6, 79.5, 75.1, 74.8, 74.2, 72.9, 71.5, 62.8, 62.0, 45.1, 33.1, 30.7, 30.7, 30.5, 30.5, 30.4, 30.0, 26.4, 23.7, 14.4. MS (ESI-TOF) [m/z (%)]: 540 ([MH]$^+$ , 25), 563 ([M +Na]$^+$ , 100). HRMS (ESI-TOF) calculated for C24H44O11SNa ([M +Na]$^+$ ) 563.2497, found 563.2499.

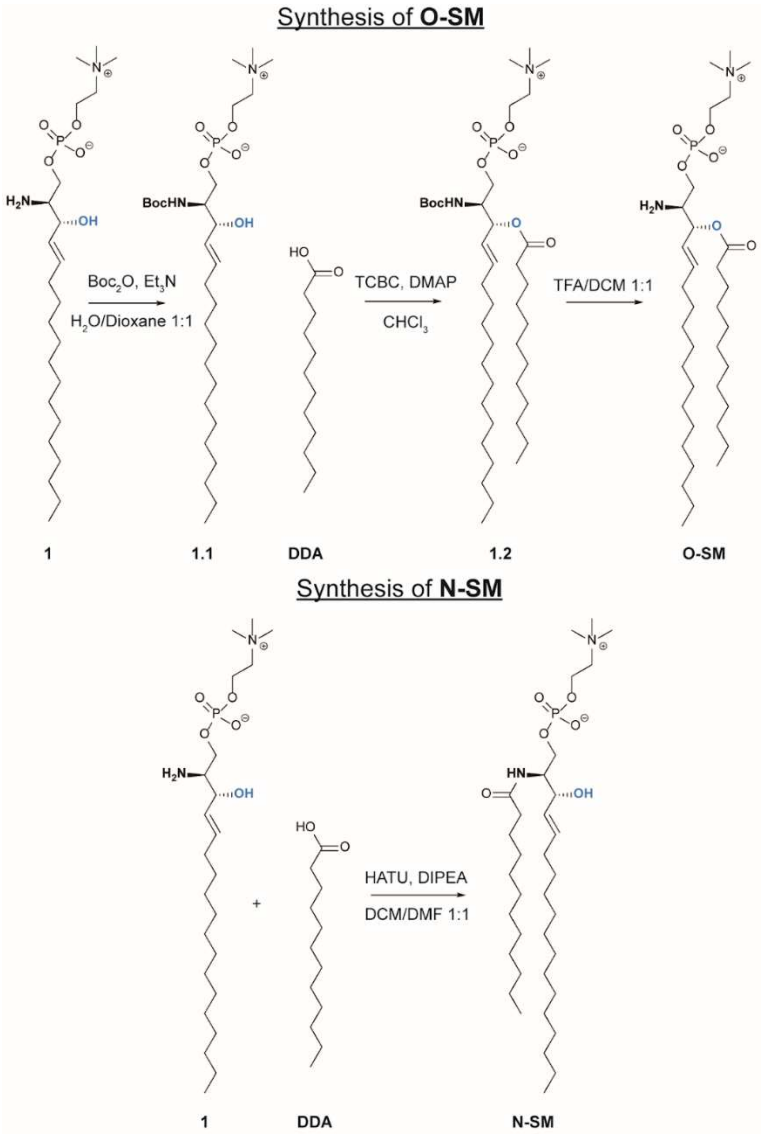


**Figure 17. Synthetic scheme for O-SM and N-SM.**

***N*-Boc-D-*erythro*-sphingosine phosphocholine** (**1.1**). To a solution of D-*erythro*-sphingosine phosphocholine (**1**, Lyso d18:1 SM-$NH_2$, 4.0 mg, 8.6 µmol) in 250 µL of $H_2O$/dioxane (1:1) was successively added $Boc_2O$ (2.8 mg, 12.9 µmol) and $Et_3N$ (3.6 µL, 25.8 µmol). After 3 h stirring at rt, the solvent was removed under reduced pressure. Then, the corresponding residue was diluted in MeOH (250 µL), filtered using a 0.2 µm syringe-driven filter, and the crude solution was purified by HPLC, affording 4.2 mg of the lysosphingolipid **1.1** as a colorless film [87%, $R_t$ = 7.5 min (Zorbax SB-C18 semipreparative

column, 5% Phase A in Phase B, 15.5 min)]. $^{1}$H NMR ($CDCl_3$, 500.13 MHz, δ): 5.81-5-57 (m, 1H, 1×CH), 5.53-5.38 (m, 1H, 1×CH), 4.59-3.52 (m, 8H, 2×CH + 3×$CH_2$), 3.31 (s, 9H, 3×$CH_3$), 2.10-1.84 (m, 2H, 1×$CH_2$), 1.39 (s, 9H, 3×$CH_3$), 1.34-1.17 (m, 22H, 11×$CH_2$), 0.88 (t, *J* = 6.9 Hz, 3H, 1×$CH_3$). $^{13}$C NMR ($CDCl_3$, 125.77 MHz, δ): 156.0, 134.0, 129.6, 79.2, 71.8, 66.5, 65.5, 59.6, 55.7, 54.6, 32.7, 32.1, 29.9, 29.9, 29.9, 29.9, 29.8, 29.8, 29.7, 29.5, 29.5, 28.7, 22.8, 14.3. MS (ESI-TOF) [m/z (%)]: 565 ([MH]$^+$, 100). HRMS (ESI-TOF) calculated for $C_{28}H_{58}N_2O_7P$ ([MH]$^+$) 565.3976, found 565.3973.

***N*-Boc-D-*erythro*-dodecanoyl-sphingosylphosphocholine** (**1.2**). A solution of *N*-Boc-D-*erythro*-sphingosine phosphocholine (**1.1**, 4.0 mg, 7.1 μmol), dodecanoic acid (3.6 mg, 17.7 μmol), DMAP (5.2 mg, 42.5 μmol) and $Et_3N$ (3.5 μL) in $CDCl_3$ (275 μL) was stirred for 10 min at rt. Then, 2,4,6-trichlorobenzoyl chloride (TCBC, 7.2 μL) was added and the reaction was stirred for 12 h at rt. Afterwards, $H_2O$ (7.5 μL) was added to the reaction mixture to quench the acid chloride, and the solvent was removed by rotary evaporation to give a yellow oil. Then, the corresponding residue was diluted in MeOH (250 μL), filtered using a 0.2 μm syringe-driven filter, and the crude solution was purified by HPLC, affording 4.6 mg of the sphingophingolipid **1.2** as a colorless film [87%, $R_t$ = 10.1 min (Zorbax SB-C18 semipreparative column, Phase B, 23.5 min)]. $^{1}$H NMR ($CD_3OD$, 500.13 MHz, δ): 6.89 (d, *J* = 9.4 Hz, 1H, 1×NH), 5.80 (dt, *J1* = 15.3 Hz, *J2* = 6.8 Hz, 1H, 1×CH), 5.45 (ddt, *J1* = 15.3 Hz, *J2* = 7.9 Hz, *J3* = 1.5 Hz, 1H, 1×CH), 5.37-5.25 (m, 1H, 1×CH), 4.35-4.18 (m, 2H, 1×$CH_2$), 4.01-3.94 (m, 1H, 1×CH), 3.93-3.82 (m, 2H, 1×$CH_2$), 3.70-3.58 (m, 2H, 1×$CH_2$), 3.23 (s, 9H, 3×$CH_3$), 2.32 (t, *J* = 7.4 Hz, 2H, 1×$CH_2$), 2.05 (ddt, *J1* = 7.2 Hz, *J2* = 3.6 Hz, *J3* = 2.0 Hz, 2H, 1×$CH_2$), 1.69-1.54 (m, 2H, 1×$CH_2$), 1.43 (s, 9H, 3×$CH_3$), 1.36-1.18 (m, 38H, 19×$CH_2$), 0.90 (t, *J* = 7.0 Hz, 6H, 2×$CH_3$). $^{13}$C NMR ($CD_3OD$, 125.77 MHz, δ): 174.4, 158.1, 138.4, 125.8, 80.2, 75.1, 67.4, 65.4, 60.5, 54.6, 54.3, 35.4, 33.4, 33.1, 30.9, 30.8, 30.8, 30.8, 30.7, 30.7, 30.6, 30.5, 30.5, 30.3, 30.2, 30.0, 28.8, 26.1, 23.8, 14.5. MS (ESI-TOF) [m/z (%)]: 769 ([M+Na]$^+$, 14), 747 ([MH]$^+$, 8), 393 ([M+H+K]$^{2+}$, 100). HRMS (ESI-TOF) calculated for $C_{40}H_{80}N_2O_8P$ ([MH]$^+$) 747.5647, found 747.5649.

**D-*erythro*-dodecanoyl-sphingosylphosphocholine** (**O-SM**). A solution of *N*-Boc-D-*erythro*-dodecanoyl-sphingosylphosphocholine (**1.2**, 4.0 mg, 5.4 μmol) in 500 μL of TFA/CH2Cl2 (1:1) was stirred

at rt for 15 min. After removal of the solvent, the residue was dried under high vacuum for 3 h. Then, the corresponding residue was diluted in MeOH (500 µL), filtered using a 0.2 µm syringe-driven filter, and the crude solution was purified by HPLC, affording 2.7 mg of **O-SM** as a colorless oil [77%, $t_R$ = 4.9 min (Zorbax SB-C18 semipreparative column, Phase B, 23.5 min)]. $^1$H NMR ($CD_3OD$, 500.13 MHz, δ): 6.02-5.82 (m, 1H, 1×CH), 5.53-5.39 (m, 2H, 2×CH), 4.36-4.24 (m, 2H, 1×$CH_2$), 4.12 (ddd, *J1* = 11.5 Hz, *J2* = 6.1 Hz, *J3* = 3.6 Hz, 1H, 0.5×$CH_2$), 3.96 (dt, *J1* = 11.4 Hz, *J2* = 7.1 Hz, 1H, 0.5×$CH_2$), 3.65 (dd, *J1* = 6.0 Hz, *J2* = 3.4 Hz, 2H, 1×$CH_2$), 3.59-3.53 (m, 1H, 1×CH), 3.23 (s, 9H, 3×$CH_3$), 2.40 (t, *J* = 7.4 Hz, 2H, 1×$CH_2$), 2.18-2.01 (m, 2H, 1×$CH_2$), 1.68-1.56 (m, 2H, 1×$CH_2$), 1.47-1.26 (m, 38H, 19×$CH_2$), 0.90 (t, *J* = 6.9 Hz, 6H, 2×$CH_3$). $^{13}$C NMR ($CD_3OD$, 125.77 MHz, δ): 172.4, 139.1, 127.2 and 122.4, 71.6, 66.0, 62.5, 59.2, 53.8, 53.2, 33.6, 32.0, 31.7, 29.5, 29.4, 29.4, 29.4, 29.4, 29.3, 29.2, 29.1, 29.1, 29.1, 28.8, 28.8, 28.5, 24.6, 22.4, 13.1. MS (ESI-TOF) [m/z (%)]: 647 ($[MH]^+$, 11), 343 ($[M+H+K]^{2+}$, 100). HRMS (ESI-TOF) calculated for $C_{35}H_{72}N_2O_6P$ ($[MH]^+$) 647.5123, found 647.5108.

***N*-dodecanoyl-D-*erythro*-sphingosylphosphorylcholine** (**N-SM**). A solution of dodecanoic acid (1.5 mg, 7.5 µmol) in DCM/DMF (1:1) (250 µL) was stirred at 0 °C for 10 min, and then HATU (3.2 mg, 8.3 µmol) and DIPEA (5.3 µL, 30.1 µmol) were successively added. After 10 min stirring at 0 °C, D-*erythro*-sphingosine phosphocholine (Lyso d18:1 SM-$NH_2$, 3.5 mg, 7.5 µmol) was added. After 1 h stirring at rt, the mixture was concentrated under reduced pressure. The corresponding residue was dissolved in MeOH (500 µL), filtered using a 0.2 µm syringe-driven filter, and the crude solution was purified by HPLC, affording 3.5 mg of X4 as a colorless film [72%, $t_R$ = 7.9 min (Zorbax SB-C18 semipreparative column, Phase B, 23.5 min)]. $^1$H NMR ($CD_3OD$, 500.13 MHz, δ): 7.98 (d, *J* = 9.0 Hz, 1H, 1×NH), 5.70 (dt, *J1* = 15.3 Hz, *J2* = 6.7 Hz, 1H, 1×CH), 5.70 (ddt, *J1* = 15.3 Hz, *J2* = 7.8 Hz, *J3* = 1.5 Hz, 1H, 1×CH), 4.71-4.58 (m, 1H, 1×CH), 4.36-4.21 (m, 2H, 1×$CH_2$), 4.14-3.92 (m, 3H, 1×CH2 + 1×CH), 3.71-3.55 (m, 2H, 1×$CH_2$), 3.22 (s, 9H, 3×$CH_3$), 2.18 (td, *J1* = 7.7 Hz, *J2* = 6.9 Hz, *J3* = 1.9 Hz, 2H, 1×$CH_2$), 2.03 (ddt, *J1* = 12.6 Hz, *J2* = 8.4 Hz, *J3* = 4.0 Hz, 2H, 1×$CH_2$), 1.66-1.46 (m, 2H, 1×$CH_2$), 1.42-1.24 (m, 38H, 19×$CH_2$), 0.90 (t, *J* = 6.9 Hz, 6H, 2×$CH_3$). $^{13}$C NMR ($CD_3OD$, 125.77 MHz, δ): 174.5, 133.8, 129.8, 71.1, 66.0, 64.4, 59.0,

53.8, 53.2, 36.0, 35.9, 32.1, 31.7, 31.7, 29.5, 29.5, 29.4, 29.4, 29.4, 29.4, 29.3, 29.3, 29.2, 29.1, 29.1, 29.1, 29.1, 29.0, 25.8, 22.4, 13.1. MS (ESI-TOF) [m/z (%)]: 647 ($[MH]^+$, 8), 343 ($[M+H+K]^{2+}$, 100). HRMS (ESI-TOF) calculated for $C_{35}H_{72}N_2O_6P$ ($[MH]^+$) 647.5123, found 647.5124.

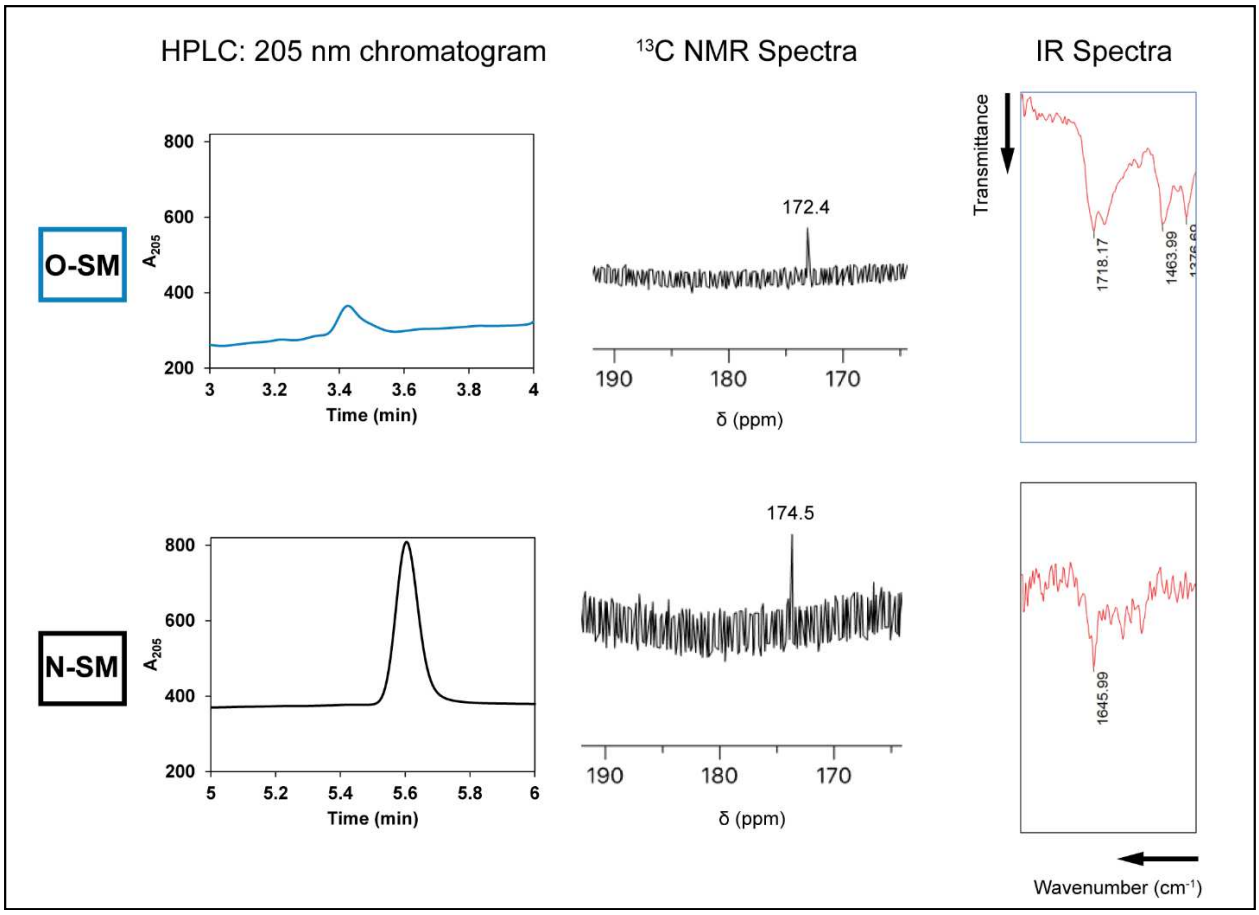


**Figure 18. Comparison of 205 nm chromatograms (20 nmol each), IR spectra, and 13C NMR spectra (carbonyl peaks) of pure O-SM and N-SM.**

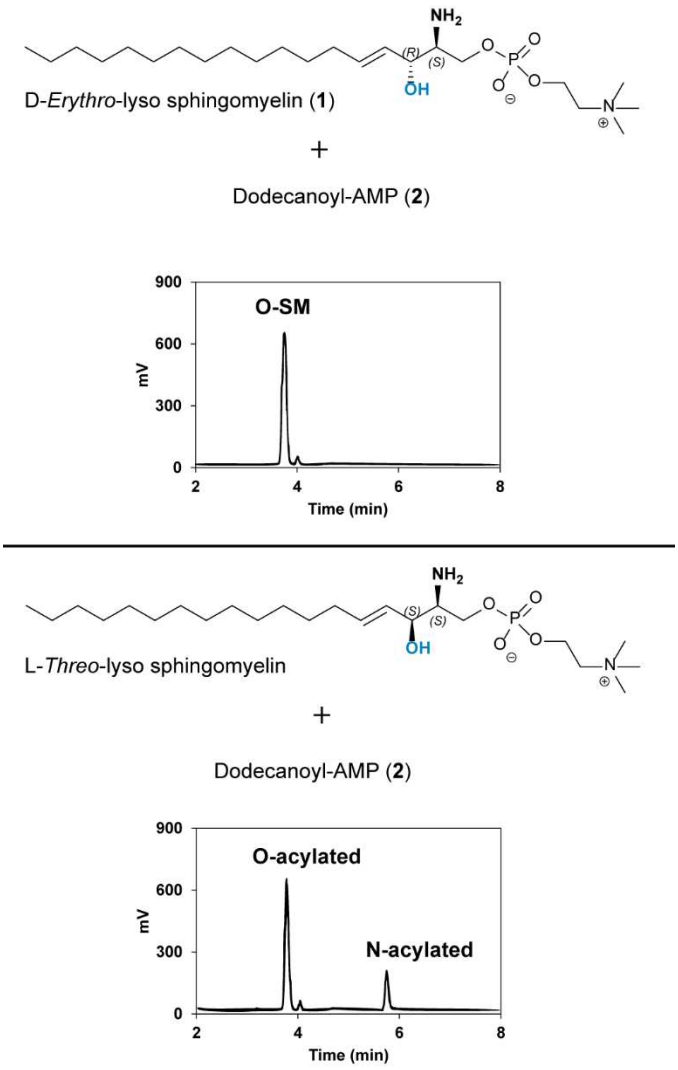


**Figure 19. Reaction between 1 mM of erythro (1) and threo stereoisomers of lyso-sphingomyelin and dodecanoyl-AMP (2) at pH 7.5 (50 mM HEPES)). HPLC-ELSD chromatograms are shown corresponding to each reaction.**

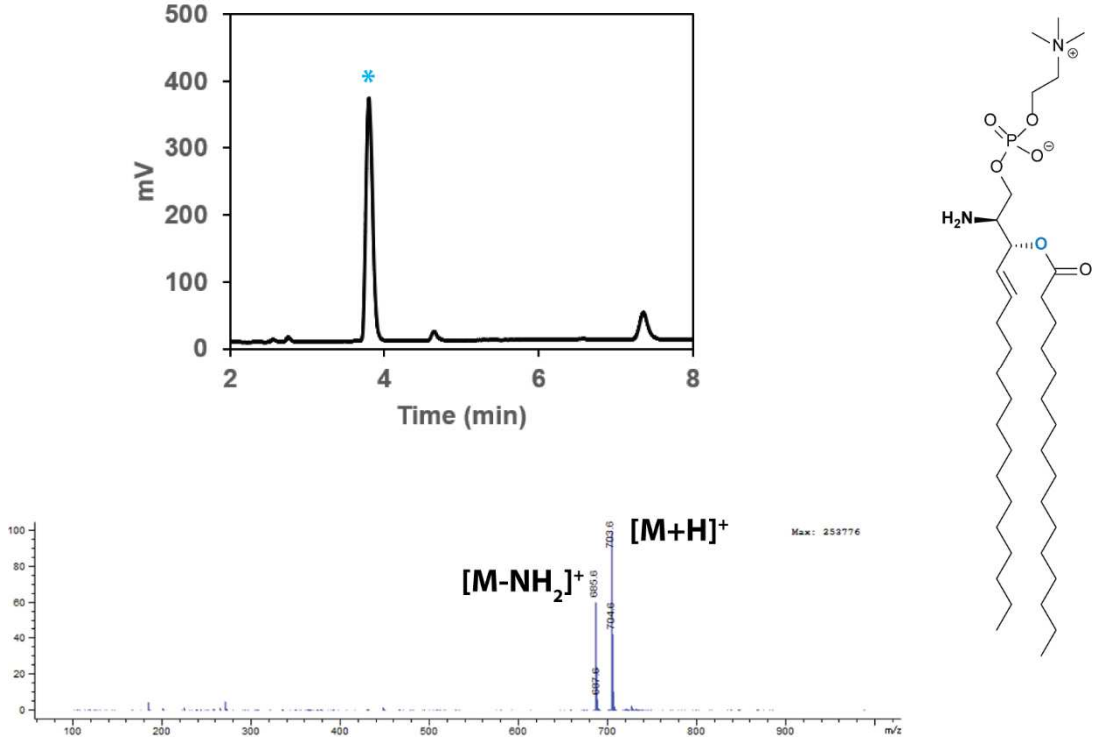


**Figure 20. Reaction between 1 mM of lyso-sphingomyelin (1) and palmitoyl CoA in 50 mM HEPES buffer pH 7.5 at 37 °C.**

HPLC-ELSD chromatogram and the mass spectrum is shown corresponding to the O-acylated product peak (indicated with an asterisk). The MS peaks corresponding to the species $[M+H]^+$ (m/z = 703) and $[M-NH_2]^+$ (m/z = 685) are shown.

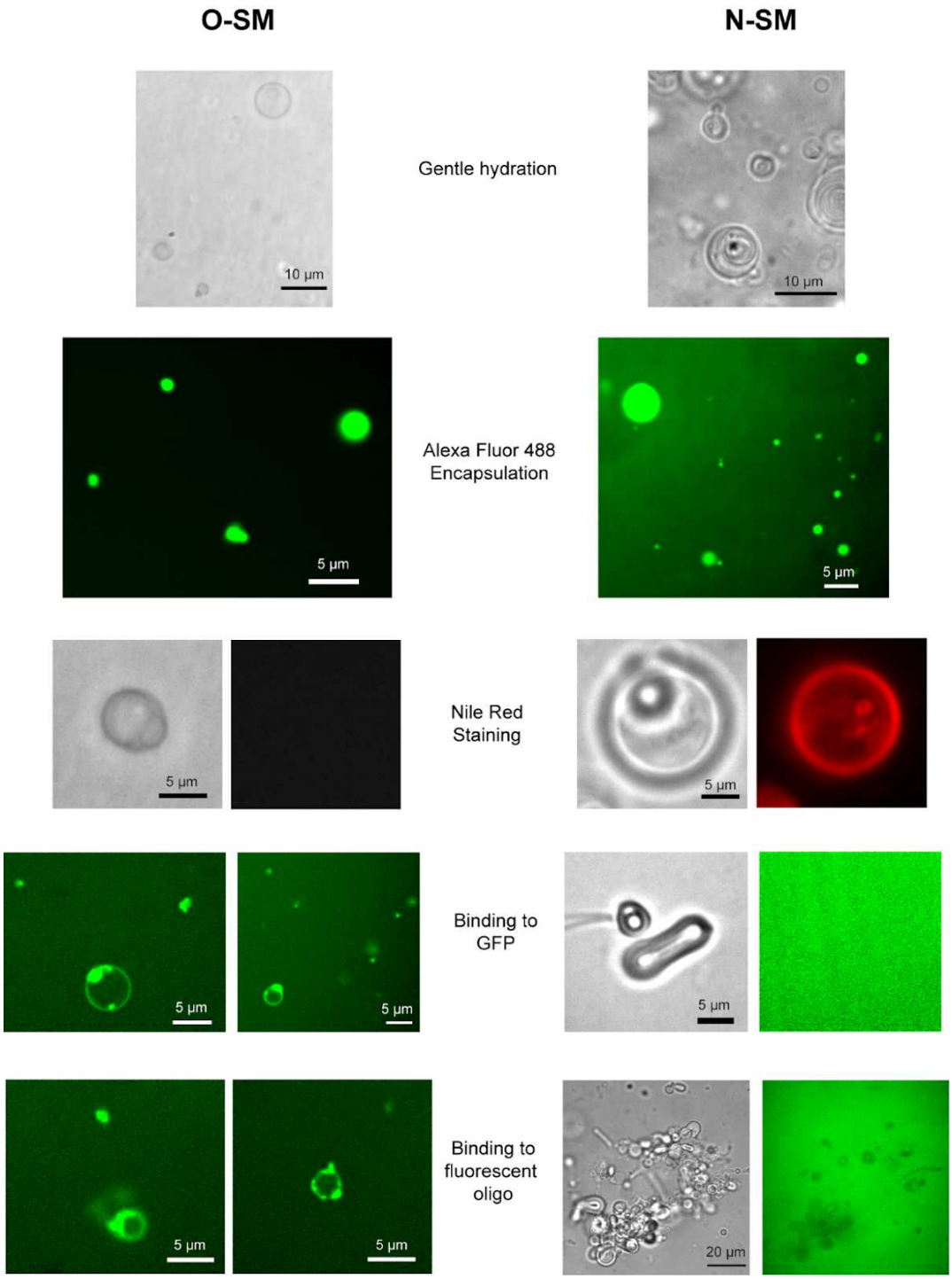


**Figure 21. Microscopy of O-SM and N-SM vesicles.**

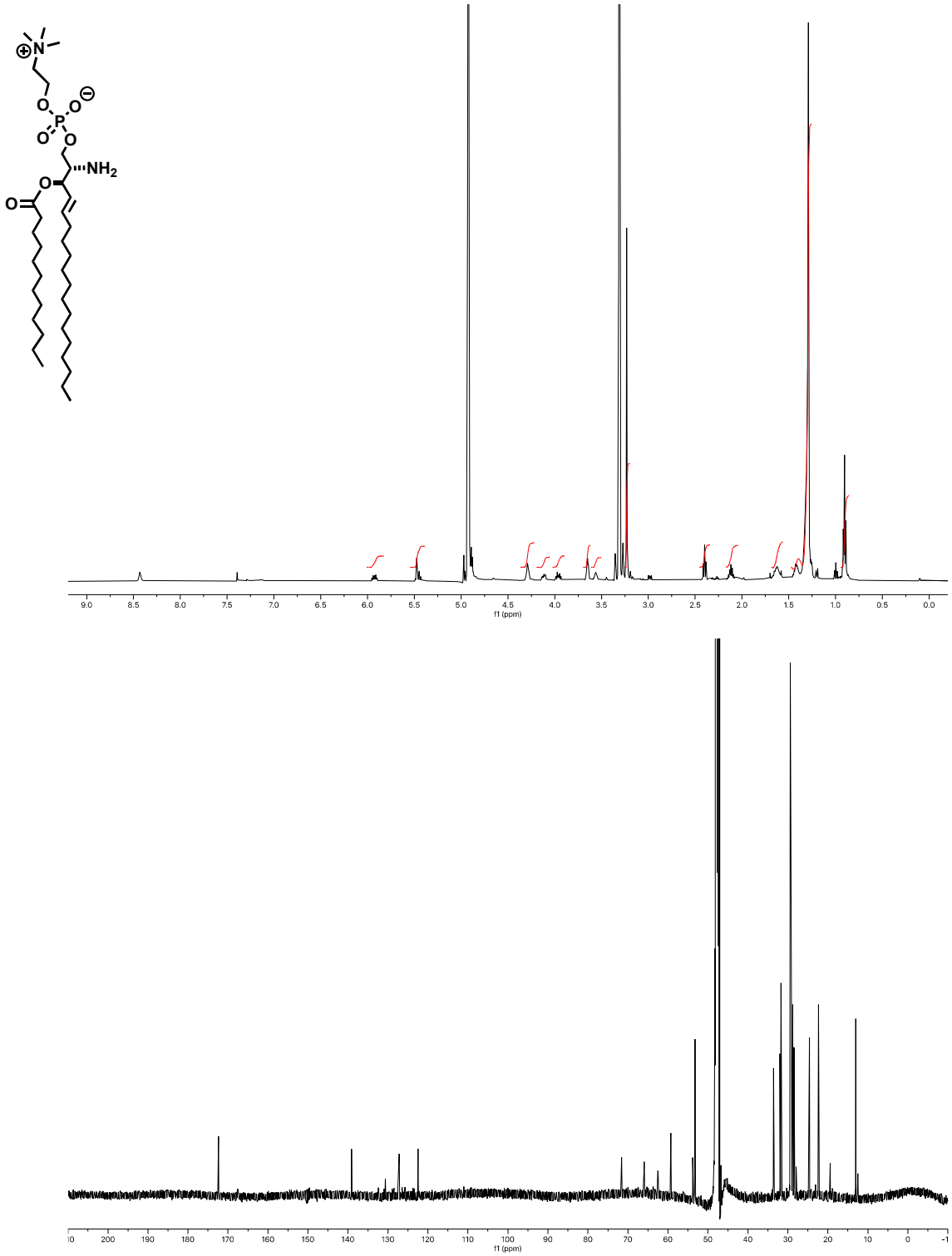


$^{1}$H (*top*) and $^{13}$C (*bottom*) NMR spectra of compound **O-SM**.

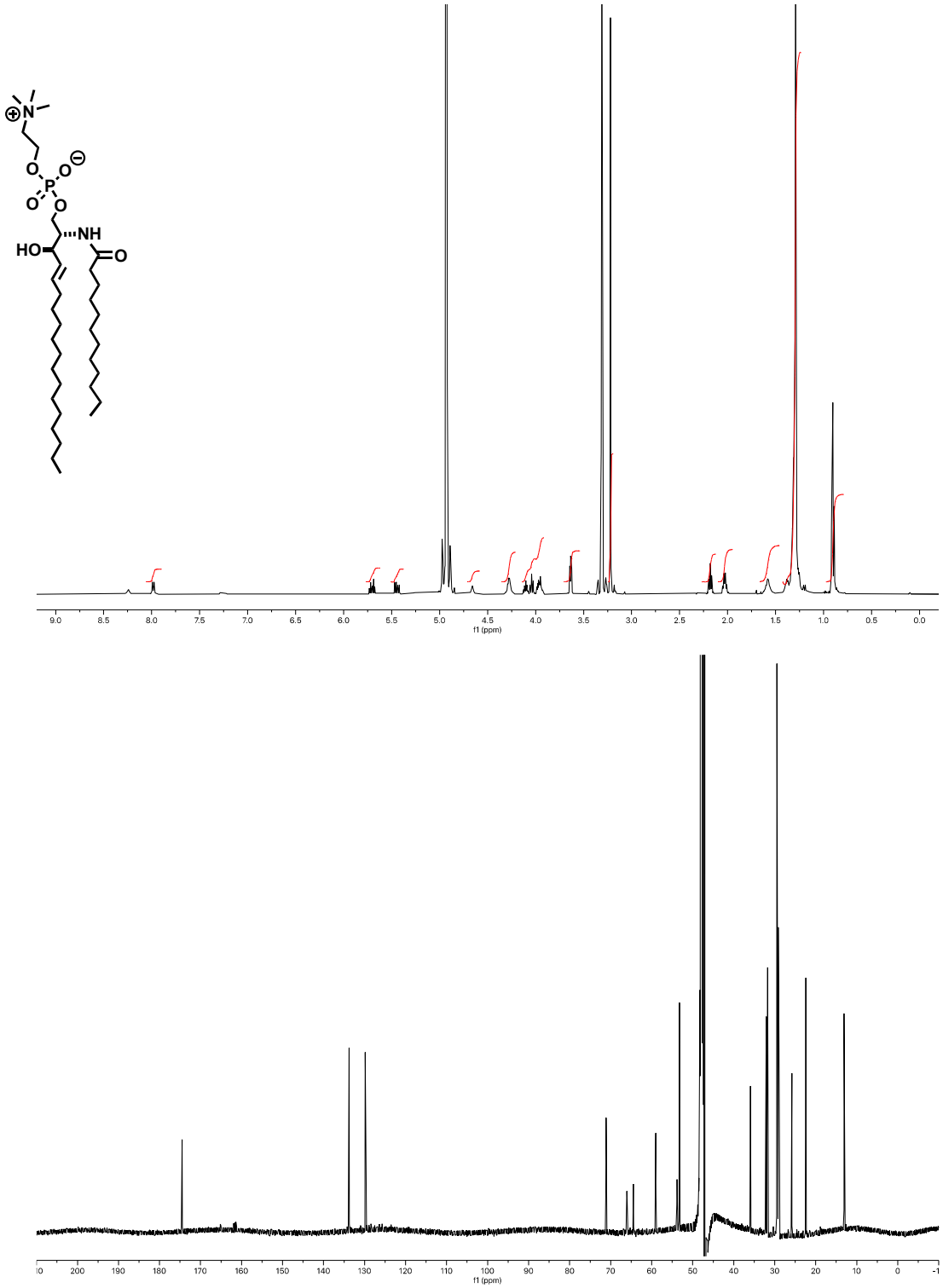


$^{1}$H (*top*) and $^{13}$C (*bottom*) NMR spectra of compound **N-SM**.

## 4.7 Acknowledgements

Chapter Four, in full, is a reprint of the material as it appears in the manuscript: Bhattacharya, A., Brea, R., J., Khanal, S., Salvador-Castell, M., Sinha, S., K., and Devaraj, N., K. Catalytic ion-directed synthesis of O-acylated sphingomyelin analogues in aqueous media and their self-assembly into vesicles. **2021**. *Submitted*. My contribution to this chapter was the optimization of the sphingolipid formation reactions under various conditions while using different metal ions. I would like to thank Ahanjit Bhattacharya for his contributions to this chapter, which includes the initial observations of different sphingolipid products made under different conditions, screening the reactions with various metal ions, optimization and characterization of the lipids made as well as, HPLC-MS, fluorescent microscopy as well as the biochemical assays. I would also like to thank Roberto Brea for the synthesis and characterization of the sphingolipid precursors as well as the lipids made and the microscopy experiments. Additionally, I would like to thank Marta Salvador-Castell for the x-ray diffraction experiments. I would like to thank Sunil Sinha for his insight and contributions to the manuscript. I would finally like to thank Neal Devaraj for his guidance for the project and assistance with the preparation of the manuscript.

## 5. Conclusion

In summary, we have developed a chemoenzymatic route to synthesize noncanonical phospholipids from simple, minimal, and biologically relevant precursors. Constructing an artificial cell from with a bottom-up approach depends on step-by-step development of chemistry to mimic the biological processes and understand these mechanisms closely to gain insight into life itself. Compartmentalization is an essential feature of life,[8,9] and the synthesis of life-like compartments will be a necessity for the construction of an artificial cell. The most common way by which biological cells compartmentalize themselves from the environment, and even organelles inside eukaryotic cells, is using lipid membranes. Understanding the necessary ways in which primitive cells may have constructed their lipid membranes is a huge area of study.[130] Additionally, these insights will help construct artificial cells as biomimetically as possible. Given our approach, there is a lot of opportunity to explore various facets moving forward. With the chemoenzymatic scheme used in our work, there should be a lot of flexibility to diversify the lipid species generated. One aspect of this is diversifying the fatty acid tails of the lipid analogs. Even though we utilized cgFAS I to selectively produce palmitoyl-CoA, the use of fatty acid synthases from other organisms could enable the formation of a diverse array of fatty acyl-CoA species, which could be subsequently coupled to reactive lysophospholipids or small reactive head groups such as cysteine to give several noncanonical lipid species. For instance, many bacterial FASs are known to synthesize terminally branched iso-, anteiso-, or omega-alicyclic fatty acids from branched, short-chain carboxylic acid precursors such as methylmalonyl-CoA.[18,131,132] This would afford us unique lipid analogs that would have very different biophysical properties and therefore their assemblies in solution would be extremely interesting to explore. For example, having methylmalonyl-CoA as the starting precursor would lead to lipid species with branched tails, which leads to a more fluid profile of membranes. Similarly, we also envision using a diverse set of modified cysteine head groups to couple with the tails to lead to lipid analogs with vastly different biophysical properties to those characterized in previous efforts. Specifically, reactive lysophospholipids with choline (LPC), ethanolamine (LPE) and inositol (LPI) head groups can be synthesized to then couple

them with fatty acyl-CoAs to create synthetic non-canonical phospholipids. This will lead to cylindrical lipids that mimic phosphatidylcholine (PC), conical lipids with positive curvature resembling phosphatidylinositol (PI) as well as inverted conical lipids with negative curvature resembling phosphatidylethanolamine (PE).

Once we have an array of analogs, we plan on utilizing the *in situ* synthesis of diverse phospholipid species to facilitate investigations of how lipid membrane composition affects vesicle assembly, growth, and division. Furthermore, we can also use this work as the foundation for building artificial cell organelle membranes. A very interesting direction to take this would be to build a programmable synthetic endoplasmic reticulum (ER). In living systems, the characteristic morphologies of cellular organelles are established through interactions between proteins and lipids that shape membranes.[133] Membrane curvature plays a critical role in defining the morphology of cells, organelles, and local membrane subdomains.[134,135] Therefore, the generation and maintenance of curvature is of central importance for membrane trafficking and cellular functions. While there has been tremendous progress in understanding how proteins and lipids cooperate to form membrane-bound organelles,[136–138] many outstanding questions persist. For instance, it is still unclear how organelle size and shape is determined and maintained. From an evolutionary biology perspective, it is unclear what physicochemical principles were essential for the *de novo* formation of membrane-bound organelles like the endoplasmic reticulum. Bottom-up designer synthetic organelles using minimal and well-defined lipids and proteins would shed light on these questions. Furthermore, the ER is the principal site for lipid synthesis,[139] and in many ways is the progenitor for all cellular membranes. Additionally, the ER is a critical site for protein synthesis, modification, and transport.[140] Finally, the ER can adopt various structures, including a reticulated network, and thus a minimal ER could shed light on what determines organelle shape and in turn inform how shape affects physical properties and function.

In living cells, the ER is maintained through the constant synthesis of fatty acids that couple to form phospholipids and is shaped by the action of several membrane proteins. To generate a synthetic ER *de novo*, we plan to combine the chemoenzymatic synthesis of non-canonical phospholipids with recombinant proteins that influence membrane curvature and fusion. The previous chapters demonstrated that we could

use minimal water-soluble precursors such as acetate can be used as the primary carbon feedstock to generate reactive precursors such as acetyl-CoA and malonyl-CoA. These, in turn, can react with cysteine and cysteine derived lysolipids to form lipids that spontaneously assemble to form membrane-bound vesicles. Building on this methodology, we imagine creating a library of non-canonical lipids that vary in chain length, unsaturation, and head group functionality. These lipid analogs can then be characterized to understand how the intrinsic curvature of the lipids affects their assembly into membranes and consequently how curvature, fluidity, and head group identity dictate interactions with membrane stabilizing and fusion proteins that are known to facilitate ER-like reticulate network generation. Furthermore, we will determine the minimal lipid composition requirements necessary for generating tubular structures and ER-like reticulate membrane networks with Yop1p and Sey1p, two membrane-bound proteins that play a critical role in membrane curvature stabilization and fusion respectively in yeast[141], and characterize the resulting membrane morphologies.

More generally, this work explores the *de novo* membrane generation starting from very minimal, small molecule precursors utilizing an elegant approach of applying a unique synthetic route coupled with ubiquitous enzymes that are used to build fatty acids in living systems. This approach of building the membranes "from scratch" gives us a lot of room to explore different reactivities and combinations to get lipids with varying curvatures and biophysical properties, which we can then leverage in building interesting systems like a programmable synthetic ER in the future. Similarly, we also explored the use of metal ions to develop yet another example of noncanonical sphingolipid that is acylated on the –OH group rather than the $–NH_2$, with the goal of further understanding the parameters that go into *de novo* membrane generation.

## 6. References


(1) Khanal, S.; Brea, R. J.; Burkart, M. D.; Devaraj, N. K. Chemoenzymatic Generation of Phospholipid Membranes Mediated by Type I Fatty Acid Synthase. *J. Am. Chem. Soc.* **2021**, *143* (23), 8533–8537.

(2) Chuong, C. M.; Nickoloff, B. J.; Elias, P. M.; Goldsmith, L. A.; Macher, E.; Maderson, P. A.; Sundberg, J. P.; Tagami, H.; Plonka, P. M.; Thestrup-Pedersen, K.; Bernard, B. A.; Schröder, J. M.; Dotto, P.; Chang, C. H.; Williams, M. L.; Feingold, K. R.; King, L. E.; Kligman, A. M.; Rees, J. L.; Christophers, E. What Is the 'True' Function of Skin? *Exp. Dermatol.* **2002**, *11* (2), 159.

(3) Bhattacharya, A.; Brea, R. J.; Devaraj, N. K. De Novo Vesicle Formation and Growth: An Integrative Approach to Artificial Cells. *Chem. Sci.* **2017**, *8* (12), 7912–7922.

(4) Chaffey, N.; Alberts, B.; Johnson, A.; Lewis, J.; Raff, M., Roberts, K.; Walter, P. Molecular Biology of the Cell. 4th Edn. *Ann. Bot.* **2003**, *91* (3), 401–401.

(5) Sunshine, H.; Iruela-Arispe, M. L. Membrane Lipids and Cell Signaling. *Current Opinion in Lipidology*. Lippincott Williams and Wilkins October 1, 2017, pp 408–413.

(6) Goñi, F. M. The Basic Structure and Dynamics of Cell Membranes: An Update of the Singer-Nicolson Model. *Biochimica et Biophysica Acta - Biomembranes*. Elsevier B.V. 2014, pp 1467–1476.

(7) Monnard, P.A.; Deamer, D. W. Membrane Self-Assembly Processes: Steps toward the First Cellular Life. *Anat. Rec.* **2002**, *268* (3), 196–207.

(8) Hanczyc, M. M.; Fujikawa, S. M.; Szostak, J. W. Experimental Models of Primitive Cellular Compartments: Encapsulation, Growth, and Division. *Science* **2003**, *302* (5645), 618–622.

(9) Blain, J. C.; Szostak, J. W. Progress Toward Synthetic Cells. *Annu. Rev. Biochem.* **2014**, *83*, 615–640.

(10) Budin, I.; Szostak, J. W. Physical Effects Underlying the Transition from Primitive to Modern Cell Membranes. *Proc. Natl. Acad. Sci. U. S. A.* **2011**, *108* (13), 5249–5254.

(11) Szostak, J. W.; Bartel, D. P.; Luisi, P. L. Synthesizing Life. *Nature* **2001**, *409* (6818), 387–390.

(12) Li, C.; Wang, L. X. Chemoenzymatic Methods for the Synthesis of Glycoproteins. *Chem. Rev.* **2018**, *118* (17), 8359–8413.

(13) Göpfrich, K.; Platzman, I.; Spatz, J. P. Mastering Complexity: Towards Bottom-up Construction of Multifunctional Eukaryotic Synthetic Cells. *Trends Biotechnol.* **2018**, *36* (9), 938–951.

(14) Roberts, M. A. J.; Cranenburgh, R. M.; Stevens, M. P.; Oyston, P. C. F. Synthetic Biology: Biology by Design. *Microbiology* **2013**, *159* (Pt 7), 1219.

(15) Yao, J.; Rock, C. O. Phosphatidic Acid Synthesis in Bacteria. *Biochim. Biophys. Acta.* **2013**, *1831* (3), 495–502.

(16) Moessinger, C.; Klizaite, K.; Steinhagen, A.; Philippou-Massier, J.; Shevchenko, A.; Hoch, M.; Ejsing, C. S.; Thiele, C. Two Different Pathways of Phosphatidylcholine Synthesis, the Kennedy Pathway and the Lands Cycle, Differentially Regulate Cellular Triacylglycerol Storage. *BMC Cell Biol.* **2014**, *15* (1), 1–17.

(17) Yamashita, A.; Sugiura, T.; Waku, K. Acyltransferases and Transacylases Involved in Fatty Acid Remodeling of Phospholipids and Metabolism of Bioactive Lipids in Mammalian Cells. *J. Biochem.* **1997**, *122* (1), 1–16.

(18) Maier, T.; Leibundgut, M.; Boehringer, D.; Ban, N. Structure and Function of Eukaryotic Fatty Acid Synthases. *Q. Rev. Biophys.* **2010**, *43* (03), 373–422.

(19) Chen, A.; Re, R. N.; Burkart, M. D. Type II Fatty Acid and Polyketide Synthases: Deciphering Protein-Protein and Protein-Substrate Interactions. *Nat. Prod. Rep*. **2018**, *35* (10), 1029–1045.

(20) Shen, H. H.; Lithgow, T.; Martin, L. L. Reconstitution of Membrane Proteins into Model Membranes: Seeking Better Ways to Retain Protein Activities. *Int. J. Mol. Sci.* **2013**, *14* (1), 1589.

(21) Scott, A.; Noga, M. J.; De Graaf, P.; Westerlaken, I.; Yildirim, E.; Danelon, C. Cell-Free Phospholipid Biosynthesis by Gene-Encoded Enzymes Reconstituted in Liposomes. *PLoS One* **2016**, *11* (10), e0163058.

(22) Flores, J.; White, B. M.; Brea, R. J.; Baskin, J. M.; Devaraj, N. K. Lipids: Chemical Tools for Their Synthesis, Modification, and Analysis. *Chem. Soc. Rev.* **2020**, *49* (14), 4602–4614.

(23) Shindou, H.; Hishikawa, D.; Harayama, T.; Yuki, K.; Shimizu, T. Recent Progress on Acyl CoA: Lysophospholipid Acyltransferase Research. *J. Lipid Res.* **2009**, *50* (Suppl), S46.

(24) Budin, I.; Devaraj, N. K. Membrane Assembly Driven by a Biomimetic Coupling Reaction. *J. Am. Chem. Soc.* **2012**, *134* (2), 751–753.

(25) Deamer, D. W.; Gavino, V. Lysophosphatidylcholine Acyltransferase: Purification and Applications in Membrane Studies. *Ann. N. Y. Acad. Sci.* **1983**, *414* (1), 90–96.

(26) Deamer, D. W.; Boatman, D. E. An Enzymatically Driven Membrane Reconstitution from Solubilized Components. *J. Cell Biol.* **1980**, *84* (2), 461–467.

(27) Brea, R. J.; Cole, C. M.; Devaraj, N. K. In Situ Vesicle Formation by Native Chemical Ligation. *Angew. Chemie - Int. Ed.* **2014**, *53* (51), 14102–14105.

(28) Brea, R. J.; Bhattacharya, A.; Devaraj, N. K. Spontaneous Phospholipid Membrane Formation by Histidine Ligation. *Synlett* **2017**, *28* (1), 108–112.

(29) Bhattacharya, A.; Brea, R. J.; Niederholtmeyer, H.; Devaraj, N. K. A Minimal Biochemical Route

towards de Novo Formation of Synthetic Phospholipid Membranes. *Nat. Commun.* **2019**, *10* (1).

(30) Mariani, A.; Russell, D. A.; Javelle, T.; Sutherland, J. D. A Light-Releasable Potentially Prebiotic Nucleotide Activating Agent. *J. Am. Chem. Soc.* **2018**, *140* (28), 8657–8661.

(31) Zhang, S. J.; Duzdevich, D.; Szostak, J. W. Potentially Prebiotic Activation Chemistry Compatible with Nonenzymatic RNA Copying. *J. Am. Chem. Soc.* **2020**, *142* (35), 14810–14813.

(32) Foden, C. S.; Islam, S.; Fernández-García, C.; Maugeri, L.; Sheppard, T. D.; Powner, M. W. Prebiotic Synthesis of Cysteine Peptides That Catalyze Peptide Ligation in Neutral Water. *Science* **2020**, *370* (6518), 865–869.

(33) Islam, S.; Bučar, D. K.; Powner, M. W. Prebiotic Selection and Assembly of Proteinogenic Amino Acids and Natural Nucleotides from Complex Mixtures. *Nat. Chem. 2017 96* **2017**, *9* (6), 584–589.

(34) Xu, J.; Chmela, V.; Green, N. J. J.; Russell, D. A. A.; Janicki, M. J. J.; Góra, R. W. W.; Szabla, R.; Bond, A. D. D.; Sutherland, J. D. D. Selective Prebiotic Formation of RNA Pyrimidine and DNA Purine Nucleosides. *Nature* **2020**, *582* (7810), 60–66.

(35) Patel, B. H.; Percivalle, C.; Ritson, D. J.; Duffy, C. D.; Sutherland, J. D. Common Origins of RNA, Protein and Lipid Precursors in a Cyanosulfidic Protometabolism. *Nat. Chem.* **2015**, *7* (4), 301–307.

(36) Eichberg, J.; Sherwood, E.; Epps, D. E.; Oró, J. Cyanamide Mediated Syntheses under Plausible Primitive Earth Conditions. IV. The Synthesis of Acylglycerols. *J. Mol. Evol.* **1977**, *10* (3), 221–230.

(37) Hargreaves, W. R.; Mulvihill, S. J.; Deamer, D. W. Synthesis of Phospholipids and Membranes in Prebiotic Conditions. *Nature* **1977**, *266* (5597), 78–80.

(38) Epps, D. E.; Sherwood, E.; Eichberg, J.; Oró, J. Cyanamide Mediated Syntheses under Plausible

Primitive Earth Conditions. V. The Synthesis of Phosphatidic Acids. *J. Mol. Evol.* **1978**, *11* (4), 279–292.

(39) Rao, M.; Eichberg, J.; Oró, J. Synthesis of Phosphatidylcholine under Possible Primitive Earth Conditions. *J. Mol. Evol.* **1982**, *18* (3), 196–202.

(40) Fayolle, D.; Altamura, E.; D'Onofrio, A.; Madanamothoo, W.; Fenet, B.; Mavelli, F.; Buchet, R.; Stano, P.; Fiore, M.; Strazewski, P. Crude Phosphorylation Mixtures Containing Racemic Lipid Amphiphiles Self-Assemble to Give Stable Primitive Compartments. *Sci. Reports* **2017**, *7* (1), 1–11.

(41) Dibrova, D. V.; Galperin, M. Y.; Mulkidjanian, A. Y. Phylogenomic Reconstruction of Archaeal Fatty Acid Metabolism. *Environ. Microbiol.* **2014**, *16* (4), 907.

(42) Lynen, F. [3] Yeast Fatty Acid Synthase. *Methods Enzymol.* **1969**, *14* (C), 17–33.

(43) Vagelos, P. R.; Alberts, A. W.; Majerus, P. W. [5] Mechanism of Saturated Fatty Acid Biosynthesis in Escherichia Coli. *Methods Enzymol.* **1969**, *14* (C), 39–43.

(44) Vagelos, P. R. Regulation of Fatty Acid Biosynthesis. *Curr. Top. Cell. Regul.* **1971**, *4* (C), 119–166.

(45) Toomey, R. E.; Wakil, S. J. Studies on the Mechanism of Fatty Acid Synthesis: XVI. *J. Biol. Chem.* **1966**, *241* (5), 1159–1165.

(46) Schweizer, E.; Hofmann, J. Microbial Type I Fatty Acid Synthases (FAS): Major Players in a Network of Cellular FAS Systems. *Microbiol. Mol. Biol. Rev.* **2004**, *68* (3), 501–517.

(47) Bloch, K.; Vance, D. Control Mechanisms in the Synthesis of Saturated Fatty Acids. *Annu. Rev. Biochem.* **1977**, *46*, 263–298.

(48) Gajewski, J.; Buelens, F.; Serdjukow, S.; Janßen, M.; Cortina, N.; Grubmüller, H.; Grininger, M.

Engineering Fatty Acid Synthases for Directed Polyketide Production. *Nat. Chem. Biol.* **2017**, *13* (4), 363–365.

(49) Marrakchi, H.; Zhang, Y. M.; Rock, C. O. Mechanistic Diversity and Regulation of Type II Fatty Acid Synthesis. *Biochem. Soc. Trans.* **2002**, *30* (Pt 6), 1050–1055.

(50) Rock, C. O.; Cronan, J. E. Escherichia Coli as a Model for the Regulation of Dissociable (Type II) Fatty Acid Biosynthesis. *Biochim. Biophys. Acta* **1996**, *1302* (1), 1–16.

(51) Smith, S. The Animal Fatty Acid Synthase: One Gene, One Polypeptide, Seven Enzymes. *FASEB J.* **1994**, *8* (15), 1248–1259.

(52) Smith, S.; Witkowski, A.; Joshi, A. K. Structural and Functional Organization of the Animal Fatty Acid Synthase. *Prog. Lipid Res.* **2003**, *42* (4), 289–317.

(53) Bajerski, F.; Wagner, D.; Mangelsdorf, K. Cell Membrane Fatty Acid Composition of Chryseobacterium Frigidisoli PB4T, Isolated from Antarctic Glacier Forefield Soils, in Response to Changing Temperature and PH Conditions. *Front. Microbiol.* **2017**, *8* (APR), 677.

(54) Kikuchi, S.; Rainwater, D. L.; Kolattukudy, P. E. Purification and Characterization of an Unusually Large Fatty Acid Synthase from Mycobacterium Tuberculosis Var. Bovis BCG. *Arch. Biochem. Biophys.* **1992**, *295* (2), 318–326.

(55) Fernandas, N. D.; Kolattukudy, P. E. Cloning, Sequencing and Characterization of a Fatty Acid Synthase-Encoding Gene from Mycobacterium Tuberculosis Var. Bovis BCG. *Gene* **1996**, *170* (1), 95–99.

(56) Kawaguchi, A.; Okuda, S. Fatty Acid Synthetase from Brevibacterium Ammoniagenes: Formation of Monounsaturated Fatty Acids by a Multienzyme Complex. *Proc. Natl. Acad. Sci. U. S. A.* **1977**, *74* (8), 3180–3183.

(57) Meurer, G.; Biermann, G.; Schütz, A.; Harth, S.; Schweizer, E. Molecular Structure of the

Multifunctional Fatty Acid Synthetase Gene of Brevibacterium Ammoniagenes: Its Sequence of Catalytic Domains Is Formally Consistent with a Head-to-Tail Fusion of the Two Yeast Genes FAS1 and FAS2. *Mol. Gen. Genet.* **1992**, *232* (1), 106–116.

(58) Stuible, H. P.; Wagner, C.; Andreou, I.; Huter, G.; Haselmann, J.; Schweizer, E. Identification and Functional Differentiation of Two Type I Fatty Acid Synthases in Brevibacterium Ammoniagenes. *J. Bacteriol.* **1996**, *178* (16), 4787–4793.

(59) Cole, S. T.; Brosch, R.; Parkhill, J.; Garnier, T.; Churcher, C.; Harris, D.; Gordon, S. V.; Eiglmeier, K.; Gas, S.; Barry, C. E.; Tekaia, F.; Badcock, K.; Basham, D.; Brown, D.; Chillingworth, T.; Connor, R.; Davies, R.; Devlin, K.; Feltwell, T.; Gentles, S.; Hamlin, N.; Holroyd, S.; Hornsby, T.; Jagels, K.; Krogh, A.; McLean, J.; Moule, S.; Murphy, L.; Oliver, K.; Osborne, J.; Quail, M. A.; Rajandream, M. A.; Rogers, J.; Rutter, S.; Seeger, K.; Skelton, J.; Squares, R.; Squares, S.; Sulston, J. E.; Taylor, K.; Whitehead, S.; Barrell, B. G. Deciphering the Biology of Mycobacterium Tuberculosis from the Complete Genome Sequence. *Nature* **1998**, *393* (6685), 537–544.

(60) Stuible, H. P.; Meier, S.; Schweizer, E. Identification, Isolation and Biochemical Characterization of a Phosphopantetheine:Protein Transferase That Activates the Two Type-I Fatty Acid Synthases of Brevibacterium Ammoniagenes. *Eur. J. Biochem.* **1997**, *248* (2), 481–487.

(61) Eggeling, L.; Sahm, H. L-Glutamate and l-Lysine: Traditional Products with Impetuous Developments. *Appl. Microbiol. Biotechnol. 1999 522* **1999**, *52* (2), 146–153.

(62) Kramer, R.; Lambert, C.; Hoischen, C.; Ebbighausen, H. Uptake of Glutamate in Corynebacterium Glutamicum. *Eur. J. Biochem.* **1990**, *194* (3), 929–935.

(63) Nampoothiri, K.; Hoischen, C.; Bathe, B.; Möckel, B.; Pfefferle, W.; Krumbach, K.; Sahm, H.; Eggeling, L. Expression of Genes of Lipid Synthesis and Altered Lipid Composition Modulates L-Glutamate Efflux of Corynebacterium Glutamicum. *Appl. Microbiol. Biotechnol. 2001 581* **2002**,

*58* (1), 89–96.

(64) Jarlier, V.; Nikaido, H. Mycobacterial Cell Wall: Structure and Role in Natural Resistance to Antibiotics. *FEMS Microbiol. Lett.* **1994**, *123* (1–2), 11–18.

(65) Sun, S.; Ding, Y.; Liu, M.; Xian, M.; Zhao, G. Comparison of Glucose, Acetate and Ethanol as Carbon Resource for Production of Poly(3-Hydroxybutyrate) and Other Acetyl-CoA Derivatives. *Front. Bioeng. Biotechnol.* **2020**, *8*, 833.

(66) Serpa, J. Cysteine as a Carbon Source, a Hot Spot in Cancer Cells Survival. *Front. Oncol.* **2020**, *10*, 947.

(67) Bean, R. C.; Shepherd, W. C.; Chan, H. Permeability of Lipid Bilayer Membranes to Organic Solutes. *J. Gen. Physiol.* **1968**, *52* (3), 495–508.

(68) Novak, K.; Pflügl, S. Towards Biobased Industry: Acetate as a Promising Feedstock to Enhance the Potential of Microbial Cell Factories. *FEMS Microbiol. Lett.* **2018**, *365* (20), 226.

(69) Wu, H.; Green, M.; Scranton, M. I. Acetate Cycling in the Water Column and Surface Sediment of Long Island Sound Following a Bloom. *Limnol. Oceanogr.* **1997**, *42* (4), 705–713.

(70) Zhuang, G. C.; Peña-Montenegro, T. D.; Montgomery, A.; Montoya, J. P.; Joye, S. B. Significance of Acetate as a Microbial Carbon and Energy Source in the Water Column of Gulf of Mexico: Implications for Marine Carbon Cycling. *Global Biogeochem. Cycles* **2019**, *33* (2), 223–235.

(71) Rittner, A.; Paithankar, K. S.; Huu, K. V.; Grininger, M. Characterization of the Polyspecific Transferase of Murine Type i Fatty Acid Synthase (FAS) and Implications for Polyketide Synthase (PKS) Engineering. *ACS Chem. Biol.* **2018**, *13* (3), 723–732.

(72) Matsuo, M.; Ohyama, S.; Sakurai, K.; Toyota, T.; Suzuki, K.; Sugawara, T. A Sustainable Self-Reproducing Liposome Consisting of a Synthetic Phospholipid. *Chem. Phys. Lipids* **2019**, *222*, 1–7.

(73) Cole, C. M.; Brea, R. J.; Kim, Y. H.; Hardy, M. D.; Yang, J.; Devaraj, N. K. Spontaneous Reconstitution of Functional Transmembrane Proteins during Bioorthogonal Phospholipid Membrane Synthesis. *Angew. Chemie - Int. Ed.* **2015**, *54* (43), 12738–12742.

(74) Brea, R. J.; Cole, C. M.; Lyda, B. R.; Ye, L.; Prosser, R. S.; Sunahara, R. K.; Devaraj, N. K. In Situ Reconstitution of the Adenosine A2A Receptor in Spontaneously Formed Synthetic Liposomes. *J. Am. Chem. Soc.* **2017**, *139* (10), 3607–3610.

(75) Iwasaki, Y.; Yamane, T. Enzymatic Synthesis of Structured Lipids. *Advances in biochemical engineering/biotechnology*. Springer, Berlin, Heidelberg 2004, pp 151–171.

(76) Radmacher, E.; Alderwick, L. J.; Besra, G. S.; Brown, A. K.; Gibson, K. J. C.; Sahm, H.; Eggeling, L. Two Functional FAS-I Type Fatty Acid Synthases in Corynebacterium Glutamicum.

(77) Haushalter, R. W.; Groff, D.; Deutsch, S.; The, L.; Chavkin, T. A.; Brunner, S. F.; Katz, L.; Keasling, J. D. Development of an Orthogonal Fatty Acid Biosynthesis System in E. Coli for Oleochemical Production. *Metab. Eng.* **2015**, *30*, 1–6.

(78) Seoane, A. A.; Brea, R. J.; Fuertes, A.; Podolsky, K. A.; Devaraj, N. K. Biomimetic Generation and Remodeling of Phospholipid Membranes by Dynamic Imine Chemistry. **2018**.

(79) Krause, M. R.; Regen, S. L. The Structural Role of Cholesterol in Cell Membranes: From Condensed Bilayers to Lipid Rafts. *Acc. Chem. Res.* **2014**, *47* (12), 3512–3521.

(80) Douliez, J. P.; Houinsou-Houssou, B.; Fameau, A. L.; Novales, B.; Gaillard, C. Self Assembly of Anastomosis-like Superstructures in Fatty Acid/Guanidine Hydrochloride Aqueous Dispersions. *J. Colloid Interface Sci.* **2010**, *341* (2), 386–389.

(81) Fameau, A. L.; Houinsou-Houssou, B.; Ventureira, J. L.; Navailles, L.; Nallet, F.; Novales, B.; Douliez, J. P. Self-Assembly, Foaming, and Emulsifying Properties of Sodium Alkyl Carboxylate/Guanidine Hydrochloride Aqueous Mixtures. *Langmuir* **2011**, *27* (8), 4505–4513.

(82) Douliez, J. P.; Houssou, B. H.; Fameau, A. L.; Navailles, L.; Nallet, F.; Grélard, A.; Dufourc, E. J.; Gaillard, C. Self-Assembly of Bilayer Vesicles Made of Saturated Long Chain Fatty Acids. *Langmuir* **2016**, *32* (2), 401–410.

(83) Suryabrahmam, B.; Agrawal, A.; Raghunathan, V. A. Fluid-Fluid Coexistence in Phospholipid Membranes Induced by Decanol. *Soft Matter* **2020**, *16* (39), 9002–9005.

(84) Semrau, S.; Schmidt, T. Membrane Heterogeneity-from Lipid Domains to Curvature Effects †. *Biochim. Biophys. Acta.* **1997**, *46* (1), 172–185.

(85) Lingwood, D.; Kaiser, H. J.; Levental, I.; Simons, K. Lipid Rafts as Functional Heterogeneity in Cell Membranes. *Biochem. Soc. Trans.* **2009,** 37 (Pt 5), 955–960.

(86) Kaneda, T. Fatty Acids of the Genus Bacillus: An Example of Branched Chain Preference. *Bacteriol. Rev*. **1977**, *41* (2), 391–418.

(87) Kaneda, T. Iso- and Anteiso-Fatty Acids in Bacteria: Biosynthesis, Function, and Taxonomic Significance. *Microbiol. Rev*. **1991**, *55* (2), 288–302.

(88) Radmacher, E.; Alderwick, L. J.; Besra, G. S.; Brown, A. K.; Gibson, K. J. C.; Sahm, H.; Eggeling, L. Two Functional FAS-I Type Fatty Acid Synthases in Corynebacterium Glutamicum. *Microbiology* **2005**, *151* (7), 2421–2427.

(89) Making your own electrocompetent cells | NEB https://www.neb.com/protocols/2012/06/21/making-your-own-electrocompetent-cells (accessed Sep 29, 2020).

(90) Brea, R. J.; Rudd, A. K.; Devaraj, N. K. Nonenzymatic Biomimetic Remodeling of Phospholipids in Synthetic Liposomes. *Proc. Natl. Acad. Sci. U. S. A.* **2016**, *113* (31), 8589–8594.

(91) Liu, L.; Zou, Y.; Bhattacharya, A.; Zhang, D.; Lang, S. Q.; Houk, K. N.; Devaraj, N. K. Enzyme-Free Synthesis of Natural Phospholipids in Water. *Nat. Chem.* **2020**, *12* (11), 1029–1034.

(92) Henriksen, J. R.; Andresen, T. L.; Feldborg, L. N.; Duelund, L.; Ipsen, J. H. Understanding Detergent Effects on Lipid Membranes: A Model Study of Lysolipids. *Biophys. J.* **2010**, *98* (10), 2199.

(93) Koynova, R.; Tenchov, B. Interactions of Surfactants and Fatty Acids with Lipids. *Curr. Opin. Colloid Interface Sci.* **2001**, *6* (3), 277–286.

(94) De Mets, F.; Van Melderen, L.; Gottesman, S. Regulation of Acetate Metabolism and Coordination with the TCA Cycle via a Processed Small RNA. *Proc. Natl. Acad. Sci. U. S. A.* **2019**, *116* (3), 1043–1052.

(95) Gao, X.; Lin, S. H.; Ren, F.; Li, J. T.; Chen, J. J.; Yao, C. B.; Yang, H. Bin; Jiang, S. X.; Yan, G. Q.; Wang, D.; Wang, Y.; Liu, Y.; Cai, Z.; Xu, Y. Y.; Chen, J.; Yu, W.; Yang, P. Y.; Lei, Q. Y. Acetate Functions as an Epigenetic Metabolite to Promote Lipid Synthesis under Hypoxia. *Nat. Commun. 2016 71* **2016**, *7* (1), 1–14.

(96) Castaño□Cerezo, S.; Bernal, V.; Post, H.; Fuhrer, T.; Cappadona, S.; Sánchez□Díaz, N. C.; Sauer, U.; Heck, A. J.; Altelaar, A. M.; Cánovas, M. Protein Acetylation Affects Acetate Metabolism, Motility and Acid Stress Response in Escherichia Coli. *Mol. Syst. Biol.* **2014**, *10* (11), 762.

(97) Kumari, S.; Beatty, C. M.; Browning, D. F.; Busby, S. J. W.; Simel, E. J.; Hovel-Miner, G. Regulation of Acetyl Coenzyme A Synthetase in Escherichia Coli. *J. Bacteriol.* **2000**, *182* (15), 4173.

(98) Shi, L.; Tu, B. P. Acetyl-CoA and the Regulation of Metabolism: Mechanisms and Consequences. **2015**.

(99) Theodoulou, F. L.; Sibon, O. C. M.; Jackowski, S.; Gout, I. Coenzyme A and Its Derivatives: Renaissance of a Textbook Classic. *Biochem. Soc. Trans.* **2014**, *42* (4), 1025–1032.

(100) Mosbach, K. Immobilized Coenzymes in General Ligand Affinity Chromatography and Their Use

as Active Coenzyme. *Adv. Enzymol. Relat. Areas Mol. Biol.* **2006,** 46, pp 205–278.

(101) Brown, T. D. K.; Jones-Mortimer, M. C.; Kornberg, H. L. The Enzymic Interconversion of Acetate and Acetyl-Coenzyme A in Escherichia Coli. *J. Gen. Microbiol.* **1977**, *102* (2), 327–336.

(102) Dirkmann, M.; Nowack, J.; Schulz, F. An in Vitro Biosynthesis of Sesquiterpenes Starting from Acetic Acid. *ChemBioChem* **2018**, *19* (20), 2146–2151.

(103) Gulbins, E. Sphingolipids: Basic Science and Drug Development. **2013**.

(104) Taha, T. A.; Mullen, T. D.; Obeid, L. M. A House Divided: Ceramide, Sphingosine, and Sphingosine-1-Phosphate in Programmed Cell Death. *Biochim. Biophys. Acta* **2006**, *1758* (12), 2027–2036.

(105) Bartke, N.; Hannun, Y. A. Bioactive Sphingolipids: Metabolism and Function. *J. Lipid Res.* **2009**, *50 Suppl* (Suppl).

(106) Malyarenko, T. V.; Kicha, A. A.; Stonik, V. A.; Ivanchina, N. V. Sphingolipids of Asteroidea and Holothuroidea: Structures and Biological Activities. *Mar. Drugs 2021, Vol. 19, Page 330* **2021**, *19* (6), 330.

(107) Kramer, J. K. G.; Blackwell, B. A.; Dugan, M. E. R.; Sauer, F. D. Identification of a New Sphingolipid 3-O-Acyl-D-Erythro-Sphingomyelin in Newborn Pig and Infant Plasma. *Biochim. Biophys. Acta* **1996**, *1303* (1), 47–55.

(108) Berger, A.; Rosenthal, D.; Spiegel, S. Sphingosylphosphocholine, a Signaling Molecule Which Accumulates in Niemann-Pick Disease Type A, Stimulates DNA-Binding Activity of the Transcription Activator Protein AP-1. *Proc. Natl. Acad. Sci. U. S. A.* **1995**, *92* (13), 5885.

(109) Breilyn, M. S.; Zhang, W.; Yu, C.; Wasserstein, M. P. Plasma Lyso-Sphingomyelin Levels Are Positively Associated with Clinical Severity in Acid Sphingomyelinase Deficiency. *Mol. Genet. Metab. Reports* **2021**, *28*, 100780.

(110) Maulik, P. R.; Shipley, G. G. N-Palmitoyl Sphingomyelin Bilayers: Structure and Interactions with Cholesterol and Dipalmitoylphosphatidylcholine. *Biochemistry* **1996**, *35* (24), 8025–8034.

(111) Nyholm, T. K. M.; Özdirekcan, S.; Antoinette Killian, J. How Protein Transmembrane Segments Sense the Lipid Environment. *Biochemistry* **2007**, *46* (6), 1457–1465.

(112) Bhattacharya, A.; Cho, C. J.; Brea, R. J.; Devaraj, N. K. Expression of Fatty Acyl-CoA Ligase Drives One-Pot de Novo Synthesis of Membrane-Bound Vesicles in a Cell-Free Transcription-Translation System. *J. Am. Chem. Soc.* **2021**, *143* (29), 11235–11242.

(113) Bhattacharya, A.; Niederholtmeyer, H.; Podolsky, K. A.; Bhattacharya, R.; Song, J. J.; Brea, R. J.; Tsai, C. H.; Sinha, S. K.; Devaraj, N. K. Lipid Sponge Droplets as Programmable Synthetic Organelles. *Proc. Natl. Acad. Sci. U. S. A.* **2020**, *117* (31), 18206–18215.

(114) Mancin, F.; Tecilla, P.; Tonellato, U. Metallomicelles Made of Ni(II) and Zn(II) Complexes of 2-Pyridinealdoxime-Based Ligands as Catalyst of the Cleavage of Carboxylic Acid Esters. *Langmuir* **2000**, *16* (1), 227–233.

(115) Ohshima, T.; Iwasaki, T.; Maegawa, Y.; Yoshiyama, A.; Mashima, K. Enzyme-like Chemoselective Acylation of Alcohols in the Presence of Amines Catalyzed by a Tetranuclear Zinc Cluster. *J. Am. Chem. Soc.* **2008**, *130* (10), 2944–2945.

(116) Schmelz, S.; Naismith, J. H. Adenylate-Forming Enzymes. *Curr. Opin. Struct. Biol.* **2009**, *19* (6), 666–671.

(117) Tristram-Nagle, S. A. Preparation of Oriented, Fully Hydrated Lipid Samples for Structure Determination Using X-Ray Scattering. *Methods Mol. Biol.* **2007**, *400*, 63.

(118) Bhattacharya, A.; Brea, R. J.; Song, J.-J.; Bhattacharya, R.; Sinha, S. K.; Devaraj, N. K. Single-Chain β-D-Glycopyranosylamides of Unsaturated Fatty Acids: Self-Assembly Properties and Applications to Artificial Cell Development. **2019**, *123* (17), 3711–3720.

(119) Nahmany, M.; Melman, A. Chemoselectivity in Reactions of Esterification. *Org. Biomol. Chem.* **2004**, *2* (11), 1563–1572.

(120) Kristensen, T. E. Chemoselective O-Acylation of Hydroxyamino Acids and Amino Alcohols under Acidic Reaction Conditions: History, Scope and Applications. *Beilstein J. Org. Chem. 1151* **2015**, *11* (1), 446–468.

(121) Himiyama, T.; Okamoto, Y. Artificial Metalloenzymes: From Selective Chemical Transformations to Biochemical Applications. *Mol.* **2020**, *25* (13), 2989.

(122) Fiore, M.; Chieffo, C.; Lopez, A.; Fayolle, D.; Ruiz, J.; Soulère, L.; Oger, P.; Altamura, E.; Popowycz, F.; Buchet, R. Synthesis of Phospholipids Under Plausible Prebiotic Conditions and Analogies with Phospholipid Biochemistry for Origin of Life Studies. *Astrobiology* **2022**, *22* (5), 598–627.

(123) Greenspan, L. Humidity Fixed Points of Binary Saturated Aqueous Solutions. *J. Res. Natl. Bur. Stand. Phys. Chem.* **1977**, *81A* (1).

(124) Ma, Y.; Ghosh, S. K.; Dilena, D. A.; Bera, S.; Lurio, L. B.; Parikh, A. N.; Sinha, S. K. Cholesterol Partition and Condensing Effect in Phase-Separated Ternary Mixture Lipid Multilayers. *Biophys. J.* **2016**, *110* (6), 1355–1366.

(125) Katsaras, J. X-Ray Diffraction Studies of Oriented Lipid Bilayers. *Biochem. Cell Biol.* **2011**, *73* (5–6), 209–218.

(126) Lyatskaya, Y.; Liu, Y.; Trisiram-Nagle, S.; Katsaras, J.; Kagle, J. F. Method for Obtaining Structure and Interactions from Oriented Lipid Bilayers. *Phys. Rev. E* **2000**, *63* (1), 011907.

(127) Zhang, R.; Suter, R. M.; Nagle, J. F. Theory of the Structure Factor of Lipid Bilayers. *Phys. Rev. E* **1994**, *50* (6), 5047.

(128) Torbet, J.; Wilkins, M. H. F. X-Ray Diffraction Studies of Lecithin Bilayers. *J. Theor. Biol.* **1976**,

*62* (2), 447–458.

(129) Nagle, J. F.; Tristram-Nagle, S. Structure of Lipid Bilayers. *Biochim. Biophys. Acta.* **2000**, *1469* (3), 159–195.

(130) Szostak, J. W.; Bartel, D. P.; Luisi, P. L. Synthesizing Life. *Nature* **2001**, *409* (6818), 387–390.

(131) Gajewski, J.; Pavlovic, R.; Fischer, M.; Boles, E.; Grininger, M. Engineering Fungal de Novo Fatty Acid Synthesis for Short Chain Fatty Acid Production. *Nat. Commun.* **2017**, *8* (1), 1–8.

(132) Johansson, P.; Wiltschi, B.; Kumari, P.; Kessler, B.; Vonrhein, C.; Vonck, J.; Oesterhelt, D.; Grininger, M. Inhibition of the Fungal Fatty Acid Synthase Type I Multienzyme Complex. *Proc. Natl. Acad. Sci.* **2008**, *105* (35), 12803–12808.

(133) Kozlov, M. M.; Campelo, F.; Liska, N.; Chernomordik, L. V.; Marrink, S. J.; McMahon, H. T. Mechanisms Shaping Cell Membranes. *Curr. Opin. Cell Biol*. **2014**, *29*, 53–60.

(134) McMahon, H. T.; Boucrot, E. Membrane Curvature at a Glance. *J. Cell Sci.* **2015**, *128* (6), 1065–1070.

(135) Jarsch, I. K.; Daste, F.; Gallop, J. L. Membrane Curvature in Cell Biology: An Integration of Molecular Mechanisms. *J. Cell Biol*. **2016**, *214* (4), 375–387.

(136) Henne, W. M.; Boucrot, E.; Meinecke, M.; Evergren, E.; Vallis, Y.; Mittal, R.; McMahon, H. T. FCHo Proteins Are Nucleators of Clathrin-Mediated Endocytosis. *Science* **2010**, *328* (5983), 1281–1284.

(137) Chang-Ileto, B.; Frere, S. G.; Chan, R. B.; Voronov, S. V.; Roux, A.; Di Paolo, G. Synaptojanin 1-Mediated PI(4,5)P2 Hydrolysis Is Modulated by Membrane Curvature and Facilitates Membrane Fission. *Dev. Cell* **2011**, *20* (2), 206–218.

(138) Westrate, L. M.; Lee, J. E.; Prinz, W. A.; Voeltz, G. K. Form Follows Function: The Importance

of Endoplasmic Reticulum Shape. *Annu. Rev. Biochem.* **2015**, *84* (1), 791–811.

(139) Jacquemyn, J.; Cascalho, A.; Goodchild, R. E. The Ins and Outs of Endoplasmic Reticulum□ controlled Lipid Biosynthesis. *EMBO Rep.* **2017**, *18* (11), 1905–1921.

(140) Vitale, A.; Ceriotti, A.; Denecke, J. *The Role of the Endoplasmic Reticulum in Protein Synthesis, Modification and Intracellular Transport. J. Exp. Bot.* **1993**, *44* (9), 1417-1444.

(141) Powers, R. E.; Wang, S.; Liu, T. Y.; Rapoport, T. A. Reconstitution of the Tubular Endoplasmic Reticulum Network with Purified Components. *Nature* **2017**, *543* (7644), 257–260.